University of Alberta

Cellular Osmotic Properties and Cellular Responses to Cooling

by

Lisa Ula Ross-Rodriguez

A thesis submitted to the Faculty of Graduate Studies and Research
in partial fulfillment of the requirements for the degree of

Doctor of Philosophy

in

Medical Sciences – Laboratory Medicine and Pathology

Department of Laboratory Medicine and Pathology

Fall 2009

Edmonton, Alberta

Examining Committee

Co-Supervisors:
Dr. Locksley E. McGann, Laboratory Medicine and Pathology
Dr. Janet A. W. Elliott, Chemical and Materials Engineering

Dr. Judith Hugh, Laboratory Medicine and Pathology

Dr. Gregory Korbutt, Surgery

Dr. Thomas Churchill, Surgery

Dr. John Critser, Veterinary Pathobiology, University of Missouri-Columbia

This achievement is dedicated to my parents,

Carlyle and Betty Anne Ross.

Thank you for your unconditional support and instilling

faith into my life.

Abstract

Cellular Osmotic Properties and Cellular Responses to Cooling

Recent advances in the fundamental theories in cryobiology using thermodynamic principles have created new opportunities for innovative methodologies in cryobiology. This thesis tested the hypothesis that calculated indicators of the two-factor hypothesis of cryoinjury, depending on cellular osmotic properties, will describe outcomes of cryobiological experiments. In addition, this thesis demonstrated that knowledge gained from improved descriptions of cellular osmotic parameters allows better understanding of cryoinjury and cryoprotection.

The main objective of this thesis was to develop approaches using simulations that can be applied to development of cryopreservation procedures for cell types of interest for therapies. In order for this approach to be successful, a method to more accurately describe the osmotic solution properties of the cell (i.e. osmolality as a function of molality for the cytoplasm) was developed. Also, in-depth examination into the correlation between predictions of the two types of cryoinjury and measured post-thaw biological outcomes was required.

The work presented in this thesis has shown that simulations, based on cell-specific osmotic characteristics, and coupled with interrupted cooling procedures can be used to determine conditions that minimize the two identified damaging factors in cryopreservation. Based on results from this research, both intracellular supercooling and

osmolality, as indicators of intracellular ice formation and solution effects injury, respectively, should be calculated when attempting to compare simulations with biological experimentation. This thesis has also shown a novel method of obtaining the solution properties (i.e. osmolality as a function of molality) of the cytoplasm of living cells using equilibrium cell volume measurements. Using these newly calculated parameters, this research also demonstrated the magnitude of error introduced by making dilute solution assumptions of the solution properties in cellular responses to low temperatures, including simulations of interrupted freezing procedures.

Overall, the research work presented in this thesis has extended the approach to cryopreservation to include the properties of the cell and the physical conditions of the freezing environment, which was only possible through the linkage between biological experimentation and simulations.

Acknowledgements

I wish to express my heartfelt appreciation and gratitude to the following individuals for their contribution to the realization of this thesis.

To Dr. Locksley McGann, my supervisor and mentor. Thank you for your wisdom, encouragement and belief in me.

To Dr. Janet Elliott, my supervisor and mentor. Thank you for your support, enthusiasm, and dedication.

To my committee members, Drs. Judith Hugh and Gregory Korbutt. Thank you for your time, encouragement, and insightful comments.

To Drs. John Critser and Thomas Churchill, my external examiners. Thank you for your feedback and support.

To Yuri Shardt and Jamie Lewis for their technical assistance.

To all the undergraduate students that I helped supervise. Thank you for allowing me to play a role in your introduction to research and to develop my teaching skills.

To past and present members of the McGann/Elliott and Acker Cryolabs, including Alireza Abazari, Adele Hansen, Tamir Kanias, Garson Law, and Kenneth Wong for their support, friendship, and even their blood…literally.

To the MANGO girls: Dr. Heidi Elmoazzen, Dr. Jelena Holovati, and Richelle Prickett. Thank you for sharing your knowledge with me. Also, thank you for your unconditional friendship, constant encouragement, and for your love of coffee breaks, sushi, and shopping.

To my friends all over the world. Thank you for your prayers, love, and support.

To the Ross and Rodriguez families. Thank you for your prayers, understanding, encouragement, patience, and unconditional love.

To Andres, my husband. Thank you for supporting me and helping me to reach my goals.

Table of Contents Page:

List of Tables

List of Figures Page:

List of Symbols and Abbreviations

Symbols

L_p	hydraulic conductivity	$\mu m^3/\mu m^2/min/atm$
		$\mu m/min/atm$
b	osmotically-inactive fraction	
E_a	activation energy	kcal/mol
T	absolute temperature	K
V	equilibrium cell volume	μm^3
V_o	isotonic cell volume	μm^3
π^o	isotonic osmolality	Osm/kg
π	experimental osmolality	Osm/kg
t	time	min
A	cell surface area	μm^2
R	universal gas constant	μm^3 atm/mol/K
		J/moleK
ρ	density of water	1.0×10^{-15} kg/μm^3
S	number of solute molecules	mole
P_s	solute permeability	$\mu m^3/\mu m^2/min$
m_s	solute concentration	moles/kg solvent
k	fitting constant	
L_p^o	reference water permeability	$\mu m^3/\mu m^2/min/atm$
P_s^o	reference solute permeability	$\mu m^3/\mu m^2/min$
m	molality of the solute	moles/kg solvent

B	fitting constant	$(\text{mole/kg})^{-1}$
C	fitting constant	$(\text{mole/kg})^{-2}$
K	electrolyte dissociation constant	
$m(\pi^o)$	isotonic molality as a function of osmolality	
$m(\pi)$	anisotonic molality as a function of osmolality	
b^*	non-ideal osmotically-inactive fraction of the cell volume	
T_{FP}^o	freezing point of the pure solvent (water)	
T_{FP}	freezing point of the solution	
R^2	coefficient of determination	
n	number of data points	
p	number of parameters	

Abbreviations

ANOVA	analysis of variance
EB	ethidium bromide
FBS	fetal bovine serum
HES	hydroxyethyl starch
HSC	hematopoietic stem cell
HUVEC	human umbilical vein endothelial cell
KCl	potassium chloride
Me_2SO	dimethyl sulfoxide
NaCl	sodium chloride
OSM	osmolality

OVE	osmotic virial equation
PBS	phosphate buffered saline
SC	supercooling
UCB	umbilical cord blood

Superscripts

e	extracellular
i	intracellular

Chapter 1: Introduction

1.1 Cryopreservation for cellular therapies and tissue engineering

Cryobiology is the study of the effects of low temperatures on biological systems. Although freezing is lethal to most living systems, cryobiologists have been able to preserve cells and tissues at a range of subzero temperatures, as low as liquid nitrogen temperatures (-196 °C). Cryobiology plays a key role in the long-term storage of native and engineered cells and tissues for research and clinical applications [26,70]. Currently, it is the only feasible method for the long-term maintenance of biological structure and function.

Recent developments in the utilization of a variety of cells, such as hematopoietic stem cells (HSC), for therapies [5,9,33,44,75] and tissue engineering [29,78] have revived interest in maximizing survival and preserving cell function during collection, processing, and preservation. As new sources of cells are being explored, it is becoming clear that using conventional approaches to cryopreservation often results in low survival of valuable cells and/or unnecessary complications. For example, the growing use of high-dose chemotherapy followed by stem cell transplantation requires efficient HSC collection, cryopreservation and storage. Currently, cryopreservation of these HSCs has been most successful with the use of dimethyl sulfoxide (Me_2SO) as a cryoprotectant. There are, however, limitations to the use of Me_2SO. Toxicities have been

associated with infusion of stem cells preserved with Me_2SO [10,11,18,52,77,90]. For cord blood samples, high cell recovery is critical because of the small, limited sample volume. There is significant interest in designing a cryopreservation protocol for HSCs, which limits toxicity, as well as maintains the cell viability while not requiring Me_2SO as a cryoprotectant. Some researchers have attempted to reduce the amount of Me_2SO [1,3] or to combine it with a non-permeating cryoprotectant, such as hydroxyethyl starch (HES) [15,30,36]. However, to our knowledge, complete removal of Me_2SO from the cryopreservation procedure for HSCs has not been documented. Higher standards for cell banking, specifically HSC banking, are required to meet future needs of cell banking, and therefore optimal cryopreservation procedures are fundamental.

1.2 Cryoinjury

"All of the obstacles to the preservation of life at low temperatures are apparently involved in the crystallization of ice" Harold T. Meryman [64]

During cryopreservation, a cell is slowly cooled to subzero temperatures, where ice is formed extracellularly, leaving the intracellular water unfrozen. This unfrozen fraction is supercooled below its freezing point. Intracellular supercooling is the extent to which a cell is cooled below the phase-change temperature before the formation of ice inside

the cell (intracellular ice). As water is removed by the formation of ice in the extracellular environment, the concentration of extracellular solutes is increased [47]. There is a resultant increase in intracellular solute concentration as well, as water flows out of the cell by exosmosis or through aquaporins (water channels). The cell can only maintain equilibrium with the extracellular solution if the cooling rate is low enough that the cell can dehydrate at the same rate as ice is forming. However, if the cooling rate is too rapid for the cell to lose water to the extracellular environment, the intracellular water becomes increasingly supercooled and there is increased probability of the formation of intracellular ice.

There have been many theories proposed to explain the mechanisms of freezing injury [24,43,47,55,65,66,69,81,84]. Mazur proposed that cell injury is caused by the formation of intracellular ice [54]. During rapid cooling, the formation of intracellular ice can be caused by supercooled intracellular water, as cells have insufficient time to equilibrate with the extracellular compartment by dehydration. The response of cells to the formation of ice in the surrounding solution is largely dependent on the movement of water across the plasma membrane [55]. Cell membrane permeability limits water efflux at low temperatures, resulting in supercooling at high cooling rates. Mazur also proposed that there is a 10 °C limit to supercooling, above which the probability of the formation of intracellular ice is significantly increased [55]. The probability of intracellular ice increases with the amount of

supercooling [55].

Lovelock also proposed that during the freezing process, cells are subjected to high concentrations of sodium chloride (NaCl) due to the formation of ice in the extracellular compartment [47]. As ice is formed, water is removed from the solution as ice, resulting in increased concentrations of NaCl in the liquid phase. This results in osmotic stress on the cell, which causes water to leave the cell. The dehydration of the cell also causes increased concentration of salts inside the cell. Lovelock proposed that the increasingly high concentration of solutes both extracellularly and intracellularly is damaging to the cell as the cell membrane becomes leaky [47]. Meryman later proposed that it is not a high concentration of salt that is damaging but that there is a minimum tolerable cell volume due to cell shrinkage during the dehydration process that is damaging to the cell [66]. Therefore, there is a minimum limit to the cell volume, which, regardless of the osmotic stress imposed by the environment, the cell cannot shrink beyond. This osmotic stress results in a transient pressure gradient across the membrane, which in turn causes the membrane to become leaky [65].

Mazur et al.'s 'two-factor hypothesis', combined previous works on the types of freezing injury and proposed that there are two independent mechanisms of damage during freezing: slow cooling injury, where cell injury is due to exposure to high solute concentrations due to ice formation, and rapid cooling injury, where cell injury is caused by the

formation of intracellular ice [60]. Maximum recovery is obtained by minimizing solution effects when cells are cooled rapidly enough to avoid harmful effects of their environment, yet cooling cells slowly enough that the cells can dehydrate sufficiently to avoid intracellular ice formation.

There is also evidence suggesting that damage may not be restricted to injury during freezing. The small ice crystals formed during rapid cooling may recrystallize during warming, causing additional damage to the cell [25,58-60]. The resulting damage occurs primarily during slow warming and may be more damaging than the formation of ice itself [25,58-60]. Therefore, there exists an optimal cooling and warming rate specific for each cell type, which minimizes both types of injury.

Injury sustained during a cryopreservation procedure can be further minimized by the use of cryoprotectants. Cryoprotectants are classified, as permeating and non-permeating, based on their ability to traverse the cell membrane [67]. Permeating agents, such as Me_2SO, protect the cell against slow cool injury by reducing the amount of ice formed, thereby minimizing cell dehydration [67]. Glycerol, has also been shown to protect the cell when present both inside and outside the cell, by reducing the excessive concentration of salts [48,71]. The criteria for an effective permeating cryoprotectant are that it must permeate the cell and exhibit low-toxicity at multimolar concentrations [67]. Me_2SO protects the cell by depressing the freezing point, which lowers the temperature at which ice is formed and in turn lowers the temperature where a specific concentration

of electrolytes occurs [11]. The movement of permeating cryoprotectants is also dependent on the membrane permeability and is limited at low temperatures. Non-permeating cryoprotectants are high molecular weight additives, such as starches (e.g. HES) and sugars, which do not permeate the cell membrane. These agents confer protection by promoting water loss at higher subzero temperatures and are responsible for osmotic stress on the cell [11]. McGann reported that freezing Chinese hamster fibroblasts with 20 % HES, resulted in comparable cell recovery to using 10 % Me_2SO/media [61]; therefore, it is feasible to attempt to eliminate Me_2SO from cryopreservation protocols.

1.3 Interrupted freezing procedures

In cryopreservation procedures, cells are cooled at a finite rate which is optimized for the cell type and cryoprotectant. This optimization has typically been approached empirically by varying cooling rates and the cryoprotectants. However, it has long been known that there are critical subzero temperature ranges where interrupting the cooling process improves cell recovery [50]. In addition to cooling at a constant rate, there are two interrupted freezing procedures which have been used to examine the effects of low temperatures on cells: a two-step freezing procedure and a graded freezing procedure. The two-step freezing procedure, used by Farrant et al. is a logical method to examine the effects of osmotic interactions on cell recovery over a broad range of subzero temperatures

[23]. In this procedure, lymphocytes were cooled rapidly to various subzero temperatures and held for various periods of time before being 1) thawed directly from that holding temperature or 2) rapidly cooled to -196 °C before thawing. McGann and Farrant later reported that the subzero temperature and the length of hold time at that temperature were important factors to consider when attempting to maximize cell survival [63]. The graded freezing procedure, a modification of the two-step freezing procedure, was later developed by McGann and used to determine the temperature range through which slow cooling should be controlled [62]. Samples were cooled slowly to various subzero temperatures before being either thawed directly or plunged into liquid nitrogen first and then thawed. Both interrupted freezing procedures allow separation of damage which occurs during the initial cooling phase from that which occurs during subsequent cooling to the storage temperature. These experimental procedures provide insights into the effects of subzero temperatures and time, which can be used to further understanding of cryoinjury.

Minimizing the potential for solution effects injury and injury due to intracellular ice formation can be done by controlling the water content in the cell. Movement of water due to extracellular ice formation ultimately determines cell volume. However, the movement of the cryoprotectant also contributes to the changes in cell volume. Therefore, it is the water and solute movement which are important factors in cellular responses to

freezing.

1.4 Cellular osmotic parameters

During cryopreservation, as extracellular ice forms the external environment (ie. osmolality) changes, resulting in a cellular osmotic response in the form of a change in cell volume [57]. In a hypertonic environment, a cell will dehydrate to reach a new equilibrium with the environment, with a resultant reduction in cell volume. Conversely, in a hypotonic environment, a cell will swell, with a resultant increase in cell volume. The permeability characteristics of the cell membrane control the movement of water both into and out of the cell. There are changes in the fluidity of the membrane that occur at lower temperatures so water movement is reduced [20,45]. The cellular responses to the changes in osmolality parallel the changes in cell volume as ice is formed in the extracellular environment and are thus important in cryobiology [57].

The osmotic response of the cell determines the type of cryoinjury the cell is susceptible to: slow cool injury (cell significantly shrinks, leading to exposure to high intracellular solute concentrations); or fast cool injury (minimal cell shrinkage leading to increased likelihood of intracellular ice formation). The osmotic characteristics of the cell, which govern the movement of water, are the hydraulic conductivity, the osmotically-inactive fraction, and the Arrhenius activation energy for the hydraulic conductivity. The hydraulic conductivity (L_p) is the rate at which water crosses the cell

membrane (Eq. 2-2). Jacobs and Stewart also described L_p as the rate of volume change in anisotonic solutions at an experimental temperature [32]. The osmotically-inactive fraction (*b*) of the cell is the fraction of the cell volume not involved in the osmotic activities of the cell. The traditional Boyle van't Hoff relationship (Eq. 2-1) can be used to calculate the osmotically-inactive fraction by expressing the equilibrium cell volume as a function of osmolality after exposure to various anisotonic solutions of impermeant solutes [49]. However, this relationship assumes an ideal, dilute solution, which is not the case at infinite osmolality (i.e. the condition used to determine the osmotically-inactive fraction). Recently a modified Boyle van't Hoff equation (Eq. 6-4) has been presented which is not limited by the constraints of ideal, dilute assumptions [72]. However, this relation requires the phase diagram information of the cytoplasm (i.e. osmolality as a function of molality), which is yet to be elucidated for cells, other than red blood cells [19,68]. The Arrhenius activation energy for L_p (E_a^{Lp}) is used to describe the temperature dependence of L_p (Eq. 2-4) [86]. The E_a^{Lp} can be determined using the slope of the Arrhenius plot of the natural logarithm of L_p as a function of the inverse absolute temperature (K) [86]. It is important to determine the temperature dependence of the osmotic parameters in order to explore the cellular responses at low temperatures. A better understanding of the nature and kinetics of cellular responses to temperature-induced conditions would allow novel approaches to the cryopreservation of new cell types. Based on the

aforementioned osmotic properties of the cell membrane, which are specific to each cell type, computer simulations can be used to determine these novel approaches to cryopreservation.

1.5 Simulations of low temperature cellular responses

Even though cryopreservation protocols have traditionally been determined empirically, some researchers have explored the use of simulations as a means of predicting low temperature responses of various cell types: peripheral blood stem cells [83]; cord blood stem cells [88]; bull spermatozoa [87]; bovine erythrocytes [40]; rat embryos [46]; porcine chondrocytes [89]; yeast [79]; hamster ova [80]; and human corneal epithelial, endothelial and stromal cells [17]. Simulation of cellular responses at low temperatures is comprised of four main elements: 1) change in the composition of the extra- and intracellular solutions at low temperatures; 2) cellular osmotic responses to changes in composition of the extracellular solution; 3) the temperature dependence of the cellular osmotic permeability parameters; and 4) changes in temperature as a function of time [76]. Computer simulations of cellular responses to low temperatures are based on mathematical calculations of changes in cell volume. It is possible to use the osmotic parameters to calculate cellular responses, i.e. changes in cell volume. Modeling expresses the theoretical cellular responses to anisotonic environments based on the osmotic properties of the cell membrane and their temperature

dependencies which are specific to each cell type. These simulations can be extrapolated to low temperature responses due to changes in osmolality by the formation of ice. The formation of ice imposes osmotic stresses on the cell by the concomitant increase in concentration of extracellular solutes [47]. Thus, the permeability characteristics of the cell membrane regulate cell volume and in turn, the intracellular osmolality.

The phase diagrams of the intracellular and extracellular solution, i.e. osmolality as a function of molality, describe the composition of the solutions during the freezing process [8]. Osmolality is the basis for freezing point depression and water transport. Phase diagrams are used to calculate the changes in cell volume based on the concentration of electrolytes in the unfrozen fraction of the system. Accurate knowledge of the osmolality of biological solutions is essential for simulations in cryobiology. The osmolality of the extracellular solution has been well defined for a variety of types and combinations of solutes [19]. The phase diagram of the intracellular solution of cells (i.e. cytoplasm) has not been well defined with the exception of the cytoplasm of red blood cells [19,68]. Nucleated cells have many intracellular components, such as water, organelles, electrolytes, and proteins of varying concentrations [2]. While the solution properties are known for individual components (e.g. hemoglobin [12,19]), and the combination of known components using the osmotic virial equation (e.g. bovine serum albumin and ovalbumin) [19], the cytoplasm is too complex to make use of the individual solute solution

properties feasible. As a result, intracellular descriptions have been included in simulations with limiting assumptions, where the model system is defined as an ideal cell model (i.e. electrolytes only) [4,14,17,22,27,28,34,35,46,55,56,80,82,84,85,87,88] or by a primitive non-ideal cell model (i.e. a single specified protein and electrolytes) [41,42,51]. More accurate knowledge of the cytoplasm of nucleated cells is required.

Simulations of freezing protocols attempt to minimize freezing injury theoretically, based on the osmotic characteristics of the cell, as opposed to empirically, based on cooling rates and the addition of cryoprotectants. Furthermore, different initial concentrations of electrolytes in the extracellular and intracellular solutions can be used in simulations to calculate the increase in final concentrations during freezing and to determine the potential for injury due to exposure to electrolytes. Simulations can be used to predict the potential for intracellular ice formation based on the amount of intracellular supercooling. Mazur proposed that there was a 10 °C limit to supercooling prior to the formation of intracellular ice and the risk of intracellular ice increased based on the amount of supercooling [55]. In yeast cells, low cooling rates have been shown to reduce the amount of supercooling and thus reduce the risk of intracellular ice [55]. Diller further examined the probability of intracellular ice formation based on the interaction of cooling rates and supercooling on human erythrocytes [13]. During freezing, the cell maintains equilibrium across the plasma membrane either through osmotic

dehydration and/or the formation of intracellular ice [13]. Sub-optimal or supra-optimal cooling rates will cause damage to a cell either by solution effects or intracellular ice formation, respectively. Karlsson et al. developed a theoretical model for predicting intracellular ice formation during cryopreservation by coupling crystal-growth, ice nucleation, and water transport models [34]. Ebertz et al. also demonstrated the use of simulations for cryopreserving corneal cells by examining supercooling as a function of cooling rates to reduce the amount of experimentation required and define a starting point for experimental verification of predicted optimal cooling rates [16,17]. However, these examples assumed ideal dilute solution. The research performed in this thesis will further the use of simulations to interpret injury associated with intracellular ice formation and solution effects.

1.6 Hypotheses

Based on cellular osmotic properties, calculated indicators of the two-factor hypothesis of cryoinjury will describe outcomes of cryobiological experiments. Knowledge gained from improved descriptions of cellular osmotic parameters will allow better understanding of cryoinjury and cryoprotection.

1.7 Overall approach and objectives

Recent advances in the fundamental theories in cryobiology using

thermodynamic principles have created new opportunities for innovative methodologies in cryobiology. In our laboratory, these advances have been implemented in improved thermodynamic models [19,21,72-74], allowing the development of cryopreservation protocols to meet specific design criteria (e.g. specific cell type and no permeating cryoprotectant). An in-house computer program (*CryoSim6*, Dr. Locksley McGann, University of Alberta, Canada), has been developed using these models, to simulate cellular osmotic responses at low temperatures. The approach of this thesis is to use detailed knowledge of cellular osmotic properties, including osmotic solution properties of the intra- and extracellular solutions, to manipulate cooling profiles in order to replace cryoprotectants as the method to minimize the two types of cryoinjury. This will aid in the design of optimal cryopreservation protocols [76]. In order for this approach to be successful, a more accurate description of the osmotic solution properties of the cell (i.e. osmolality as a function of molality for the cytoplasm) is required. Also, in-depth examination into the correlation between predictions of the two types of cryoinjury and measured post-thaw biological outcomes is necessary. TF-1 cells have been used in this research as a model cell type for HSC, as they express the CD34+ antigen, are able to differentiate into the various hematopoietic lineages [37,38,53], and have been used as HSC models in various other studies [6,7,31,39,53]. The overall goal of this thesis is to develop approaches using simulations that can be applied to development of cryopreservation

procedures for HSCs and other cell types of interest for cellular therapies.

The specific objectives of this doctoral thesis are:

1. Determine the osmotic parameters, hydraulic conductivity, osmotically-inactive fraction, and Arrhenius activation energy for the hydraulic conductivity, of TF-1 cells, human umbilical vein endothelial cells (HUVECs), and porcine chondrocytes.

In Chapter 2, the complexity of cellular responses to anisotonic conditions was investigated. We measured the osmotic parameters using an electronic particle counter fitted with a cell size analyzer. Changes in cell volume as a function of time were monitored, while exposing cells to hypertonic solutions at various temperatures.

2. Characterize the cryobiological responses of TF-1 cells to interrupted freezing procedures.

In Chapter 3, cellular responses to low temperatures were explored. We empirically investigated TF-1 cell recovery following interrupted freezing procedures: two-step freezing (rapid interrupted cooling with hold time); and graded freezing (slow interrupted cooling without hold time).

3. Demonstrate the use of calculated intracellular supercooling, as an indicator of intracellular ice formation, to understand post-thaw biological

outcomes.

In Chapter 4, correlation between freezing experiments and simulations was used to further our understanding of two-step freezing. We used the osmotic parameters of TF-1 cells to model the cellular responses to low temperatures. These models were based on actual experimental procedures, i.e. two-step freezing protocols (rapid interrupted cooling with hold time), which were used to examine the effects of subzero temperatures and time spent at subzero temperatures on intracellular ice formation. The results of the simulations were then used to interpret the TF-1 cell recovery.

4. Dissect the components of cryoinjury using simulations of a graded freezing procedure (slow interrupted cooling without hold time).

In Chapter 5, predicted intracellular osmolality was investigated as an indicator for solution effects injury in simulations. We used the osmotic parameters of TF-1 cells to model cellular responses to low temperatures based on a graded freezing protocol (slow interrupted cooling without hold time), which has been used to examine the two types of freezing injuries: solution effects and intracellular ice formation using calculated indicators of injury. The results were then used to interpret post-thaw TF-1 cell recovery.

5. Develop a new procedure to measure the osmotic solution properties of the cytoplasm of living cells and evaluate the effect of using these measured properties on calculated indicators of cryoinjury in simulations.

In Chapter 6, the solution properties of the cytoplasm for various nucleated cell types were determined. We calculated the osmotically-inactive fraction of the cell (with and without ideal, dilute solution assumptions) and the solution properties of the cytoplasm using osmotic equilibrium data for various cell types of interest to cryopreservation, including TF-1 cells. The parameters of TF-1 cells were then used in simulations of interrupted freezing procedures and compared with previously used approximations.

1.8 References

[1] J.F. Abrahamsen, A.M. Bakken, and O. Bruserud, Cryopreserving human peripheral blood progenitor cells with 5-percent rather than 10-percent DMSO results in less apoptosis and necrosis in CD34+cells. Transfusion 42 (2002) 1573-1580.

[2] B. Alberts, D. Bray, J. Lewis, M. Raff, K. Roberts, and J.D. Watson, Molecular biology of the cell, Garland Publishing, Inc, New York & London, 1994.

[3] F. Beaujean, J.H. Bourhis, C. Bayle, H. Jouault, M. Divine, C. Rieux, M. Janvier, C. Le Forestier, and J.L. Pico, Successful cryopreservation of purified autologous CD34(+) cells: influence of freezing parameters on cell recovery and engraftment. Bone Marrow Transplantation 22 (1998) 1091-1096.

[4] C.M.K. Benson, J.D. Benson, and J.K. Critser, An improved cryopreservation method for a mouse embryonic stem cell line. Cryobiology 56 (2008) 120-130.

[5] C. Boucherie, and E. Hermans, Adult stem cell therapies for neurological disorders: benefits beyond neuronal replacement? Journal of Neuroscience Research 87 (2009) 1509-1521.

[6] S.S. Buchanan, S.A. Gross, J.P. Acker, M. Toner, J.F. Carpenter, and D.W. Pyatt, Cryopreservation of stem cells using trehalose: evaluation of the method using a human hematopoietic cell line. Stem Cells and Development 13 (2004) 295-305.

[7] L. Cermak, S. Simova, A. Pintzas, V. Horejsi, and L. Andera, Molecular mechanisms involved in CD43-mediated apoptosis of TF-1 cells. The Journal of Biological Chemistry 277 (2002) 7955-7961.

[8] F.H. Cocks, and W.E. Brower, Phase diagram relationships in cryobiology. Cryobiology 11 (1974) 340-358.

[9] G.Q. Daley, and D.T. Scadden, Prospects for stem cell-based therapy. Cell 132 (2008) 544-548.

[10] K. Darabi, J.R. Brown, and G.S. Kao, Paradoxical embolism after peripheral blood stem cell infusion. Bone Marrow Transplantation 36 (2005) 560-562.

[11] J.M. Davis, S.D. Rowley, H.G. Braine, S. Piantadosi, and G.W. Santos, Clinical toxicity of cryopreserved bone-marrow graft infusion. Blood 75 (1990) 781-786.

[12] D.A.T. Dick, and L.M. Lowenstein, Osmotic equilibria in human erythrocytes studied by immersion refractometry. Proceedings of the Royal Society of London Series B-Biological Sciences 148 (1958) 241-256.

[13] K.R. Diller, Intracellular freezing - effect of extracellular supercooling. Cryobiology 12 (1975) 480-485.

[14] K.R. Diller, and M.E. Lynch, An irreversible thermodynamic analysis of cell freezing in the presence of membrane-permeable additives .2. Transient electrolyte and additive concentrations. Cryoletters 5 (1984) 117-130.

[15] C. Donaldson, W.J. Armitage, P.A. DenningKendall, A.J. Nicol, B.A. Bradley, and J.M. Hows, Optimal cryopreservation of human umbilical cord blood. Bone Marrow Transplantation 18 (1996) 725-731.

[16] S.L. Ebertz, Fundamental cryobiology of cells from a bioengineered human corneal equivalent, Medical Sciences - Laboratory Medicine and Pathology, University of Alberta, Edmonton, Alberta, 2002, pp. 161.

[17] S.L. Ebertz, and L.E. McGann, Osmotic parameters of cells from a bioengineered human corneal equivalent and consequences for cryopreservation. Cryobiology 45 (2002) 109-117.

[18] M.J. Egorin, D.M. Rosen, R. Sridhara, L. Sensenbrenner, and M. Cottler-Fox, Plasma concentrations and pharmacokinetics of dimethylsulfoxide and its metabolites in patients undergoing peripheral-blood stem-cell transplants. Journal of Clinical Oncology 16 (1998) 610-615.

[19] J.A.W. Elliott, R.C. Prickett, H.Y. Elmoazzen, K.R. Porter, and L.E. McGann, A multi-solute osmotic virial equation for solutions of interest in biology. Journal of Physical Chemistry B 111 (2007) 1775-1785.

[20] H.Y. Elmoazzen, J.A.W. Elliott, and L.E. McGann, The effect of temperature on membrane hydraulic conductivity. Cryobiology 45 (2002) 68-79.

[21] H.Y. Elmoazzen, J.A.W. Elliott, and L.E. McGann, Osmotic Transport across Cell Membranes in Nondilute Solutions: A New Nondilute Solute Transport Equation. Biophysical Journal 96 (2009) 2559-2571.

[22] G.M. Fahy, Simplified calculation of cell water-content during freezing and thawing in nonideal solutions of cryoprotective agents and its possible application to the study of solution effects injury. Cryobiology 18 (1981) 473-482.

[23] J. Farrant, S.C. Knight, L.E. McGann, and J. O'Brien, Optimal recovery of lymphocytes and tissue culture cells following rapid cooling. Nature 249 (1974) 452-3.

[24] J. Farrant, and G.J. Morris, Thermal shock and dilution shock as the causes of freezing injury. Cryobiology 10 (1973) 134-140.

[25] M. Forsyth, and D.R. Macfarlane, Recrystallization revisited. Cryo-Letters 7 (1986) 367-378.

[26] D. Gao, and J.K. Critser, Mechanisms of cryoinjury in living cells. ILAR Journal 41 (2000) 187-196.

[27] D.Y. Gao, C. Liu, C.T. Benson, J. Liu, E.S. Critser, J.K. Critser, L.E. McGann, and S. Lin, Theoretical and experimental analyses of optimal experimental design for determination of hydraulic conductivity of cell membrane. in: L.J. Hayes, and R.B. Roemer, (Eds.), Advances in heat and mass transfer in biological systems., American Society of Mechanical Engineers., New York, N. Y.,

1994, pp. 151-158.

[28] J.A. Gilmore, J. Liu, E.J. Woods, A.T. Peter, and J.K. Critser, Cryoprotective agent and temperature effects on human sperm membrane permeabilities: convergence of theoretical and empirical approaches for optimal cryopreservation methods. Human Reproduction 15 (2000) 335-343.

[29] L. Guerra, E. Dellambra, L. Panacchia, and E. Paionni, Tissue engineering for damaged surface and lining epithelia: stem cells, current clinical applications, and available engineered tissues. Tissue Engineering Part B-Reviews 15 (2009) 91-112.

[30] P. Halle, O. Tournilhac, W. Knopinska-Posluszny, J. Kanold, P. Gembara, N. Boiret, C. Rapatel, M. Berger, P. Travade, S. Angielski, J. Bonhomme, and F. Demeocq, Uncontrolled-rate freezing and storage at-80 degrees C, with only 3.5-percent DMSO in cryoprotective solution for 109 autologous peripheral blood progenitor cell transplantations. Transfusion 41 (2001) 667-673.

[31] G. Hansen, T.R. Hercus, B.J. McClure, F.C. Stomski, M. Dottore, J. Powell, H. Ramshaw, J.M. Woodcock, Y.B. Xu, M. Guthridge, W.J. McKinstry, A.F. Lopez, and M.W. Parker, The structure of the GM-CSF receptor complex reveals a distinct mode of cytokine receptor activation. Cell 134 (2008) 496-507.

[32] M.H. Jacobs, and D.R. Stewart, A simple method for the quantitative measurement of cell permeability. Journal of Cellular and

Comparative Physiology 1 (1932) 71-82.

[33] K.B. Jones, T. Seshadri, R. Krantz, A. Keating, and P.C. Ferguson, Cell-based therapies for osteonecrosis of the femoral head. Biology of Blood and Marrow Transplantation 14 (2008) 1081-1087.

[34] J.O.M. Karlsson, E.G. Cravalho, and M. Toner, A model of diffusion-limited ice growth inside biological cells during freezing. Journal of Applied Physics 75 (1994) 4442-4445.

[35] J.O.M. Karlsson, A. Eroglu, T.L. Toth, E.G. Cravalho, and M. Toner, Fertilization and development of mouse oocytes cryopreserved using a theoretically optimized protocol. Human Reproduction 11 (1996) 1296-1305.

[36] Y. Katayama, T. Yano, A. Bessho, S. Deguchi, K. Sunami, N. Mahmut, K. Shinagawa, E. Omoto, S. Makino, T. Miyamoto, S. Mizuno, T. Fukuda, T. Eto, T. Fujisaki, Y. Ohno, S. Inaba, Y. Niho, and M. Harada, The effects of a simplified method for cryopreservation and thawing procedures on peripheral blood stem cells. Bone Marrow Transplantation 19 (1997) 283-287.

[37] T. Kitamura, F. Takaku, and A. Miyajima, IL-1 up-regulates the expression of cytokine receptors on a factor-dependent human hemopoietic cell line, TF-1. International Immunology 3 (1991) 571-577.

[38] T. Kitamura, A. Tojo, T. Kuwaki, S. Chiba, K. Miyazono, A. Urabe, and F. Takaku, Identification and analysis of human erythropoietin

receptors on a factor-dependent cell-line, TF-1. Blood 73 (1989) 375-380.

[39] A. Kolonics, A. Apati, J. Janossy, A. Brozik, R. Gati, A. Schaefer, and M. Magocsi, Activation of Raf/ERK1/2 MAP kinase pathway is involved in GM-CSF-induced proliferation and survival but not in erythropoietin-induced differentiation of TF-1 cells. Cellular Signalling 13 (2001) 743-754.

[40] S.P. Leibo, Freezing damage of bovine erythrocytes - simulation using glycerol concentration changes at subzero temperatures. Cryobiology 13 (1976) 587-598.

[41] R.L. Levin, E.G. Cravalho, and C.E. Huggins, Effect of hydration on water-content of human erythrocytes. Biophysical Journal 16 (1976) 1411-1426.

[42] R.L. Levin, E.G. Cravalho, and C.E. Huggins, Effect of solution non-ideality on erythrocyte volume regulation. Biochimica et Biophysica Acta 465 (1977) 179-190.

[43] J. Levitt, Sulfhydryl-disulfide hypothesis of frost injury and resistance in plants. Journal of Theoretical Biology 3 (1962) 355-391.

[44] A.C. Lindsay, and J.P. Halcox, Stem cells as future therapy in cardiology. Hospital Medicine 66 (2005) 215-220.

[45] C. Liu, C.T. Benson, D.Y. Gao, B.W. Haag, L.E. Mcgann, and J.K. Critser, Water permeability and Its activation-energy for individual hamster pancreatic-islet cells. Cryobiology 32 (1995) 493-502.

[46] J. Liu, E.J. Woods, Y. Agca, E.S. Critser, and J.K. Critser, Cryobiology of rat embryos II: A theoretical model for the development of interrupted slow freezing procedures. Biology of Reproduction 63 (2000) 1303-1312.

[47] J.E. Lovelock, The haemolysis of human red blood-cells by freezing and thawing. Biochimica et Biophysica Acta 10 (1953) 414-426.

[48] J.E. Lovelock, The Mechanism of the Protective Action of Glycerol Against Haemolysis by Freezing and Thawing. Biochimica et Biophysica Acta 11 (1953) 28-36.

[49] B. Lucke, and M. McCutcheon, The living cell as an osmotic system and its permeability to water. Physiological Reviews 12 (1932) 68-139.

[50] B. Luyet, and J. Keane, A critical temperature range apparently characterized by sensitivity of bull semen to high freezing velocity. Biodynamica 7 (1955) 281-292.

[51] G.A. Mansoori, Kinetics of water-loss from cells at subzero centigrade temperatures. Cryobiology 12 (1975) 34-45.

[52] G. Marcacci, G. Corazzelli, C. Becchimanzi, M. Arcamone, G. Capobianco, F. Russo, F. Frigeri, and A. Pinto, DMSO-associated encephalopathy during autologous peripheral stem cell infusion: a predisposing role of preconditioning exposure to CNS-penetrating agents? Bone Marrow Transplantation 44 (2009) 133-135.

[53] M. Marone, G. Scambia, G. Bonanno, S. Rutella, D. de Ritis, F. Guidi,

G. Leone, and L. Pierelli, Transforming growth factor-beta 1 transcriptionally activates CD34 and prevents induced differentiation of TF-1 cells in the absence of any cell-cycle effects. Leukemia 16 (2002) 94-105.

[54] P. Mazur, Physical factors implicated in the death of micro-organisms at subzero temperatures. Annals of the New York Academy of Sciences 85 (1960) 610-629.

[55] P. Mazur, Kinetics of water loss from cells at subzero temperatures and the likelihood of intracellular freezing. The Journal of General Physiology 47 (1963) 347-369.

[56] P. Mazur, Studies on rapidly frozen suspensions of yeast cells by differential thermal analysis and conductometry, 1963, pp. 323-353.

[57] P. Mazur, The role of cell membranes in the freezing of yeast and other cells. Annals of the New York Academy of Science 125 (1965) 658-76.

[58] P. Mazur, Role of Intracellular Freezing in Death of Cells Cooled at Supraoptimal Rates. Cryobiology 14 (1977) 251-272.

[59] P. Mazur, Freezing of living cells - mechanisms and implications. American Journal of Physiology 247 (1984) C125-C142.

[60] P. Mazur, S.P. Leibo, and E.H. Chu, A two-factor hypothesis of freezing injury. Evidence from Chinese hamster tissue-culture cells. Experimental Cell Research 71 (1972) 345-55.

[61] L.E. McGann, Differing actions of penetrating and nonpenetrating

cryoprotective agents. Cryobiology 15 (1978) 382-90.

[62] L.E. McGann, Optimal temperature ranges for control of cooling rate. Cryobiology 16 (1979) 211-216.

[63] L.E. McGann, and J. Farrant, Survival of tissue culture cells frozen by a two-step procedure to -196 degrees C. II. Warming rate and concentration of dimethyl sulphoxide. Cryobiology 13 (1976) 269-273.

[64] H.T. Meryman, General principles of freezing and freezing injury in cellular materials. Annals of the New York Academy of Sciences 85 (1960) 503-509.

[65] H.T. Meryman, Modified model for the mechanism of freezing injury in erythrocytes. Nature 218 (1968) 333-336.

[66] H.T. Meryman, The exceeding of a minimum tolerable cell volume in hypertonic suspension as a cause of freezing injury. in: G.W.a.M. O'Conner, (Ed.), The frozen cell, London, 1970, pp. 51-64.

[67] H.T. Meryman, Cryoprotective agents. Cryobiology 8 (1971) 173-183.

[68] M.M. Moronne, R.J. Mehlhorn, M.P. Miller, L.C. Ackerson, and R.I. Macey, ESR measurement of time-dependent and equilibrium volumes in red-cells. Journal of Membrane Biology 115 (1990) 31-40.

[69] K. Muldrew, and L.E. McGann, The osmotic rupture hypothesis of intracellular freezing-injury. Biophysical Journal 66 (1994) 532-541.

[70] D.E. Pegg, The current status of tissue cryopreservation. Cryo Letters

22 (2001) 105-114.

[71] C. Polge, A.U. Smith, and A.S. Parkes, Revival of spermatozoa after vitrification and dehydration at low temperatures. Nature 164 (1949) 666.

[72] R.C. Prickett, J.A.W. Elliott, S. Hakda, and L.E. McGann, A non-ideal replacement for the Boyle van't Hoff equation. Cryobiology 57 (2008) 130-136.

[73] R.C. Prickett, J.A.W. Elliott, and L.E. McGann, Application of multisolute osmotic virial equation to solutions containing electrolytes. In preparation (2009).

[74] R.C. Prickett, J.A.W. Elliott, and L.E. McGann, Application of the osmotic virial equation in cryobiology. Cryobiology (accepted) (2009).

[75] C.M. Rice, and N.J. Scolding, Adult stem cells-reprogramming neurological repair? Lancet 364 (2004) 193-199.

[76] L.U. Ross-Rodriguez, Using simulations to design a cryopreservation procedure for hematopoietic stem cells without DMSO, Medical Sciences - Laboratory Medicine and Pathology, University of Alberta, Edmonton, 2003, pp. 111.

[77] N.C. Santos, J. Figueira-Coelho, J. Martins-Silva, and C. Saldanha, Multidisciplinary utilization of dimethyl sulfoxide: pharmacological, cellular, and molecular aspects. Biochemical Pharmacology 65 (2003) 1035-1041.

[78] A. Schaffler, and C. Buchler, Concise review: Adipose tissue-derived stromal cells - Basic and clinical implications for novel cell-based therapies. Stem Cells 25 (2007) 818-827.

[79] G.J. Schwartz, and K.R. Diller, Osmotic response of individual cells during freezing .1. Experimental volume measurements. Cryobiology 20 (1983) 61-77.

[80] M. Shabana, and J.J. Mcgrath, Cryomicroscope investigation and thermodynamic modeling of the freezing of unfertilized hamster ova. Cryobiology 25 (1988) 338-354.

[81] P.L. Steponkus, J. Wolfe, and M.F. Dowget, Stresses induced by contraction and expansion during a freeze-thaw cycle: a membrane perspective. in: G.J. Morris, and A. Clarke, (Eds.), Effects of Low Temperatures on Biological Membranes, Academic Press, Toronto, 1981.

[82] S. Thirumala, and R.V. Devireddy, A simplified procedure to determine the optimal rate of freezing biological systems. Journal of Biomechanical Engineering 127 (2005) 295-300.

[83] M.R. Tijssen, H. Woelders, A. de Vries-van Rossen, C.E. van der Schoot, C. Voermans, and J.M. Lagerberg, Improved postthaw viability and in vitro functionality of peripheral blood hematopoietic progenitor cells after cryopreservation with a theoretically optimized freezing curve. Transfusion 48 (2008) 893-901.

[84] M. Toner, E.G. Cravalho, and M. Karel, Thermodynamics and kinetics

of intracellular ice formation during freezing of biological cells. Journal of Applied Physics 67 (1990) 1582-1593.

[85] M. Toner, E.G. Cravalho, and M. Karel, Cellular-response of mouse oocytes to freezing stress - prediction of intracellular ice formation. Journal of Biomechanical Engineering-Transactions of the Asme 115 (1993) 169-174.

[86] D. Voet, and J.G. Voet, Biochemistry, John Wiley & Sons, Inc., New York, 1995, pp. 288-289.

[87] H. Woelders, and A. Chaveiro, Theoretical prediction of 'optimal' freezing programmes. Cryobiology 49 (2004) 258-271.

[88] E.J. Woods, J. Liu, K. Pollok, J. Hartwell, F.O. Smith, D.A. Williams, M.C. Yoder, and J.K. Critser, A theoretically optimized method for cord blood stem cell cryopreservation. J Hematother Stem Cell Res 12 (2003) 341-350.

[89] W.T. Wu, S.-R. Lyu, and W.H. Hsieh, Cryopreservation and biophysical properties of articular cartilage chondrocytes. Cryobiology 51 (2005) 330-338.

[90] A. Zambelli, G. Poggi, G. Da Prada, P. Pedrazzoli, A. Cuomo, D. Miotti, C. Perotti, P. Preti, and G.R. Della Cuna, Clinical toxicity of cryopreserved circulating progenitor cells infusion. Anticancer Research 18 (1998) 4705-4708.

Chapter 2. Osmotic permeability characteristics of various cell types[1]

2.1 Introduction

Cryobiology plays a key role in the long-term storage of native and engineered cells and tissues for research and clinical applications. Cryopreservation, which involves storing cells and tissues at low subzero temperatures, is currently the only feasible method for the long-term maintenance of biological structure and function [8,28]. Recently developed cellular therapies critically depend on the number of functional cells transplanted, thus reviving interest in maximizing survival and preserving cell function during collection, processing, and preservation. As new sources of cells are being explored, it is becoming clear that using conventional approches to cryopreservation often results in low survival of valuable cells.

The survival of cells after being subjected to freezing and thawing depends on the ability of the cells to withstand a variety of stresses imposed by the cryopreservation protocol. As extracellular ice forms during cryopreservation, there is a resulting increase in extracellular solute concentration, which imposes osmotic stresses on the cell [23]. The osmotic response of the cell is largely dependent on the movement of

[1]This chapter with modifications, including all TF-1 cell data, has been accepted to Cryobiology (2009) as "Characterization of cryobiological responses in TF-1 cells using interrupted freezing procedures", L.U. Ross-Rodriguez, J.A.W. Elliott, and L.E. McGann

water across the plasma membrane [22]. The movement of water across the membrane is the result of movement of water molecules by diffusion through the membrane or through water channels (aquaporins). The osmotic parameters governing the movement of water and cryoprotectants across the membrane are specific to each cell type; thus the osmotic responses to anisotonic conditions are different for different cell types. If a permeating cryoprotectant is present then both the net water and cryoprotectant movements depend on the osmotic parameters of the cell membrane. Therefore, measuring the osmotic parameters of the cell membrane is important to further understand the cryobiology of a cell.

Electronic particle counters have been used to measure cell volumes as a function of time for cells exposed to anisotonic solutions [26]. In kinetic studies, sequential measurements of cell volumes allow determination of cell permeability characteristics by fitting the experimental data with theoretical models. Using this method, osmotic parameters have been determined for a variety of cell types including: human lymphocytes [14]; bovine chondrocytes [25]; pancreatic islet cells [19,32]; human corneal endothelial, stromal, and epithelial cells [3]; several African mammalian spermatozoa [10]; and HSC [9,15,31].

The purpose of this study was to determine the osmotic permeability characteristics of various cell types, including TF-1 cells, human umbilical vein endothelial cells (HUVECs), and porcine chondrocytes.

2.2 Materials and methods

2.2.1 *Cell types*

TF-1 cells[2]

TF-1 cells ((Lot #2056376) ATCC, Manassas, VA, USA) were cultured at 37 °C in 5 % CO_2 in Modified RPMI 1640 Medium (ATCC) with 10 % fetal bovine serum (ATCC), and supplemented with 2 ng/mL recombinant human GM-CSF (Stemcell Technologies, Vancouver, BC, Canada). Prior to experiments, cells were washed twice with serum-free RPMI media and incubated in serum-free RPMI overnight to accumulate the cells in the G_1/G_0 phase of the cell cycle [18], resulting in a more uniform cell size distribution. Cells were then centrifuged and re-suspended in serum-free RPMI (4×10^6 cells/mL) prior to experiments. Serum-free media was chosen for experiments in order to compare experimental results with and without different types of cryoprotectants.

HUVECs

Human umbilical vein endothelial cells ((Lot #7F3659) LONZA, Walkersville, MD, USA) were cultured at 37 °C in 5 % CO_2 in EBM-2 Bulletkit (LONZA), which includes Endothelial Cell Basal Medium-2 supplemented with human fibroblast growth factor-B, hydrocortisone,

[2] Data for TF-1 cells were previously published (L. U. Ross-Rodriguez, Using simulations to design a cryopreservation procedure for hematopoietic stem cells without DMSO, MSc thesis, Medical Sciences – Laboratory Medicine and Pathology, University of Alberta, Edmonton, 2003, pp.111); however the analysis and discussion are new.

vascular endothelial growth factor, R3-insulin-like growth factor, ascorbic acid, heparin, fetal bovine serum, human endothelial growth factor, GA-1000 (Gentamicin, Amphotericin-B). Cell culture medium was changed every 48 hours, as per LONZA instructions. Prior to experiments, cells were trypsinized using trypsin-EDTA (LONZA) once they had reached ~70% confluency. Cells were then centrifuged and re-suspended in media (4 x 10^6 cells/mL) for experiments. Cells from different passages were used for experiments.

Chondrocytes

Porcine chondrocytes were isolated by graduate student Andrew Weiss from the laboratory of Dr. Nadr Jomha (University of Alberta), as previously described [30]. Briefly, intact stifle joints were harvested from six sexually mature pigs sacrificed for meat consumption (Sturgeon Valley Pork, St. Albert, AB, Canada). Portions of full thickness cartilage (3-4g per joint) were removed from the femoral chondyles and placed in a 100 mm petri dish containing 1X Dulbecco's phosphate buffered saline solution (PBS; GIBCO Invitrogen Corp., Carlsbad, CA, USA). The PBS was removed and supplemented with 20 mL of Dulbecco's modified Eagle's medium with F-12 nutritional supplement and 1 % penicillin-streptomycin (DMEM/F-12, GIBCO) containing 1mg/mL of collagenase 1A (Sigma-Aldrich Canada, Oakville, ON, Canada). The cartilage was incubated with shaking at 37 °C and 5 % CO_2 for 6 hours and then the

solution was passed through a 40 μm nylon cell strainer (BD biosciences, Mississauga, ON, Canada). The solution was centrifuged at 500 rcf (relative centrifugal force) for 6 minutes to pellet the chondrocytes; they were washed once in PBS, and then incubated in DMEM/F-12 with 10% fetal bovine serum (FBS, GIBCO) at 37 °C and 5 % CO_2 for 24-36 hrs. Prior to experiments, cells were trypsinized using 0.25% Trypsin-EDTA (GIBCO). Cells were then centrifuged and re-suspended in media (4×10^6 cells/mL) for experiments. Cell from different pigs were used for experiments.

2.2.2 Cell volume measurements

A Coulter Electronic Particle Counter (ZB1, Coulter Inc., Hialeah, FL, USA), fitted with a pulse-height analyzer (The Great Canadian Computer Company, Spruce Grove, AB, Canada) was used to monitor cell volume as a function of time as cells passed through the 100 μm aperture [11-13,26]. This system has been previously used to monitor changes in cell volume for a variety of cells in suspension [2,3,14,19,32,36], including HSC [9,31].

Cells (200 μL) were injected into well-mixed hypertonic experimental solutions (10 mL) at experimental temperatures that were maintained using a circulating water bath and a custom insulated jacket. Pulse heights, proportional to the cell volumes, were digitized and the time recorded as each cell traversed the aperture of the Coulter counter [26].

Various concentrations of PBS were prepared by diluting 10X PBS (GIBCO) with distilled water. Volume measurements to determine the permeability of dimethyl sulfoxide ((Me_2SO) Sigma, Missisauga, ON, Canada)) for TF-1 cells used Me_2SO in 1X PBS for a final concentration of 1 M Me_2SO. Osmolalities were measured using a freezing-point depression Osmometer (Precision Systems Inc., Natick, MA, USA), calibrated using 0.1, 0.3, 0.5, and 1.5 Osm/kg osmometry standards (Precision Systems Inc.).

For all experimental solutions, the experimental temperatures were measured using a Digi-Sense thermocouple thermometer (Cole Parmer, Anjou, QC, Canada). For each experiment, 3 replicate measurements were performed for each solution at each temperature. The experiments were repeated a minimum of 3 times using cells from different passages or pigs (chondrocytes). Latex beads (10, 15, or 20 μm diameter; Beckman Coulter, Miami, FL, USA) were used as calibrators to convert pulse heights to actual volumes in 1X PBS and in the experimental solutions.

2.2.3 Calculations of cell permeability parameters

Osmotically-inactive fraction

Cellular osmotic parameters relevant to cryopreservation are the osmotically-inactive fraction, the hydraulic conductivity, and the solute permeability for permeating cryoprotectants and their activation energies. The osmotically-inactive fraction (*b*) of the cell is the fraction of the cell

volume not involved in the osmotic transport. The Boyle van't Hoff relationship [21] has been used to express equilibrium cell volume in solutions of impermeant solutes:

$$\frac{V}{V_o} = \frac{\pi^o}{\pi}(1-b)+b\,; \qquad 2\text{-}1$$

where V is the equilibrium cell volume (μm^3), V_o is the isotonic cell volume (μm^3), π^o is the isotonic osmolality (osmoles/kg water), π is the experimental osmolality (osmoles/kg water), and b is the osmotically-inactive fraction of the cell volume, a parameter found by fitting Eq. 2-1 to data.

Hydraulic conductivity

Jacobs and Stewart [16,17] used the following equation to describe the rate of water movement across the plasma membrane:

$$\frac{dV}{dt} = L_p ART\rho(\pi_i - \pi_e)\,; \qquad 2\text{-}2$$

where V is the volume of the cell (μm^3), t is the time (min), L_p is the hydraulic conductivity (μm^3/μm^2/min/atm or μm/min/atm), A is the cell surface area (μm^2), R is the universal gas constant (μm^3·atm/mol/K), T is the absolute temperature (K), ρ is the density of water (assumed to be

constant at 1.0 x 10^{-15} kg/μm^3), π_e is the extracellular osmolality (osmoles/kg of water), and π_i is the intracellular osmolality (osmoles/kg of water). Experimental measurements of cell volume as a function of time in the presence of an impermeant solute were fit to Eq. 2-2, with the following initial conditions: i) the intracellular solution was at isotonic concentration and the extracellular solution was at the experimental concentration; ii) the intracellular osmolality was calculated from the Boyle-van't Hoff equation (Eq. 2-1). The differential equation Eq. 2-2 was integrated using Euler's method with sufficiently small discretization in EXCEL (e.g. time increment approximately 8 x 10^{-4} min). Experimental data were fit to the differential equation solutions using the least squares method (EXCEL Solver) to estimate a best fit value for L_p (computer program written by L.E. McGann). The assumptions used in these equations are: i) intracellular and extracellular solutions are dilute, so the values of osmolality and molality are the same; ii) the density of water is 1 g/mL; and iii) the cell surface area was calculated from the spherical cell volume.

Solute permeability

Jacobs and Stewart coupled Eq. 2-2 with the following equation to describe the volume changes and solute movement across a membrane as a function of time:

$$\frac{dS}{dt} = P_s A\left(m_s^e - m_s^i\right)\rho \; ; \qquad 2\text{-}3$$

where S is the number of solute molecules in the cell (mole), P_s is the solute permeability ($\mu m^3/\mu m^2/min$), m_s is the solute concentration (moles/kg solvent), the superscript e denotes extracellular, and the superscript i denotes intracellular. In the presence of a permeant solute, TF-1 experimental data were fit to Eqs. 2-2 and 2-3 using the following conditions: i) the initial conditions were that the intracellular solution was at isotonic concentration, containing no permeant solute; and ii) the experimental conditions were that the extracellular solution consisted of the permeant solute at the experimental concentration and an impermeant solute at the isotonic concentration. The differential equation Eq. 2-3 was integrated using Euler's method with sufficiently small discretization in EXCEL, and the experimental data were fit to the differential equation solutions using the least squares method (EXCEL Solver) to estimate either P_s or both P_s and L_p (computer program written by L.E. McGann).

Temperature dependencies of permeability parameters

Also relevant to cryopreservation are the temperature dependencies of L_p and P_s, which are normally described with Arrhenius relationships [27]:

$$L_p = k_1 \exp(\frac{-E_a^{Lp}}{RT}); \quad \text{2-4}$$

$$P_s = k_2 \exp\left(\frac{-E_a^{Ps}}{RT}\right); \quad \text{2-5}$$

where k_1 and k_2 are fitting constants, R is the universal gas constant (kcal/mol/K) and T is the absolute temperature (K). The equations can also be written:

$$L_p = L_p^o \exp\left(-\frac{E_a{}^{Lp}}{R}\left(\frac{1}{T}-\frac{1}{T_o}\right)\right); \quad \text{2-6}$$

$$P_s = P_s^o \exp\left(-\frac{E_a{}^{Ps}}{R}\left(\frac{1}{T}-\frac{1}{T_o}\right)\right); \quad \text{2-7}$$

where L_p^o and P_s^o are the reference water and solute permeabilities, respectively, at the temperature T_o, E_a are the Arrhenius activation energies (kcal/mol), R is the universal gas constant (kcal/mol/K), and T is the absolute temperature (K). The Arrhenius activation energies for L_p or P_s, described by Eqs. 2-4 and 2-5 respectively, were determined by fits using linear regression of the natural logarithm of L_p or P_s as a function of the inverse absolute temperature.

2.2.4 Statistical analysis

Statistical comparisons used a standard two-way analysis of

variance (ANOVA) (α=0.05 level of significance) for estimates of L_p and b respectively between the 4 groups of experimental temperatures and PBS concentrations, including evaluation of interactions between these parameters. A one-way ANOVA (α=0.05) was used to further evaluate statistical differences between temperatures for L_p. Post hoc analysis was done to evaluate the homogeneity of the variances of the population when performing ANOVA.

A Kruskal-Wallis non-parametric statistical test (α=0.05) was used to compare estimates of P_s when solved for separately from L_p, with estimates of P_s when solved for simultaneously with L_p. It was chosen for the statistical test because it makes no assumptions about the underlying distribution of the data due to the small sample size [35]. For all mean values reported, the standard error of the mean was also calculated and included in the result (i.e. mean ± sem).

2.3 Results

2.3.1 Isotonic cell volume

The isotonic volumes of TF-1, HUVECs and porcine chondrocytes were different, with mean isotonic volumes of 916 ± 15, 1481 ± 6, and 730 ± 14 μm^3 (mean ± repeat sem), respectively. The width of the distributions were 916 ± 35, 1481 ± 41, and 730 ± 60 μm^3 (mean ± sd of the distribution), respectively. The correction factor for cell density was investigated and changed the values by approximately 2 % [5]. Given that

the standard error of the mean was greater than 2 %, the correction factor was not used.

2.3.2 Osmotic parameters (b, L_p, Ea^{Lp})

Figure 2-1 shows a representative plot of mean cell volume as a function of time after exposure of TF-1 cells to an 860 osm/kg PBS solution (3X PBS) at 4 different temperatures. Data for TF-1, HUVECs, and chondrocytes from such experimental runs were fit to numerical solutions of Eqs. 2-1 and 2-2 (Euler's method) using the least squares method in EXCEL Solver to give the best estimates for the hydraulic conductivity (L_p) and the osmotically-inactive fraction (b). Data from different PBS experimental solutions at four different temperatures were used to examine the concentration and temperature dependence of L_p and b for each cell type and were summarized in Tables 2-1 to 2-6.

Values of the osmotically-inactive fraction calculated for all the experimental conditions in Table 2-1 show that the osmotically-inactive fraction for TF-1 cells was not dependent on solute concentration ($p>0.05$), but was dependent on temperature ($p<0.05$). Further analysis showed that among temperatures, some were statistically significant, indicating a possible slight temperature dependence. From an Arrhenius plot, the activation energy describing the temperature dependence for the osmotically-inactive fraction (E_a^b) in TF-1 cells was 0.80 $\pm$ 0.14 kcal/mol, which is very low. Furthermore, a two-way ANOVA analysis revealed that

there was no statistically significant interaction effect between osmolality and temperature on *b* ($p>0.05$). Original data for all temperatures and osmolalities were pooled and the overall mean value for the fitted osmotically-inactive fraction was 0.355 ± 0.005.

A Boyle van't Hoff plot of equilibrium cell volume as a function of inverse osmolality for the aggregate data is shown in Figure 2-2. The y-intercept of the linear regression estimates the osmotically-inactive fraction to be 0.368 ± 0.004, calculated with the LINEST function in EXCEL. There was no statistical difference between the osmotically-inactive fractions calculated by these two approaches (Mann-Whitney U test; $p>0.05$). The osmotically-inactive fraction calculated from the Boyle van't Hoff plot was used in further analysis.

Table 2-2 show that the osmotically-inactive fraction for HUVECs was not dependent on solute concentration or temperature ($p>0.05$), so all the values for all solute concentrations and temperatures were pooled. The overall mean value for the fitted osmotically-inactive fraction from all original experimental data was 0.592 ± 0.024. A Boyle van't Hoff plot of equilibrium volume as a function of inverse osmolality for the aggregate data is shown in Figure 2-3. The y-intercept of the linear regression gives an osmotically-inactive fraction of 0.598 ± 0.006, calculated with the LINEST function in EXCEL. There was no statistical difference between the osmotically-inactive fractions calculated by these two approaches (Mann-Whitney U test; $p>0.05$).

Table 2-3 show that the osmotically-inactive fraction for chondrocytes was not dependent on concentration ($p>0.05$), so data for all concentrations were pooled. The values for some temperature points were statistically different ($p<0.05$), while others were not, indicating a possible slight temperature dependence. From an Arrhenius plot, the temperature dependence for the osmotically-inactive fraction (E_a^b) was found to be 1.1 $\pm$ 0.3 kcal/mol, which is low. Therefore, data for all temperatures were pooled and the mean value for the fitted osmotically-inactive fraction was 0.678 $\pm$ 0.023. A Boyle van't Hoff plot of equilibrium cell volume as a function of inverse osmolality for the aggregate data is shown in Figure 2-4. The y-intercept of the linear regression estimates the osmotically-inactive fraction to be 0.580 $\pm$ 0.004, calculated with the LINEST function in EXCEL. There was no statistical difference between the osmotically-inactive fractions calculated by these two approaches (Mann-Whitney U test; $p>0.05$).

Tables 2-4 to 2-6 show the calculated hydraulic conductivity for the three cell types at different temperatures and extracellular osmolalities. Table 2-4 shows the calculated hydraulic conductivity for TF-1 cells at different temperatures and extracellular osmolalities. Two-way ANOVA indicated that L_p changed significantly with temperature ($p<0.001$), but did not change significantly with extracellular osmolality ($p>0.05$). This test also revealed a statistically significant interaction between the effects of osmolality and temperature on L_p ($p<0.05$), indicating evidence that the

effect of temperature is dependent on concentration in predicting L_p. Due to this interaction effect, statistical significance should be interpreted with caution. However, since the effect of temperature is highly statistically significant, values at different osmolalities were pooled for each experimental temperature. In order to calculate the activation energy of L_p, Eq. 2-4 was linearized by taking the natural logarithm of each side of the equation and the data were plotted as $\ln L_p$ as a function of inverse absolute temperature. The same calculations were used for all three cell types. The pooled mean data for 2-5X PBS values (Table 2-4; n=36), along with pooled mean data for 3X PBS values (n=9[3]), were fitted to this equation using (linear regression), giving an activation energy for L_p of 14.2 $\pm$ 1.1 kcal/mol. An Arrhenius plot of all the experimental data and the fitted line is shown in Figure 2-5 (R^2=0.95).

Table 2-5 shows the calculated hydraulic conductivity for HUVECs cells at different temperatures and extracellular osmolalities. ANOVA indicated that L_p changed significantly with temperature ($p<0.05$) but did not change significantly with extracellular osmolality ($p>0.05$). L_p values at different osmolalities were pooled for each experimental temperature. The pooled mean values in Table 2-5 gave an activation energy for L_p of 13.4 $\pm$ 0.3 kcal/mol. An Arrhenius plot of the experimental data and the fitted line is shown in Figure 2-6 (R^2=1.00).

Table 2-6 shows the calculated hydraulic conductivity for porcine

[3] 3X PBS experiments were conducted by Ruth Nelson.

chondrocytes at different temperatures and extracellular osmolalities. ANOVA indicated that L_p changed significantly with temperature ($p<0.05$) but did not change significantly with extracellular osmolality ($p>0.05$). Values at different osmolalities were pooled for each experimental temperature. The pooled mean values in Table 2-6 gave an activation energy for L_p of 11.3 $\pm$ 0.5 kcal/mol. An Arrhenius plot of the experimental data and the fitted line is shown in Figure 2-7 (R^2=1.00).

2.3.3 Me_2SO permeability properties

Figure 2-8 shows the typical volume responses when TF-1 cells are exposed to a solution containing 1 M Me_2SO at 3 different temperatures: a) 4°C; b) 10°C; and c) 22°C[4]. Using EXCEL Solver, P_s was calculated using two different approaches: 1) using values for L_p that were calculated from E_a^{Lp}, and fitting data to Eqs. 2-1, 2-2 and 2-3 to get values for P_s; and 2) fitting data to Eqs. 2-1, 2-2 and 2-3 to get values for P_s and L_p. The values for P_s and L_p in Table 2-7 show that pair-wise comparison of the two parameter estimation methods at each temperature give the values within experimental error ($p>0.05$), with the exception of L_p at 23.4 °C ($p<0.001$). A Kruskal-Wallis statistical test indicated that temperature is a significant predictor of both P_s and L_p, regardless of the calculation approach used to determine these parameters ($p<0.001$). The mean values in Table 2-7 were fitted to the linearized Arrhenius equation,

[4] Me_2SO experiments were conducted by Nelly Wu.

Eq. 2-5, (using linear regression), giving an activation energy for P_s of 13.8 ± 0.1 kcal/mol and 16.3 ± 1.1 kcal/mol, respectively for the two different methods of calculation. For the second method, the activation energy for L_p was also calculated (17.5 ± 0.9 kcal/mol).

2.4 Discussion

In the range of osmolalities studied, TF-1 cells follow the Boyle van't Hoff relationship yielding an osmotically-inactive fraction of 0.368. A previously reported value for human bone marrow hematopoietic $CD34^+$ cells was 0.205 [9], and for human umbilical cord blood $CD34^+$ cells was 0.32 [31] and 0.27 ± 0.01 [15]. The value of osmotically-inactive fraction reported here is also within the range for a variety of mammalian cell types (0.2-0.69) [1,3,9,10,14,19,24,27]. The osmotically-inactive fractions for HUVECs (0.598) and porcine chondrocytes (0.580) reported here are at the upper part of this range, which includes cells such as chimpanzee sperm [1].

Permeability parameters, calculated from cell volume measurements between 2 and 37 °C, showed that the osmotically-inactive fraction was largely independent of temperature, but that the hydraulic conductivity was strongly temperature-dependent. However, for L_p there was a statistically significant interaction between the effects of osmolality and temperature. Although partitioning the interaction between the temperature and osmolality in predicting L_p is beyond the scope of this

study, we can conclude that the findings of the significance of the temperature effect on L_p is supported by the literature [19]. The value for L_p for TF-1 cells was 0.339 μm/min/atm at 20 °C and was higher than for HUVECs (0.147 μm/min/atm at 20 °C) and for porcine chondrocytes (0.254 μm/min/atm at 20 °C). However, all the L_p values are within the range reported for many nucleated mammalian cells, such as rat megakaryocytoporietic cells, Chinese hamster lung fibroblast cells, bovine immature oocytes, chondrocytes, corneal endothelial, epithelial and stromal cells [27]. The value reported here for L_p of TF-1 cells is comparable with the L_p previously reported for human cord blood $CD34^+$ cells of 0.168 ± 0.03 μm/atm/min at 20 °C [15,31], indicating that the rate of water movement in TF-1 cells is similar to other HSC. Also, the value reported here for L_p of porcine chondrocytes was comparable with the L_p previously reported for porcine chondrocytes of 0.175 μm/atm/min at 20 °C [33] and for bovine chondrocytes of 0.214 μm/atm/min at 20 °C [25].

The Arrhenius activation energy of L_p for TF-1 (14.2 kcal/mol), HUVECs (13.4 kcal/mol), and porcine chondrocytes (11.3 kcal/mol) reported here, are within the range of some other mammalian cells (9-16 kcal/mol) [3,14,19,27]. For HSCs, based on L_p values reported by Hunt et al. at 2 temperatures [15], we calculated the E_a^{Lp} in cord blood $CD34^+$ cells to be 18.8 kcal/mol; and for porcine [33] and bovine chondrocytes [25], we calculated the E_a^{Lp} to be 8.2 kcal/mol and 16.0 kcal/mol, respectively. It has been reported that an E_a^{Lp} of

<6 kcal/mol may be indicative of channel-mediated water transport [6], and an E_a^{Lp} >10 kcal/mol may indicate transport water across the plasma membrane primarily by solubility-diffusion [6]. Based on these assumptions, water transport for all three cell types would occur primarily by solubility-diffusion.

The conventional method for cryopreserving many cell types for cellular therapies, including HSC, utilizes Me_2SO as a cryoprotectant [34]. The P_s of Me_2SO in TF-1 cells was calculated using two different approaches: 1) using values for L_p that were calculated from E_a^{Lp}, and 2) fitting data to get values for both P_s and L_p. The values for P_s and L_p in Table 3 shows that both methods of calculation give the same values for the parameters, within experimental error, which is consistent with other findings in the literature [4], indicating no influence of Me_2SO on water transport. The permeability of Me_2SO in TF-1 cells, 14.3 μm/min at 22 °C, is higher than reported for human cord blood $CD34^+$ cells (9.4 μm/min (22 °C) [31]; 4.4 μm/min (20 °C) [15]), but within the range of reported values found for a variety of mammalian cell types [27], including human corneal endothelial, keratocyte and epithelial cells [4], hamster islet cells [2], human granulocytes [29], canine red blood cells [20], and neonatal porcine islet cells [7].

TF-1 cells are used as a model for HSCs. Although similarly to other HSCs, TF-1 cells express CD34+ and differentiate into the various hematopoietic lineages, some of the osmotic parameters for TF-1 cells

differed from those of bone marrow and cord blood CD34+ cells, such as the osmotically-inactive fraction and the isotonic volumes. The average size of TF-1 cells (916 $\pm$ 31 μm^3) was higher than that previously reported for both human bone marrow $CD34^+$ cells of 345 μm^3 [9] and umbilical cord blood $CD34^+$ cells of 274 $\pm$ 13 μm^3 [15]. Model systems allow for increased learning about the characteristics of responses to low temperatures, however when parameters differ, actual protocols may depend on the precise parameters of the specific target cells.

Herein the osmotic parameters have been determined for various cell types of interest in cryobiology, including TF-1 cells, HUVECs and porcine chondrocytes. The obtained values of the osmotic parameters can be used in computer simulations of low temperature cellular responses to provide insight into cellular responses to anisotonic conditions resulting form ice formation at low temperatures during cryopreservation.

2.5 References

[1] Y. Agca, J. Liu, S. Mullen, J. Johnson-Ward, K. Gould, A. Chan, and J. Critser, Chimpanzee (Pan troglodytes) spermatozoa osmotic tolerance and cryoprotectant permeability characteristics. Journal of Andrology 26 (2005) 470-477.

[2] C.T. Benson, C. Liu, D.Y. Gao, E.S. Critser, J.D. Benson, and J.K. Critser, Hydraulic conductivity (L-p) and its activation energy (E-a), cryoprotectant agent permeability (P-s) and its E-a, and reflection coefficients (sigma) for golden hamster individual pancreatic islet cell membranes. Cryobiology 37 (1998) 290-299.

[3] S.L. Ebertz, and L.E. McGann, Osmotic parameters of cells from a bioengineered human corneal equivalent and consequences for cryopreservation. Cryobiology 45 (2002) 109-117.

[4] S.L. Ebertz, and L.E. McGann, Cryoprotectant permeability parameters for cells used in a bioengineered human corneal equivalent and applications for cryopreservation. Cryobiology 49 (2004) 169-180.

[5] C. Electronics, Instruction and service manual for the Coulter Counter (4201006), Coulter Electronics, Inc., Hialeah, Florida, 1970.

[6] H.Y. Elmoazzen, J.A.W. Elliott, and L.E. McGann, The effect of temperature on membrane hydraulic conductivity. Cryobiology 45 (2002) 68-79.

[7] C. Fedorow, L.E. McGann, G.S. Korbutt, G.R. Rayat, R.V. Rajotte, and J.R.T. Lakey, Osmotic and cryoprotectant permeation

characteristics of islet cells isolated from the newborn pig pancreas. Cell Transplantation 10 (2001) 651-659.

[8] D. Gao, and J.K. Critser, Mechanisms of cryoinjury in living cells. ILAR Journal 41 (2000) 187-196.

[9] D.Y. Gao, Q. Chang, C. Liu, K. Farris, K. Harvey, L.E. McGann, D. English, J. Jansen, and J.K. Critser, Fundamental cryobiology of human hematopoietic progenitor cells I: Osmotic characteristics and volume distribution. Cryobiology 36 (1998) 40-48.

[10] J.A. Gilmore, L.E. McGann, E. Ashworth, J.P. Acker, J.P. Raath, M. Bush, and J.K. Critser, Fundamental cryobiology of selected African mammalian spermatozoa and its role in biodiversity preservation through the development of genome resource banking. Animal Reproduction Science 53 (1998) 277-297.

[11] N.B. Grover, J. Naaman, S. Ben-Sasson, and F. Doljanski, Electrical sizing of particles in suspensions. I: Theory. Biophysical Journal 9 (1969) 1398-1414.

[12] N.B. Grover, J. Naaman, S. Ben-Sasson, and F. Doljanski, Electrical sizing of particles in suspensions. III: Rigid spheroids and red blood cells. Biophysical Journal 12 (1972) 1099-1117.

[13] N.B. Grover, J. Naaman, S. Ben-Sasson, F. Doljanski, and E. Nadav, Electrical sizing of particles in suspensions. II: Experiments with rigid spheres. Biophysical Journal 9 (1969) 1415-25.

[14] H.G. Hempling, S. Thompson, and A. Dupre, Osmotic properties of

human lymphocyte. Journal of Cellular Physiology 93 (1977) 293-302.

[15] C.J. Hunt, S.E. Armitage, and D.E. Pegg, Cryopreservation of umbilical cord blood: 1. Osmotically inactive volume, hydraulic conductivity and permeability of CD34(+) cells to dimethyl, sulphoxide. Cryobiology 46 (2003) 61-75.

[16] M.H. Jacobs, The simultaneous measurement of cell permeability to water and to dissolved substances. Journal of Cellular and Comparative Physiology 2 (1933) 427-444.

[17] M.H. Jacobs, and D.R. Stewart, A simple method for the quantitative measurement of cell permeability. J. Cell. Comp. Physiol. 1 (1932) 71-82.

[18] A. Kolonics, A. Apati, J. Janossy, A. Brozik, R. Gati, A. Schaefer, and M. Magocsi, Activation of Raf/ERK1/2 MAP kinase pathway is involved in GM-CSF-induced proliferation and survival but not in erythropoietin-induced differentiation of TF-1 cells. Cellular Signalling 13 (2001) 743-754.

[19] C. Liu, C.T. Benson, D.Y. Gao, B.W. Haag, L.E. Mcgann, and J.K. Critser, Water permeability and Its activation-energy for individual hamster pancreatic-islet cells. Cryobiology 32 (1995) 493-502.

[20] J. Liu, J.A. Christian, and J.K. Critser, Canine RBC osmotic tolerance and membrane permeability. Cryobiology 44 (2002) 258-268.

[21] B. Lucke, and M. McCutcheon, The living cell as an osmotic system

and its permeability to water. Physiol. Rev. 12 (1932) 68-139.

[22] P. Mazur, The role of cell membranes in the freezing of yeast and other cells. Annals of the New York Academy of Science 125 (1965) 658-76.

[23] P. Mazur, S.P. Leibo, and E.H. Chu, A two-factor hypothesis of freezing injury. Evidence from Chinese hamster tissue-culture cells. Experimental Cell Research 71 (1972) 345-55.

[24] L.E. McGann, M. Grant, A.R. Turner, and J.M. Turc, Osmotic limits of human-granulocytes. Cryobiology 18 (1981) 622-622.

[25] L.E. McGann, M. Stevenson, K. Muldrew, and N. Schachar, Kinetics of osmotic water-movement in chondrocytes isolated from articular-cartilage and applications to cryopreservation. Journal of Orthopaedic Research 6 (1988) 109-115.

[26] L.E. McGann, A.R. Turner, and J.M. Turc, Microcomputer interface for rapid measurements of average volume using an electronic particle counter. Medical & Biological Engineering & Computing 20 (1982) 117-120.

[27] J.J. McGrath, Membrane transport properties. in: J.J. McGrath, and K.R. Diller, (Eds.), Low temperature biotechnology emerging applications and engineering contributions, The American Society of Mechanical Engineers, New York, 1988, pp. 273-330.

[28] D.E. Pegg, The current status of tissue cryopreservation. Cryo Letters 22 (2001) 105-114.

[29] C.J. Toupin, M. Le Maguer, and L.E. McGann, Permeability of human granulocytes to dimethyl sulfoxide. Cryobiology 26 (1989) 422-430.

[30] A. Weiss, Design of aqueous vitreous solutions, Surgery, University of Alberta, Edmonton, 2009, pp. 61.

[31] E.J. Woods, J. Liu, C.W. Derrow, F.O. Smith, D.A. Williams, and J.K. Critser, Osmometric and permeability characteristics of human placental/umbilical cord blood CD34+ cells and their application to cryopreservation. Journal of Hematotherapy and Stem Cell Research 9 (2000) 161-173.

[32] E.J. Woods, J. Liu, M.A.J. Zieger, J.R.T. Lakey, and J.K. Critser, Water and cryoprotectant permeability characteristics of isolated human and canine pancreatic islets. Cell Transplantation 8 (1999) 549-559.

[33] W.T. Wu, S.-R. Lyu, and W.H. Hsieh, Cryopreservation and biophysical properties of articular cartilage chondrocytes. Cryobiology 51 (2005) 330-338.

[34] H. Yang, J.P. Acker, J. Hannon, H. Miszta-Lane, J.J. Akabutu, and L.E. McGann, Damage and protection of UC blood cells during cryopreservation. Cytotherapy 3 (2001) 377-386.

[35] J.H. Zar, Biostatistical analysis, Prentice Hall, Upper Saddle River, New Jersey, 1996.

[36] M.A.J. Zieger, E.J. Woods, J.R.T. Lakey, J. Liu, and J.K. Critser, Osmotic tolerance limits of canine pancreatic islets. Cell

Transplantation 8 (1999) 277-284.

Table 2-1. Osmotically-inactive volume, *b*, values for TF-1 cells (mean ± sem; n = 9)

Osmolality (osm/kg)	**Temperature**			
	4.8 ± 0.1 °C	12.9 ± 0.3 °C	23.3 ± 0.2 °C	37.4 ± 0.1 °C
583 ± 7	0.399 ± 0.006	0.336 ± 0.021	0.334 ± 0.008	0.294 ± 0.022
861 ± 6	0.347 ± 0.024	0.374 ± 0.014	0.338 ± 0.006	0.339 ± 0.016
1150 ± 4	0.387 ± 0.027	0.385 ± 0.019	0.355 ± 0.007	0.344 ± 0.019
1434 ± 5	0.368 ± 0.009	0.400 ± 0.012	0.371 ± 0.008	0.312 ± 0.012
pooled mean	0.375 ± 0.010^{a}	0.374 ± 0.010^{a}	$0.349 \pm 0.004^{a,b}$	0.325 ± 0.009^{b}

Same superscripts indicate no statistical difference ($p>0.05$).

Different superscripts indicate statistical difference ($p<0.05$).

Table 2-2. Osmotically-inactive volume, *b*, values for HUVECs (mean ± sem; n = 14)

Osmolality (osm/kg)	**Temperature**			
	2.2 ± 0.2 °C	10.1 ± 0.1 °C	20.5 ± 0.5 °C	36.6 ± 0.2 °C
571 ± 1	0.621 ± 0.041	0.564 ± 0.036	0.594 ± 0.028	0.590 ± 0.022
855 ± 1	0.608 ± 0.032	0.635 ± 0.023	0.627 ± 0.019	0.620 ± 0.016
1136 ± 1	0.589 ± 0.037	0.627 ± 0.019	0.628 ± 0.018	0.591 ± 0.026
1433 ± 1	0.581 ± 0.027	0.621 ± 0.017	0.614 ± 0.018	0581 ± 0.032
1729 ± 1	0.572 ± 0.030	0.592 ± 0.018	0.608 ± 0.020	0.598 ± 0.018
2028 ± 2	0.599 ± 0.030	0.604 ± 0.020	0.587 ± 0.020	0.592 ± 0.023
2327± 4	0.563 ± 0.021	0.588 ± 0.017	0.591 ± 0.027	0.596 ± 0.027
2667 ± 10	0.576 ± 0.024	0.557 ± 0.010	0.598 ± 0.022	0.552 ± 0.023
pooled mean	0.588 ± 0.009	0.601 ± 0.007	0.606 ± 0.007	0.593 ± 0.007

$p>0.05$ implying no concentration or temperature dependence

Table 2-3. Osmotically-inactive volume, *b*, values for porcine chondrocytes (mean ± sem; n = 6)

Osmolality (osm/kg)	Temperature			
	2.4 ± 0.1 °C	10.2 ± 0.3 °C	19.6 ± 0.1 °C	36.3 ± 0.2 °C
563 ± 2	0.656 ± 0.032	0.608 ± 0.045	0.500 ± 0.084	0.507 ± 0.093
840 ± 3	0.681 ± 0.013	0.564 ± 0.050	0.562 ± 0.081	0.530 ± 0.030
1123 ± 4	0.655 ± 0.022	0.631 ± 0.024	0.583 ± 0.010	0.510 ± 0.046
1418 ± 4	0.670 ± 0.017	0.507 ± 0.067	0.562 ± 0.005	0.525 ± 0.038
1733 ± 6	0.663 ± 0.023	0.595 ± 0.029	0.573 ± 0.015	0.484 ± 0.032
2016 ± 4	0.638 ± 0.027	0.560 ± 0.022	0.534 ± 0.010	0.540 ± 0.053
2324 ± 3	0.638 ± 0.018	0.607 ± 0.024	0.498 ± 0.046	0.537 ± 0.058
2682 ± 5	0.620 ± 0.034	0.581 ± 0.021	0.530 ± 0.024	0.539 ± 0.015
pooled mean	0.653 ± 0.008[a]	0.580 ± 0.014 [b]	0.538 ± 0.011 [b,c]	0.522 ± 0.015 [c]

Same superscripts indicate no statistical difference ($p>0.05$).

Different superscripts indicate statistical difference ($p<0.05$).

Table 2-4. Hydraulic conductivity, L_p, values for TF-1 cells (mean ± sem; n = 9)

Osmolality (osm/kg)	**Temperature**			
	4.8 ± 0.1 °C	12.9 ± 0.3 °C	23.3 ± 0.2 °C	37.4 ± 0.1 °C
583 ± 7	0.075 ± 0.003	0.119 ± 0.005	0.355 ± 0.012	1.348 ± 0.093
861 ± 6	0.070 ± 0.003	0.123 ± 0.005	0.395 ± 0.013	1.413 ± 0.074
1150 ± 4	0.075 ± 0.004	0.119 ± 0.004	0.407 ± 0.010	1.447 ± 0.106
1434 ± 5	0.074 ± 0.004	0.112 ± 0.002	0.386 ± 0.013	1.512 ± 0.061
pooled mean	0.074 ± 0.002[a]	0.118 ± 0.002[a]	0.386 ± 0.006[b]	1.425 ± 0.044[c]

Same superscripts indicate no statistical difference ($p>0.05$).

Different superscripts indicate statistical difference ($p<0.05$).

Table 2-5. Hydraulic conductivity, L_p, values for HUVECs (mean ± sem; n = 14)

Osmolality (osm/kg)	Temperature			
	2.2 ± 0.2 °C	10.1 ± 0.1 °C	20.5 ± 0.5 °C	36.6 ± 0.2 °C
571 ± 1	0.044 ± 0.007	0.065 ± 0.004	0.131 ± 0.013	0.521 ± 0.050
855 ± 1	0.036 ± 0.004	0.062 ± 0.005	0.155 ± 0.014	0.539 ± 0.051
1136 ± 1	0.034 ± 0.002	0.062 ± 0.005	0.147 ± 0.014	0.591 ± 0.062
1433 ± 1	0.033 ± 0.002	0.065± 0.005	0.156 ± 0.014	0.511 ± 0.064
1729 ± 1	0.034 ± 0.002	0.064 ± 0.005	0.144 ± 0.012	0.522 ± 0.054
2028 ± 2	0.032 ± 0.002	0.067 ± 0.004	0.162 ± 0.015	0.516 ± 0.052
2327± 4	0.031 ± 0.002	0.067 ± 0.005	0.150 ± 0.017	0.472 ± 0.056
2667 ± 10	0.033 ± 0.002	0.066 ± 0.004	0.137 ± 0.013	0.513 ± 0.046
pooled mean	0.034 ± 0.004[a]	0.065 ± 0.005[a]	0.148 ± 0.016[b]	0.522 ± 0.062[c]

Same superscripts indicate no statistical difference ($p>0.05$).

Different superscripts indicate statistical difference ($p<0.05$).

Table 2-6. Hydraulic conductivity, L_p, values for porcine chondrocytes (mean ± sem; n = 6)

Osmolality (osm/kg)	Temperature			
	2.4 ± 0.1 °C	10.2 ± 0.3 °C	19.6 ± 0.1 °C	36.3 ± 0.2 °C
563 ± 2	0.136 ± 0.029	0.142 ± 0.024	0.238 ± 0.043	0.452 ± 0.037
840 ± 3	0.067 ± 0.007	0.216 ± 0.070	0.248 ± 0.020	0.958 ± 0.257
1123 ± 4	0.065 ± 0.012	0.137 ± 0.008	0.247 ± 0.026	0.835 ± 0.231
1418 ± 4	0.071 ± 0.010	0.135 ± 0.027	0.221 ± 0.015	0.727 ± 0.076
1733 ± 6	0.062 ± 0.012	0.098 ± 0.013	0.214 ± 0.016	0.694 ± 0.125
2016 ± 4	0.059 ± 0.009	0.116 ± 0.011	0.193 ± 0.026	0.904 ± 0.139
2324 ± 3	0.064 ± 0.007	0.092 ± 0.013	0.228 ± 0.023	0.676 ± 0.127
2682 ± 5	0.089 ± 0.026	0.098 ± 0.011	0.223 ± 0.016	0.607 ± 0.037
pooled mean	0.077 ± 0.006^{a}	0.129 ± 0.011^{a}	0.225 ± 0.008^{b}	0.739 ± 0.054^{c}

Same superscripts indicate no statistical difference ($p>0.05$).

Different superscripts indicate statistical difference ($p<0.05$).

Table 2-7. Me_2SO permeability properties for TF-1 cells (mean ± sem; n = 9)

1M Me_2SO	**Using calculated L_p from E_a^{Lp}**		**Solving for L_p and P_s simultaneously**	
Temperature (°C)	**L_p (µm/min/atm)**	**P_s (µm/min)**	**L_p (µm/min/atm)**	**P_s (µm/min)**
4.9 ± 0.3	0.09	3.36 ± 0.40	0.08 ± 0.00	2.92 ± 0.22
10.7 ± 0.4	0.15	5.67 ± 0.51	0.17 ± 0.01	6.00 ± 0.76
23.4 ± 0.5	0.45	15.95 ± 1.08	0.61 ± 0.02*	18.8 ± 1.66
E_a (kcal/mol)	14.2	13.8 ± 0.1	17.5 ± 0.9	16.3 ± 1.1

* Signifies statistically significant difference from the P_s value estimated using the method of calculating L_p from E_a^{Lp} ($p<0.001$)

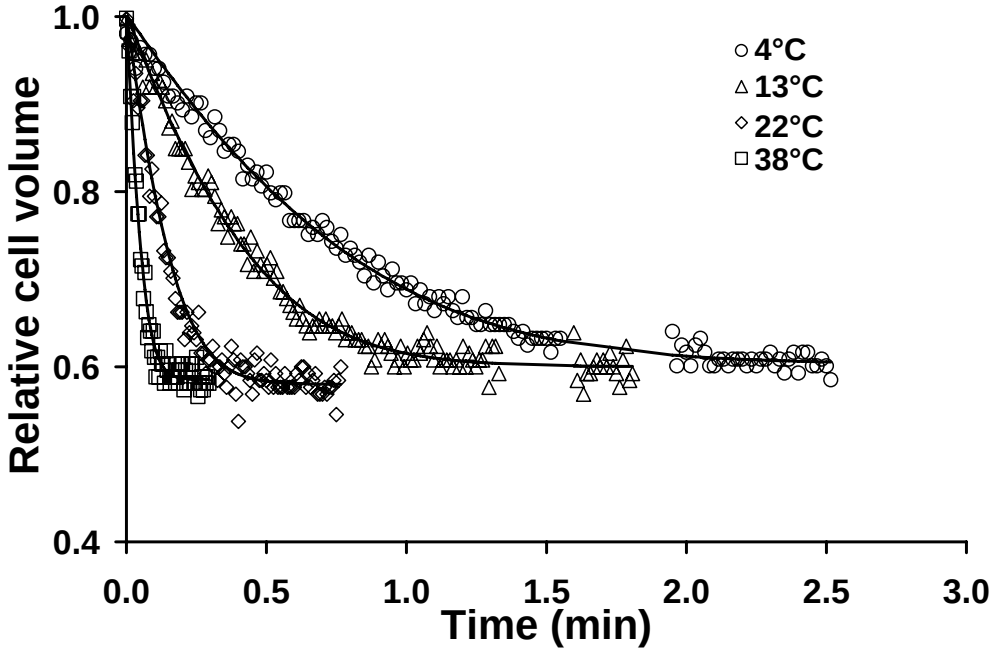

Figure 2-1. Representative cell volume kinetics of TF-1 cells exposed to 3X PBS at 4 different temperatures. The symbols show the experimental volume measurements averaged over 300 msec time intervals and the solid lines represent Eqs. 2-1 and 2-2 fitted curves to the data using the least squares method, yielding a value of L_p and b at each temperature.

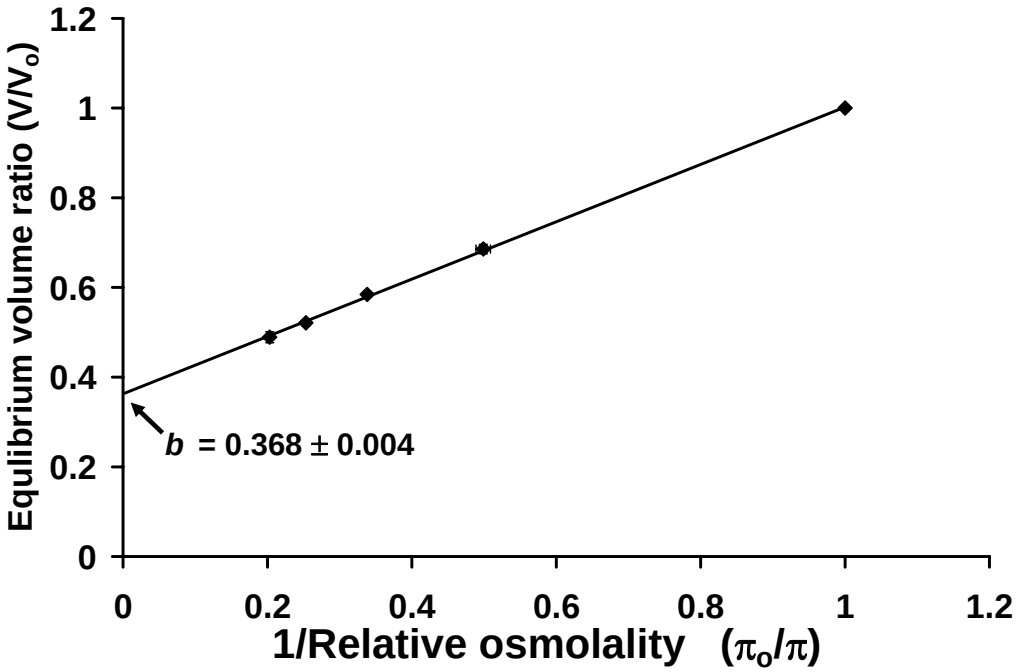

Figure 2-2. The Boyle van't Hoff plot for TF-1 cells. The symbols represent the experimental relative equilibrium cell volumes in hypertonic solutions and the solid line represents the linear regression fit of Eq. 2-1 to the data. The y-intercept gives the osmotically-inactive fraction, *b*.

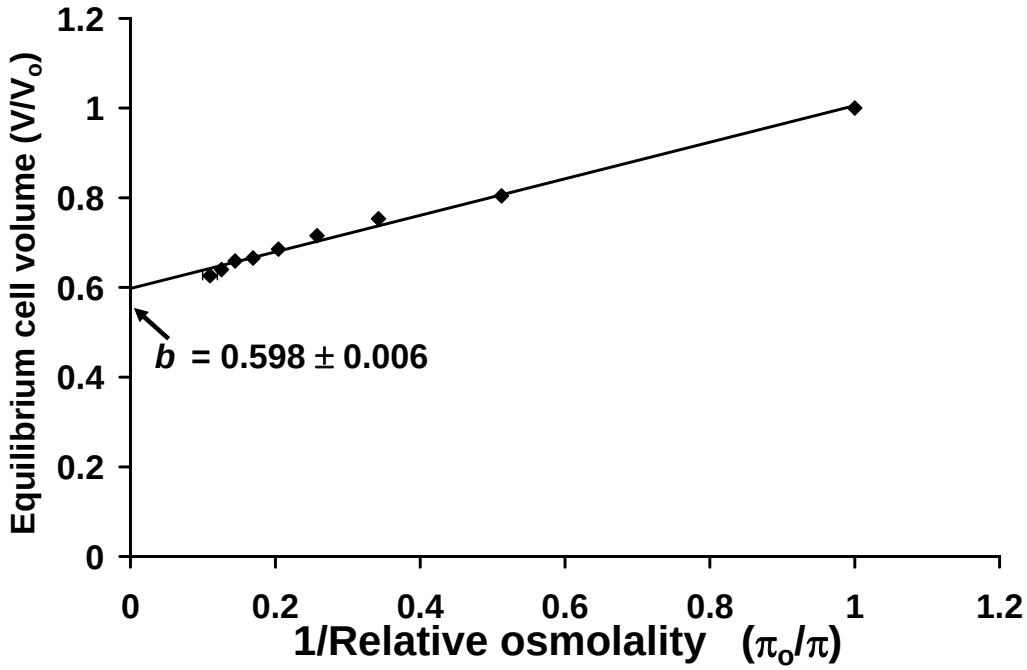

Figure 2-3. The Boyle van't Hoff plot for HUVECs. The symbols represent the experimental relative equilibrium cell volumes in hypertonic solutions and the solid line represents the linear regression fit of Eq. 2-1 to the data. The y-intercept gives the osmotically-inactive fraction, *b*.

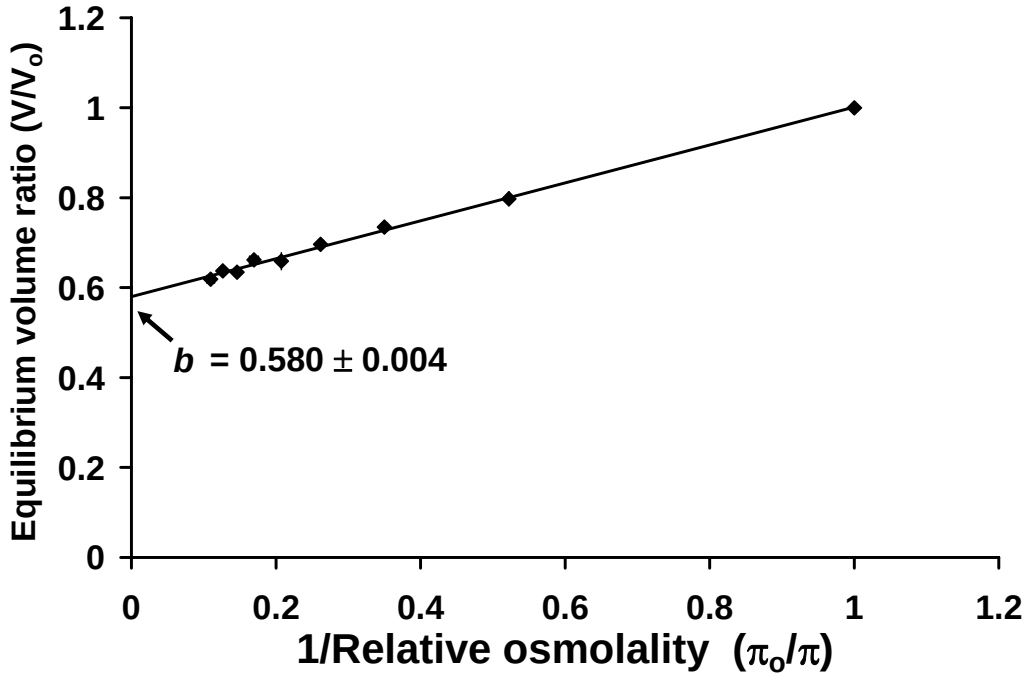

Figure 2-4. The Boyle van't Hoff plot for porcine chondrocytes. The symbols represent the experimental relative equilibrium cell volumes in hypertonic solutions and the solid line represents the linear regression fit of Eq. 2-1 to the data. The y-intercept gives the osmotically-inactive fraction, *b*.

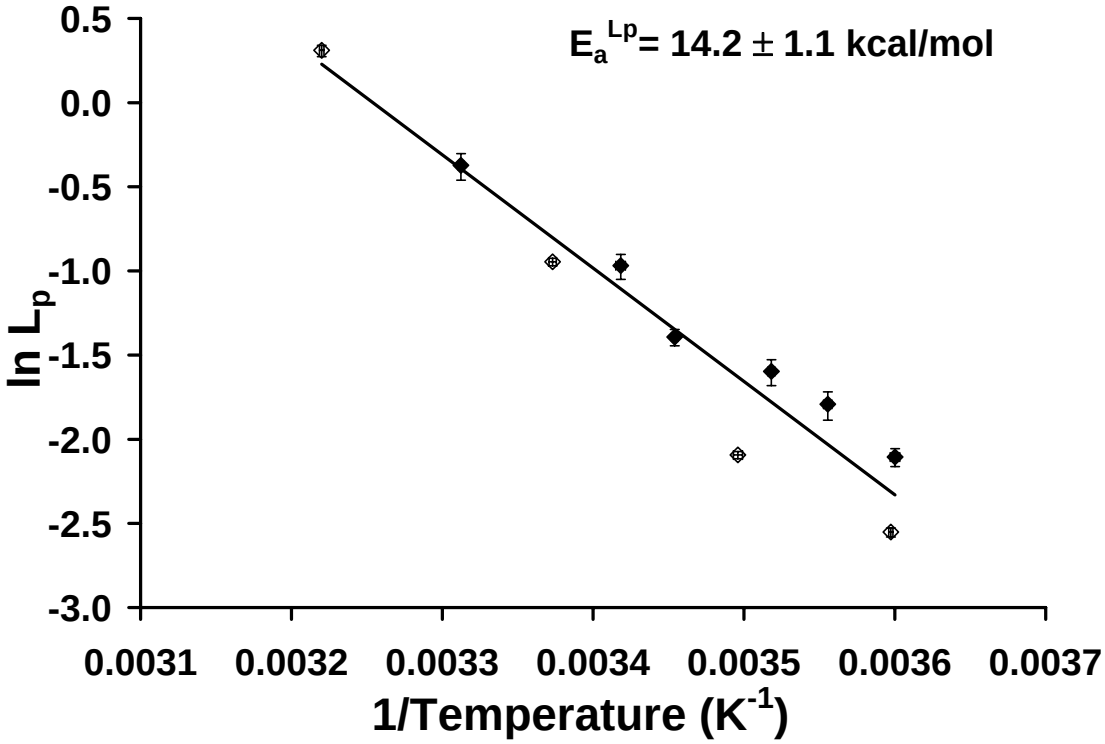

Figure 2-5. Arrhenius plot of the natural logarithm for L_p (μm/min/atm) of TF-1 cells (± sem) as a function of inverse temperature (K^{-1}) (± sem). The open diamond symbols represent all experiments done in 2-5X PBS, with different concentration data pooled (n = 36). The closed symbols represent all experiments done in 3X PBS (n = 9). The solid line represents the linear regression of all the data for calculation of the activation energy (E_a) from the slope (R^2=0.95).

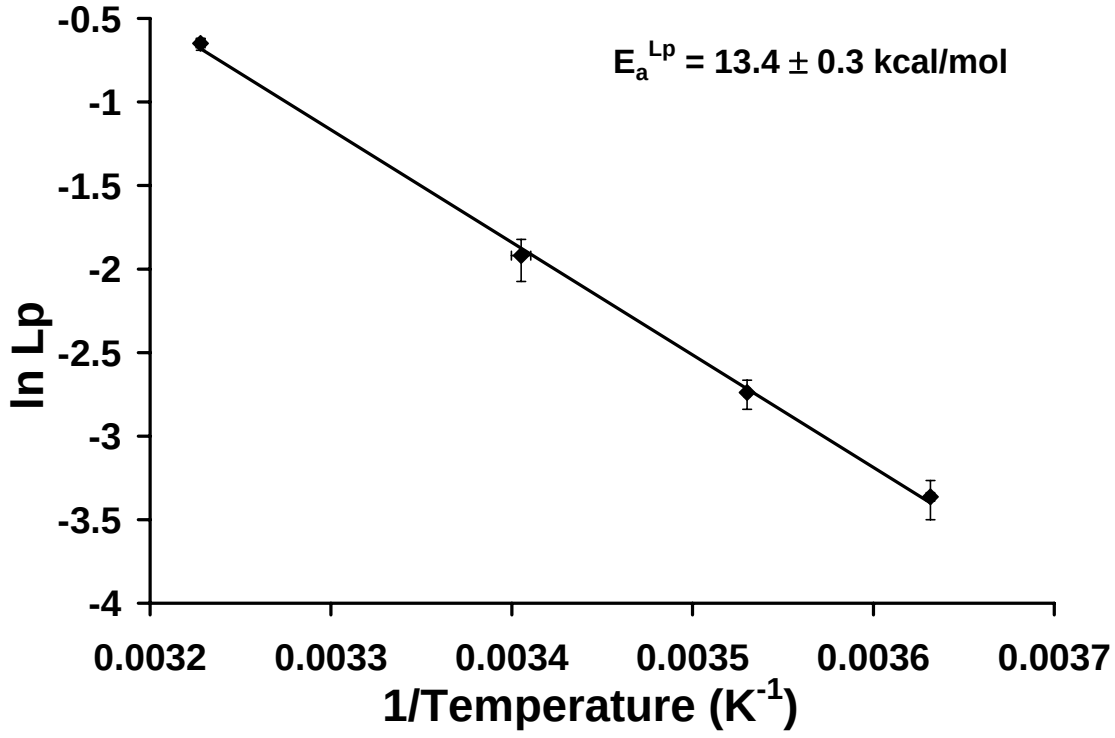

Figure 2-6. Arrhenius plot of the natural logarithm for L_p (μm/min/atm) of HVUECs (± sem) as a function of inverse temperature (K^{-1}) (± sem). The solid line represents the linear regression of the data for calculation of the activation energy (E_a) from the slope (R^2=1.00).

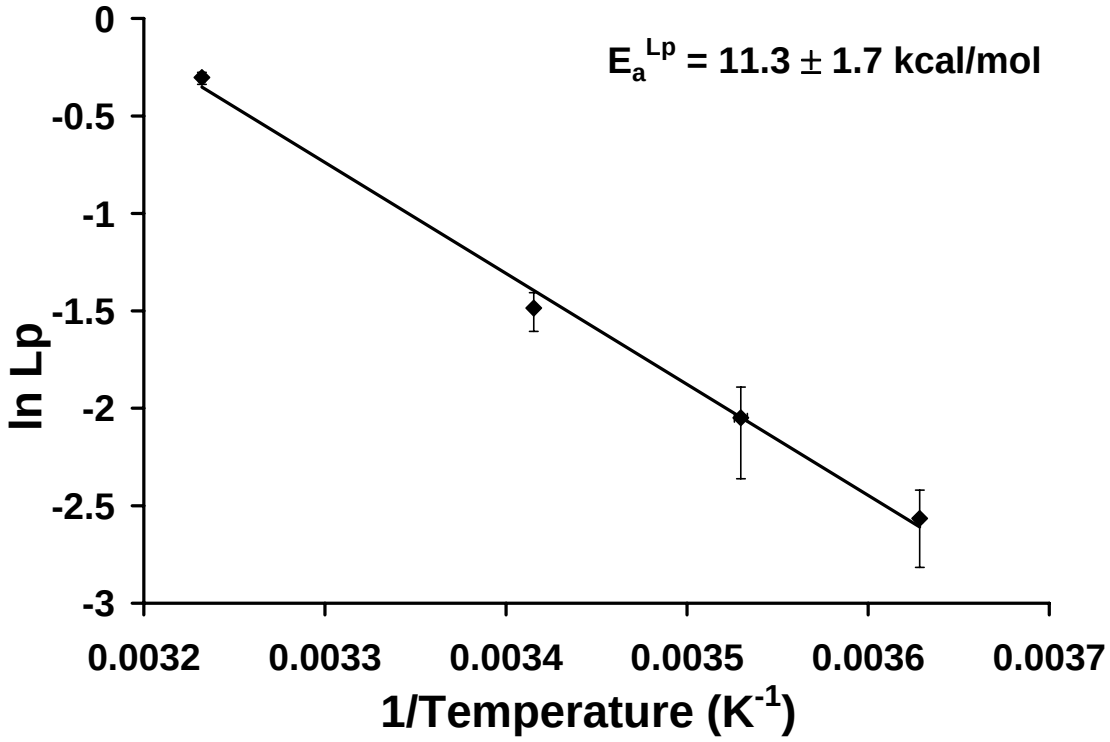

Figure 2-7. Arrhenius plot of the natural logarithm for L_p (μm/min/atm) of porcine chondrocytes (± sem) as a function of inverse temperature (K^{-1}) (± sem). The solid line represents the linear regression of the data for calculation of the activation energy (E_a) from the slope (R^2=1.00).

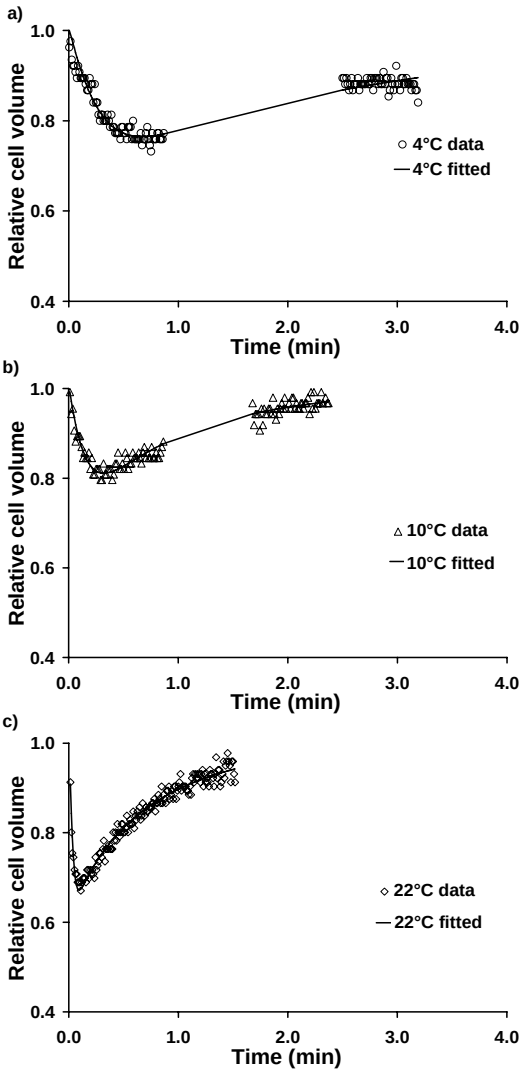

Figure 2-8. Representative plots of cell volume kinetics of TF-1 cells exposed to 1M ME_2SO at (a) 4°C, (b) 10°C, and (c) 22°C. The symbols show the experimental volume measurements averaged over 300 msec time intervals and the solid lines represent Eqs. 2-1, 2-2, and 2-3 fitted to the data using the least squares method, yielding a value of P_s at each temperature. Due to the length of time required for the cells to shrink and swell at the lower temperatures (a and b), the Coulter counter was stopped for a short duration, so as not to run out of solution (this appears as gaps in the data).

Chapter 3. Interrupted freezing procedures using TF-1 cells[1]

3.1 Introduction

The survival of cells and tissues after freezing and thawing depends on the ability of the cells to withstand a variety of stresses imposed by the cryopreservation protocol. Mazur *et al.*'s "two-factor hypothesis" of freezing injury [21] proposes that there are two independent mechanisms of damage during freezing: injury during slow cooling, where cell injury is caused by exposure to high solute concentrations as water in the extracellular solution is converted to ice [16]; and injury during rapid cooling, where cell injury is related to the presence of intracellular ice [19]. Maximum survival is normally obtained by selecting a cooling rate that is sufficiently high to avoid the injury from exposure to the concentrated solutes, yet low enough that the cells can osmotically dehydrate to avoid intracellular ice formation. This approach almost always requires a cryoprotectant, such as dimethyl sulfoxide (Me_2SO). Like other permeating cryoprotectants, Me_2SO protects the cell primarily against slow cool injury by reducing the amount of ice formed at any temperature, hence reducing the concentrations of other solutes and injury related to exposure [37]. There are, however, drawbacks to using cryoprotectants

[1] This chapter with modifications has been accepted to Cryobiology (2009) as "Characterization of cryobiological responses in TF-1 cells using interrupted freezing procedures", L.U. Ross-Rodriguez, J.A.W. Elliott, and L.E. McGann

in cryopreservation of clinical samples for cellular therapies, which include cellular osmotic stress during addition and removal, toxicity to cells during processing and preservation, and transplant-related toxicity for the patient. A better understanding of the nature and kinetics of cellular responses to temperature-induced conditions would allow novel approaches to the cryopreservation of new cell types.

In most practical cryopreservation procedures, cells are typically cooled to a low temperature (e.g. -80°C), the process being empirically optimized for each cell type by varying cooling rate and cryoprotectant type and concentration to minimize cryoinjury. However, it has long been known that there are critical subzero temperature ranges where interrupting the cooling process improves cell recovery [17]. There are two procedures specifically designed to explore cryoinjury by separating damage which occurs during the initial cooling to this critical temperature range, during time spent in this temperature range itself, and during subsequent cooling to storage temperatures. These two procedures are two-step freezing (interrupted rapid cooling with hold time) [8] and graded freezing (interrupted slow cooling without hold time) [23].

The two-step freezing procedure used by Farrant et al. is a logical method to examine the effects of interrupted rapid cooling on cell recovery over a broad range of subzero temperatures and conditions [8]. Using this procedure [8], human lymphocytes were cooled rapidly to various subzero temperatures and held for various periods of time before being either (a)

thawed directly from that holding temperature or (b) rapidly cooled to -196°C (liquid nitrogen) before thawing (see schematic - Figure 3-1a). This two-step freezing procedure is uniquely different from previous procedures using interrupted cooling as it also includes a separate analysis of damage which occurs during the initial cooling to the hold temperature. In further studies, McGann and Farrant reported that subzero temperature and the length of hold time at that temperature were important factors affecting cell survival [24]. McGann also used two-step freezing to explore the differing actions of penetrating and non-penetrating cryoprotectants and for the cryopreservation of Chinese hamster fibroblasts with 20 % hydroxyethyl starch (HES), with cell recovery comparable to 10 % Me_2SO [22]. It should be noted that the two-step procedure [8] is a modification of previously reported procedures [2,28,31], which did not include the direct thawing step from the hold temperature.

A variation of the two-step freezing procedure, the graded freezing procedure, was used by McGann to investigate progressive cell injury during slow cooling [23]. In this procedure, samples were cooled at a low linear rate to various subzero temperatures before being either (a) thawed directly or (b) rapidly cooled to -196°C (liquid nitrogen) before thawing. The difference between the two-step and graded freezing procedures is that two-step freezing uses interrupted rapid cooling with a hold step at an intermediate temperature, while graded freezing uses interrupted slow cooling to an intermediate temperature, without a hold step (see

schematic - Figure 3-1b). Both approaches allow separation of damage which occurs during the initial cooling phase from that which occurs during subsequent cooling to the storage temperature.

Although hematopoietic stem cells (HSC) are routinely cryopreserved for clinical use using Me_2SO, this cryoprotectant is associated with morbidity and mortality in some HSC transplant patients [5-7,30,38] and contributes to osmotic stresses for stem cells [32]. As with other cells used in therapies, it would be beneficial to eliminate Me_2SO from the cryopreservation protocol. TF-1 cells have been used as a model cell type for HSC. These cells express the CD34+ antigen and are able to differentiate into the various hematopoietic lineages [13,14,18], and as such have been used in various studies [3,4,9,15,18]. This study explores the cryobiology of TF-1 cells, a model for HSCs, by examining cryoinjury during interrupted rapid cooling and interrupted slow cooling procedures. Specifically, this study used two-step freezing and graded freezing procedures to characterize the cryobiological responses of TF-1 cells.

3.2 Materials and methods[2]

3.2.1 TF-1 cell culture

TF-1 cells ((Lot #2056376) ATCC, Manassas, VA, USA) were cultured at 37 °C in 5 % CO_2 in Modified RPMI 1640 Medium (ATCC) with

[2] Data for TF-1 cells were previously published (L. U. Ross-Rodriguez, Using simulations to design a cryopreservation procedure for hematopoietic stem cells without DMSO, MSc thesis, Medical Sciences – Laboratory Medicine and Pathology, University of Alberta, Edmonton, 2003, pp.111); however the analysis and discussion are new.

10 % fetal bovine serum (ATCC), and supplemented with 2 ng/mL recombinant human GM-CSF (Stemcell Technologies, Vancouver, BC, Canada). Prior to experiments, cells were washed twice with serum-free RPMI media and incubated in serum-free RPMI overnight to accumulate the cells in the G_1/G_0 phase of the cell cycle [15], resulting in a more uniform cell size distribution. Cells were then centrifuged and re-suspended in serum-free RPMI (4×10^6 cells/mL) prior to experiments. Serum-free media was chosen for experiments in order to compare experimental results with and without a cryoprotectant.

3.2.2 Interrupted freezing procedures

Two-step freezing procedure (interrupted rapid cooling with hold time)

Samples of 0.2 mL TF-1 cell suspension in serum-free RPMI were transferred to glass tubes (6x50 mm; Fisher, Edmonton, AB, Canada) and allowed to equilibrate at room temperature for 5 min. Control samples (unfrozen) were either warmed in a 37 °C water bath or plunged directly into liquid nitrogen. Experimental samples (frozen) were individually transferred into a stirred methanol bath (FTS Systems, Inc., Stone Ridge, NY, USA) preset at -3, -6, -9, -12, -15, -20, or -30 °C and allowed to equilibrate for 2 min at that temperature prior to ice nucleation with cold forceps. After nucleation, samples were held at the experimental temperature for 3 min before either thawing in a 37 °C water bath or plunging into liquid nitrogen. Plunge samples were stored in liquid nitrogen for a minimum of 1 hour prior to thawing in a 37 °C water bath. Sample

temperatures were monitored throughout the experiments using a Type T thermocouple (Omega, Laval, QC, Canada). Experiments were also performed using different hold times. Samples were cooled to various experimental hold temperatures (-5, -7, -9, -12, -25 °C), nucleated with cold forceps, and held for 0.5, 0.7, 1, 2, 3, 5, 7 or 10 min. Samples cooled to -25 °C spontaneously nucleated prior to reaching the hold temperature. Duplicate samples were used for each experimental measurement and each experiment was repeated in triplicate with cells from different passages. Samples cooled to hold temperatures of -20, -25, and -30°C spontaneously nucleated prior to reaching the hold temperature; however time zero for all experimental samples was calculated as time after manual nucleation or the 2 min equilibration time.

Graded freezing procedure (interrupted slow cooling without hold time) - no cryoprotectant

Samples of 0.2 mL cell suspension in serum-free RPMI were transferred to glass tubes and cooled in a 0 °C wet ice bath for 5 min. Control samples (unfrozen) were removed and either warmed in a 37 °C water bath or plunged into liquid nitrogen. Experimental samples (frozen) were transferred into a methanol bath preset at -3 °C and allowed to equilibrate for 5 min prior to ice nucleation in each tube with cold forceps. The bath was then cooled at 0.9 °C/min, and the temperature monitored using a Type T thermocouple. At each experimental temperature (-3, -6, -9, -12, -15, -20, -30, and -40 °C), one set of duplicate samples was

thawed directly in a 37 °C water bath and another set was plunged into liquid nitrogen. Plunge samples were kept in liquid nitrogen for a minimum of one hour prior to being thawed in a 37 °C water bath. Duplicate samples were used for each experimental temperature. Other experiments used cooling rates of 0.2 and 0.5 °C/min. Each experiment was repeated in triplicate with cells from different passages.

Graded freezing procedure with Me_2SO

Samples of 0.2 mL cell suspension in 10 % Me_2SO (Sigma, Mississauga, ON, Canada) in serum-free RPMI at room temperature were transferred to glass tubes and placed in a 0 °C ice bath for 5 min. Control samples (unfrozen) were removed and either warmed in a 37 °C water bath or plunged into liquid nitrogen. Experimental samples (frozen) were transferred into a methanol bath preset at -3 °C and allowed to equilibrate for 5 min prior to ice nucleation with cold forceps. After 5 min, the bath was cooled at 0.9 °C/min. At each experimental temperature (-3, -6, -9, -12, -15, -20, -30, and -40 °C), one set of duplicate samples was thawed directly in a 37 °C water bath and another set was plunged into liquid nitrogen. Plunge samples were kept in liquid nitrogen for a minimum of one hour prior to being thawed in a 37 °C water bath. Duplicate samples were used for each experimental temperature. Each experiment was repeated in triplicate with cells from different passages.

3.2.3 Assessment of cell recovery

Membrane integrity is widely used as an indicator of cryoinjury to

cells, and there is evidence that the plasma membrane is a primary site of freezing-thawing injury [1,20]. Although not a rigorous test of cell function, the membrane integrity assay indicates the upper limit for cell viability. In these studies, the membrane integrity assay was performed by incubating cells with SYTO® 13 (SYTO) (Molecular Probes, Eugene, OR, USA) and ethidium bromide (EB) (Sigma, Mississauga, ON, Canada) [34]. SYTO permeates the cell membrane of all cells, complexes with DNA, and fluoresces green under UV exposure. EB permeates cells with damaged plasma membranes and also complexes with DNA fluorescing red under UV conditions.

The SYTO/EB stain was prepared daily from 1X phosphate-buffered saline (PBS) and stock solutions, which were stored at 4 °C (for EB) and at -20 °C (for SYTO). Final concentrations were 0.25 mM EB and 0.125 mM SYTO. Twenty μL of stain was added to 200 μL of cell suspension, mixed, and incubated for 2 min at room temperature. Fluorescent images were captured using a Leitz Dialux 22 fluorescence (440-480nm) microscope (Leitz, Wetzlar, Germany) fitted with a PIXERA Viewfinder Pro digital camera (Pixera Corporation, Los Gatos, CA, USA). A viability assessment program (The Great Canadian Computer Company, Spruce Grove, AB, Canada) was used to quantify cell membrane integrity from digital images [11]. Cell recovery was calculated by dividing the number of intact green cells (experimental sample) by the number of intact green cells (control sample) to also account for cell loss.

3.3 Results

3.3.1 Two-step freezing experiments

Figure 3-2 shows a representative fluorescent photograph depicting membrane integrity assay for TF-1 cells with intact plasma membranes (green) and without intact plasma membranes (red). Figure 3-3 shows experimental results for TF-1 cells, suspended in serum-free RPMI without cryoprotectant, cooled rapidly to various experimental temperatures and held for 3 min, prior to direct thaw or plunge into liquid nitrogen. Data were normalized with control TF-1 samples (i.e. TF-1 samples at room temperature; 94.4 ± 0.2 %). The direct thaw samples showed little loss of membrane integrity at hold temperatures down to -9 °C, but membrane integrity declined sharply between -9 and -20 °C, indicating that damage was incurred during cooling to, or at the hold temperature. For samples plunged into liquid nitrogen, some protection against injury was conferred by holding for 3 min at -3 to -15 °C. Maximum membrane integrity after plunge and thaw was 62.2 ± 2.1 % and 61.8 ± 6.7 % at hold temperatures -12 °C and -15 °C, respectively. Membrane integrity for TF-1 cells that were plunged directly from room temperature was 6.7 ± 1.3 % and demonstrates that the absence of ice nucleation at high subzero temperatures and holding before plunging results in lower membrane integrity after thawing. Figure 3-4 shows membrane integrity of the plunge-thaw samples as a percentage of the direct thaw membrane integrity. This analysis demonstrates that at lower subzero hold

temperatures; no additional damage is incurred by the cells during plunge into liquid nitrogen.

3.3.2 Effect of hold times in two-step freezing

Figure 3-5 shows the membrane integrity of TF-1 cells as a function of hold time at -5 or -25 °C. Data were normalized with control TF-1 samples (i.e. TF-1 samples at room temperature; 91.6 ± 2.2 % and 91.3 ± 2.2 %, respectively). For direct thaw samples at -5 °C, membrane integrity remained high for hold times up to at least 10 min. Cells plunged into liquid nitrogen from -5 °C showed maximum membrane integrity with a 2 min hold time (65.4 ± 0.5 %). Comparable results for membrane integrity were obtained for hold temperatures between -7 °C and -9 °C (data not shown). Cell damage was evident during cooling to a hold temperature of -25 °C, which limited the membrane integrity of cells plunged into liquid nitrogen. Figure 3-6 shows contour plots of membrane integrity for TF-1 cells subjected to two-step freezing over a range of hold temperatures and hold times. Figure 3-6a shows that cells, directly thawed after being held for various times at the hold temperatures, show progressive decrease in membrane integrity as the hold temperature was reduced below -9 °C and to a lesser extent, as hold time was increased. Figure 3-6b shows that cells held for 1-3 min at temperatures between -5 °C and -7 °C prior to plunging into liquid nitrogen, resulted in the highest percentage of membrane integrity (60 %). A hold time of greater than 5 min resulted in a marked decrease in cell survival. These data indicates

that there is a zone of subzero hold temperatures (-5 °C to -12 °C) which, when held for 1-6 min, confers protection against cryoinjury associated with plunging to liquid nitrogen temperatures.

3.3.3 Graded freezing without cryoprotectant

Membrane integrity as a function of experimental temperature for TF-1 cells cooled at 0.9 °C/min, prior to direct thaw or plunge into liquid nitrogen is shown in Figure 3-7. Data were normalized with control TF-1 samples (i.e. TF-1 samples at 0 °C; 92.5 ± 2.9 %). Similar results were found for cooling rates of 0.2 °C/min and 0.5 °C/min (data not shown). Data from all 3 cooling rates demonstrated a progressive decline in membrane integrity for cells thawed directly from the experimental temperature, with a 50% loss at -12 °C, indicating injury related to exposure to the concentrated extracellular solution. Cells plunged into liquid nitrogen from the experimental temperature incurred additional injury. The zone of subzero experimental temperatures between -3 °C and -9 °C confers some protection against injury during plunge into liquid nitrogen (30.1 ± 0.7 % at -9 °C). Membrane integrity for TF-1 cells that were plunged directly from 0 °C was 11.8 ± 2.7 %.

Figure 3-8 also shows membrane integrity data further analyzed by calculating the plunge-thaw cell recovery as a percentage of the direct-thaw cell recovery, showing the additional damage incurred during the plunge step. This supports the view that recovery after the plunge step is only partially limited by damage incurred during the direct thaw step and

that there is significant additional damage to the cells during the plunge step.

3.3.4 Graded freezing with Me_2SO

Figure 3-9 shows the recovery of TF-1 cells cooled at 0.9 °C/min in 10 % Me_2SO to various subzero temperatures ranging from -3 to -40 °C, and either thawed directly or plunged into liquid nitrogen. Data were normalized with control TF-1 samples (i.e. TF-1 samples at 0 °C; 91.4 ± 3.2 %). Maximum membrane integrity after plunge and thaw was 71.5 ± 4.1 % at a plunge temperature of -15 °C with Me_2SO. Note, for comparison, that the membrane integrity of TF-1 cells following a conventional cryopreservation protocol (cooling 0.9 °C/min to -40 °C and then plunging into liquid nitrogen) was 63.0 ± 6.4 %. Membrane integrity for TF-1 cells in 10 % Me_2SO that were plunged directly from 0 °C was 30.9 ± 3.1 %. Figure 3-9 also shows membrane integrity data further analyzed by calculating the plunge-thaw cell recovery as a percentage of the direct-thaw cell recovery, showing that with Me_2SO, most of the damage incurred is during the plunge step.

3.4 Discussion

This study characterized the cryobiological responses on TF-1 cells to interrupted freezing procedures. In the absence of cryoprotectants, this study showed that using two-step freezing (interrupted rapid cooling with hold time), TF-1 cells sustained less injury at lower subzero hold

temperatures than using graded freezing (interrupted slow cooling without hold time). However, using two-step freezing, there was also damage associated with cooling down to and exposure at the hold temperatures. Cells thawed directly from the hold temperatures showed a decline in membrane integrity with decreasing temperature, reaching 50% at -17 °C, indicating that a major portion of cells were damaged prior to being plunged into liquid nitrogen. This damage is associated with cooling to and exposure at the hold temperature, with intracellular ice formation as a likely cause. For -25 °C hold temperatures, damage did not increase with hold time and it was cooling to -25 °C where damage occurred (Figure 3-4). Freezing results from this study also demonstrate that for hold temperatures below -15 °C, no additional damage is incurred by cooling to liquid nitrogen temperatures, implying that the cells remaining intact at the end of the hold step have lost a sufficient amount of intracellular water and that there is no additional damage due to intracellular ice formation during the plunge. The highest recovery for samples thawed from liquid nitrogen was 65.4 ± 0.5 % at a hold temperature of -5 °C with a hold time of 2 min. Avoidance of intracellular ice formation during the plunge step requires osmotic dehydration during the hold step. The hydraulic conductivity and its activation energy are different for different cell types, so the optimal hold temperature and time will be cell-type dependent.

Using the graded freezing procedure, this study demonstrated the progressive damage incurred by slow cooling TF-1 cells to subzero

experimental temperatures, indicating the deleterious effect of exposure to concentrated extracellular solutions. There was a marked difference between the membrane integrity for cells directly thawed and those plunged into liquid nitrogen, which has also been shown for other cell types [25,26,34-36]. The maximum recovery for plunge samples using graded freezing without Me_2SO was 27.8 ± 0.8 %, while results from the literature for other HSCs were 32 % for nucleated white cells and 17 % for $CD34^+$ cells [35].

Table 3-1 compares maximum recovery of TF-1 cells cooled in liquid nitrogen (plunge thaw) using the different freezing protocols. The maximum two-step freezing recovery (65.4 ± 0.5 %) was higher than recovery using graded freezing profiles without Me_2SO (30.1 ± 0.7 %). Furthermore, the two-step freezing membrane integrity (without cryoprotectant) was comparable with membrane integrity of TF-1 cells cooled using a conventional cryopreservation protocol (cooling at 0.9 °C/min in 10 % Me_2SO to -40 °C and plunging into liquid nitrogen) of 63.0 ± 6.4 %.

Although there is no true standard cryopreservation method for HSCs, there is an overall conventional approach of slow cooling in 5-10 % Me_2SO solution. Based on the HSC cryopreservation literature, this approach leads to recoveries of 79 ± 5 % (1 °C/min with plunge at -50 °C using 10 % Me_2SO) [10], 67.4 ± 2.0 % (1 °C/min with plunge at -60 °C using 10 % Me_2SO) [33], and 85.8 ± 6.8 % (4 °C/min with plunge at -44 °C

using 5 % Me_2SO) [35]. While the exact cooling protocols and Me_2SO solutions may differ to varying degrees from the present study, the influence of Me_2SO on increasing cell survival at lower temperatures during slow cooling is a commonality. The trends using graded freezing with Me_2SO, are comparable to those seen using graded freezing with nucleated white blood cells, [35], CD34+ umbilical cord blood stem cells [35], and chinese hamster fibroblasts [22]. The maximum recovery obtained using graded freezing with Me_2SO was higher than the standard procedure with Me_2SO (71.5 ± 4.1 %); however, this was using a relatively high plunge temperature of -5 °C (Table 3-1). It also demonstrates that when comparing the results to having no Me_2SO present, Me_2SO confers protection even without ice nucleation at high subzero temperatures.

The data in this study are also comparable to previously published results by Karlsson et al. using slow cooling and Me_2SO with mouse oocytes [12]. They showed low cell recovery at high plunge temperatures, which increased at lower plunge temperatures. They also suggested that the observed cell damage at high subzero plunge temperatures was the result of intracellular ice formation, based on predictions of a mechanistic model [12], which would also explain the plunge results in this study.

The use of Me_2SO as a cryoprotectant has been identified as a problem for HSC transplant patients due to its clinical toxicity [5,7,30,38]. The experimental results reported here for TF-1 cells without cryoprotectants indicate that higher cell recovery is possible by

manipulating the cooling profile. These data indicates that there is a zone of subzero hold temperatures (-5 to -12 °C) and hold times (1-6 min), that confers cryoprotection comparable to the conventional 10 % Me_2SO solution with slow cooling down to -40 °C in TF-1 cells. The pattern of recovery as a function of hold time and temperature was similar to that previously shown for fibroblasts [24].

By comparing the post-thaw recovery of TF-1 cells, following slow cooling, with water permeability results in Chapter 2, it is evident that cells with a low hydraulic conductivity are damaged during slow cooling without a cryoprotectant (27.8 ± 0.8 %). However, human erythrocytes, which have a much higher L_p (12 µm/min/atm at 22-24 °C) [27], sustain even greater injury during slow cooling (hemolysis >95 %) [29].

Practical cryopreservation procedures have largely been limited to the use of constant cooling rates. Interrupted freezing procedures, such as two-step and graded freezing, provide useful insight into the mechanisms of damage occurring at various temperatures throughout the cooling profile [23]. These procedures allow manipulation of different variables of the cryopreservation protocol, including cooling profiles, plunge temperatures, cryoprotectants, and storage temperatures. In this study, both procedures allowed additional characterization of the cryobiology of cells. It also demonstrated the ability to improve recoveries when using Me_2SO with graded freezing and, more significantly, to cryopreserve TF-1 cells (a model for HSC) without the need for Me_2SO

using a two-step procedure. As cryopreservation protocols continue to attempt to decrease the use of Me_2SO and/or include HES, the value of the two-step procedure may become more apparent. Ultimately this approach will enable to systematic exploration of alternatives to constant cooling rates and perhaps future cryopreservation protocols will benefit from using a two-step procedure.

3.5 References

[1] J.P. Acker, and L.E. McGann, Membrane damage occurs during the formation of intracellular ice. Cryoletters 22 (2001) 241-254.

[2] E. Asahina, Prefreezing as a method enabling animals to survive freezing at an extremely low temperature. Nature 184 (1959) 1003-1004.

[3] S.S. Buchanan, S.A. Gross, J.P. Acker, M. Toner, J.F. Carpenter, and D.W. Pyatt, Cryopreservation of stem cells using trehalose: evaluation of the method using a human hematopoietic cell line. Stem Cells and Development 13 (2004) 295-305.

[4] L. Cermak, S. Simova, A. Pintzas, V. Horejsi, and L. Andera, Molecular mechanisms involved in CD43-mediated apoptosis of TF-1 cells. The Journal of Biological Chemistry 277 (2002) 7955-7961.

[5] J.M. Davis, S.D. Rowley, H.G. Braine, S. Piantadosi, and G.W. Santos, Clinical toxicity of cryopreserved bone-marrow graft infusion. Blood 75 (1990) 781-786.

[6] A. Donmez, M. Tombuloglu, A. Gungor, N. Soyer, G. Saydam, and S. Cagirgan, Clinical side effects during peripheral blood progenitor cell infusion. Transfusion and Apheresis Science 36 (2007) 95-101.

[7] M.J. Egorin, D.M. Rosen, R. Sridhara, L. Sensenbrenner, and M. Cottler-Fox, Plasma concentrations and pharmacokinetics of dimethylsulfoxide and its metabolites in patients undergoing peripheral-blood stem-cell transplants. Journal of Clinical Oncology

16 (1998) 610-615.

[8] J. Farrant, S.C. Knight, L.E. McGann, and J. O'Brien, Optimal recovery of lymphocytes and tissue culture cells following rapid cooling. Nature 249 (1974) 452-453.

[9] G. Hansen, T.R. Hercus, B.J. McClure, F.C. Stomski, M. Dottore, J. Powell, H. Ramshaw, J.M. Woodcock, Y.B. Xu, M. Guthridge, W.J. McKinstry, A.F. Lopez, and M.W. Parker, The structure of the GM-CSF receptor complex reveals a distinct mode of cytokine receptor activation. Cell 134 (2008) 496-507.

[10] C.J. Hunt, S.E. Armitage, and D.E. Pegg, Cryopreservation of umbilical cord blood: 2. Tolerance of CD34(+) cells to multimolar dimethyl sulphoxide and the effect of cooling rate on recovery after freezing and thawing. Cryobiology 46 (2003) 76-87.

[11] N.M. Jomha, P.C. Anoop, J.A. Elliott, K. Bagnall, and L.E. McGann, Validation and reproducibility of computerised cell-viability analysis of tissue slices. BMC Musculoskeletal Disorders 4 (2003) 5.

[12] J.O.M. Karlsson, A. Eroglu, T.L. Toth, E.G. Cravalho, and M. Toner, Fertilization and development of mouse oocytes cryopreserved using a theoretically optimized protocol. Human Reproduction 11 (1996) 1296-1305.

[13] T. Kitamura, F. Takaku, and A. Miyajima, IL-1 up-regulates the expression of cytokine receptors on a factor-dependent human hemopoietic cell line, TF-1. International Immunology 3 (1991) 571-

577.

[14] T. Kitamura, A. Tojo, T. Kuwaki, S. Chiba, K. Miyazono, A. Urabe, and F. Takaku, Identification and analysis of human erythropoietin receptors on a factor-dependent cell-line, TF-1. Blood 73 (1989) 375-380.

[15] A. Kolonics, A. Apati, J. Janossy, A. Brozik, R. Gati, A. Schaefer, and M. Magocsi, Activation of Raf/ERK1/2 MAP kinase pathway is involved in GM-CSF-induced proliferation and survival but not in erythropoietin-induced differentiation of TF-1 cells. Cellular Signalling 13 (2001) 743-754.

[16] J.E. Lovelock, The haemolysis of human red blood-cells by freezing and thawing. Biochimica et Biophysica Acta 10 (1953) 414-426.

[17] B. Luyet, and J. Keane, A critical temperature range apparently characterized by sensitivity of bull semen to high freezing velocity. Biodynamica 7 (1955) 281-292.

[18] M. Marone, G. Scambia, G. Bonanno, S. Rutella, D. de Ritis, F. Guidi, G. Leone, and L. Pierelli, Transforming growth factor-beta 1 transcriptionally activates CD34 and prevents induced differentiation of TF-1 cells in the absence of any cell-cycle effects. Leukemia 16 (2002) 94-105.

[19] P. Mazur, Kinetics of water loss from cells at subzero temperatures and the likelihood of intracellular freezing. The Journal of General Physiology 47 (1963) 347-369.

[20] P. Mazur, The role of cell membranes in the freezing of yeast and other cells. Annals of the New York Academy of Sciences 125 (1965) 658-676.

[21] P. Mazur, S.P. Leibo, and E.H.Y. Chu, A two-factor hypothesis of freezing injury - evidence from chinese-hamster tissue-culture cells. Experimental Cell Research 71 (1972) 345-355.

[22] L.E. McGann, Differing actions of penetrating and nonpenetrating cryoprotective agents. Cryobiology 15 (1978) 382-390.

[23] L.E. McGann, Optimal temperature ranges for control of cooling rate. Cryobiology 16 (1979) 211-216.

[24] L.E. McGann, and J. Farrant, Survival of tissue culture cells frozen by a two-step procedure to -196 degrees C. I. Holding temperature and time. Cryobiology 13 (1976) 261-268.

[25] L.E. McGann, and M.L. Walterson, Cryoprotection by dimethyl sulfoxide and dimethyl sulfone. Cryobiology 24 (1987) 11-16.

[26] L.E. McGann, H.Y. Yang, and M. Walterson, Manifestations of cell damage after freezing and thawing. Cryobiology 25 (1988) 178-185.

[27] J.J. McGrath, Membrane transport properties. in: J.J. McGrath, and K.R. Diller, (Eds.), Low temperature biotechnology emerging applications and engineering contributions, The American Society of Mechanical Engineers, New York, 1988, pp. 273-330.

[28] C. Polge, Low-temperature storage of mammalian spermatozoa.

Proceedings of the Royal Society of London Series B-Biological Sciences 147 (1957) 498-507.

[29] G. Rapatz, J.J. Sullivan, and B. Luyet, Preservation of erythrocytes in blood containing various cryoprotective agents, frozen at various rates and brought to a given final temperature. Cryobiology 5 (1968) 18-25.

[30] N.C. Santos, J. Figueira-Coelho, J. Martins-Silva, and C. Saldanha, Multidisciplinary utilization of dimethyl sulfoxide: pharmacological, cellular, and molecular aspects. Biochemical Pharmacology 65 (2003) 1035-1041.

[31] A.C. Taylor, The physical state transition in the freezing of living cells. Annals of the New York Academy of Sciences 85 (1960) 595-609.

[32] E.J. Woods, J. Liu, C.W. Derrow, F.O. Smith, D.A. Williams, and J.K. Critser, Osmometric and permeability characteristics of human placental/umbilical cord blood CD34+ cells and their application to cryopreservation. Journal of Hematotherapy and Stem Cell Research 9 (2000) 161-173.

[33] H. Yang, Effects of incubation temperature and time after thawing on viability assessment of peripheral hematopoietic progenitor cells cryopreserved for transplantation. Bone Marrow Transplantation 32 (2003) 1021-1026.

[34] H. Yang, J. Acker, A. Chen, and L. McGann, In situ assessment of cell viability. Cell Transplantation 7 (1998) 443-51.

[35] H. Yang, J.P. Acker, J. Hannon, H. Miszta-Lane, J.J. Akabutu, and L.E. McGann, Damage and protection of UC blood cells during cryopreservation. Cytotherapy 3 (2001) 377-386.

[36] H. Yang, F. Arnaud, and L.E. McGann, Cryoinjury in human granulocytes and cytoplasts. Cryobiology 29 (1992) 500-510.

[37] Z.W. Yu, and P.J. Quinn, Dimethyl-Sulfoxide - a Review of Its Applications in Cell Biology. Bioscience Reports 14 (1994) 259-281.

[38] A. Zambelli, G. Poggi, G. Da Prada, P. Pedrazzoli, A. Cuomo, D. Miotti, C. Perotti, P. Preti, and G.R. Della Cuna, Clinical toxicity of cryopreserved circulating progenitor cells infusion. Anticancer Research 18 (1998) 4705-4708.

Table 3-1. Maximum recovery of TF-1 cells (plunge thaw), as assessed by membrane integrity (mean ± SEM; normalized).

Protocol	**Maximum recovery after storing in liquid nitrogen**
Standard Freezing protocol (with Me_2SO)[1]	63.0 ± 6.4 %
Graded Freezing (without Me_2SO)[2]	30.1 ± 0.7 %
Two-step Freezing (without Me_2SO)[3]	65.4 ± 0.5 %
Graded Freezing (with Me_2SO)[4]	71.5 ± 4.1 %

[1]0.9 °C/min to -40 °C and plunge
[2]0.9 °C/min to -9 °C and plunge
[3]non-linear cooling with 2 minute hold at -5 °C followed by plunge
[4]0.9 °C/min to -15 °C and plunge

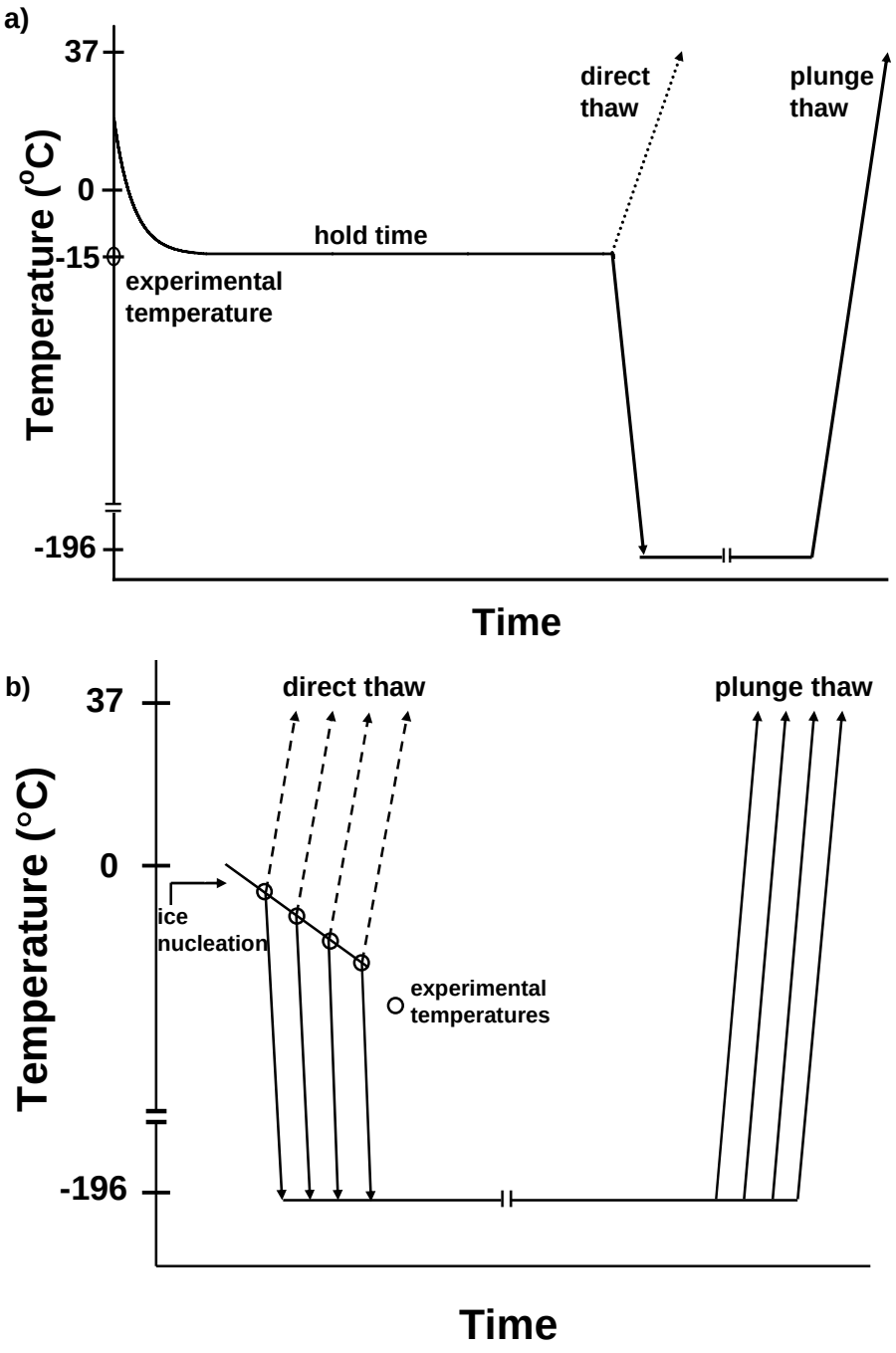

Figure 3-1. Schematics of (a) two-step freezing, including initial rapid non-linear cooling to hold temperature, hold time, and either directly thawing or plunging and then thawing following storage time, and of (b) graded freezing, including initial slow linear cooling to experimental temperatures and either direct thawing or plunging and then thawing.

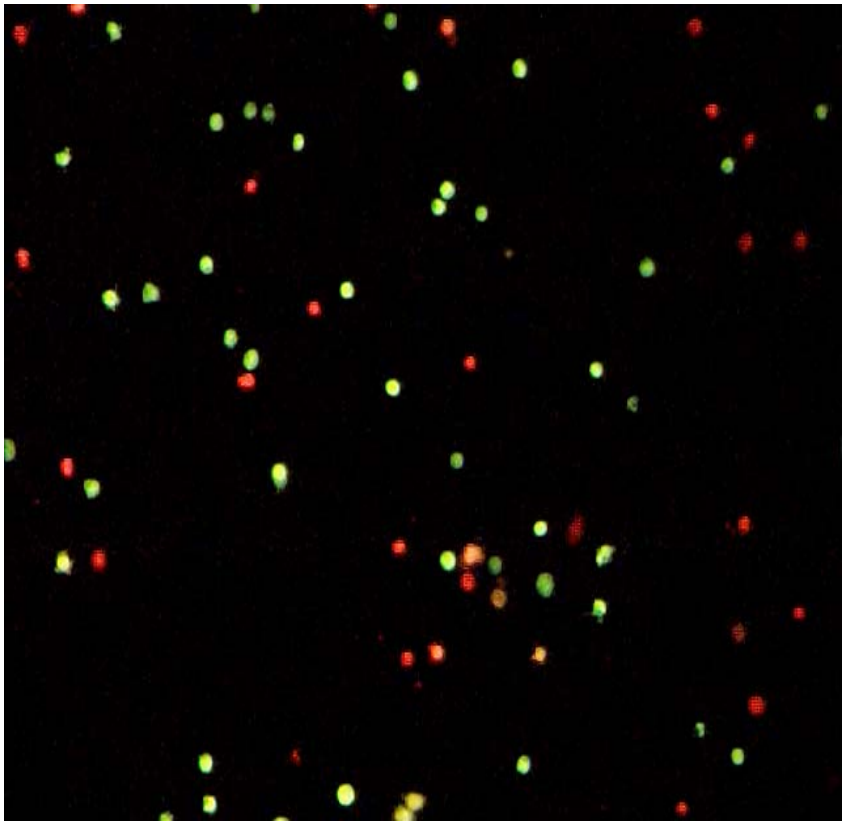

Figure 3-2. Representative fluorescent photograph depicting membrane integrity assay for TF-1 cells with intact plasma membranes (green) and without intact plasma membranes (red).

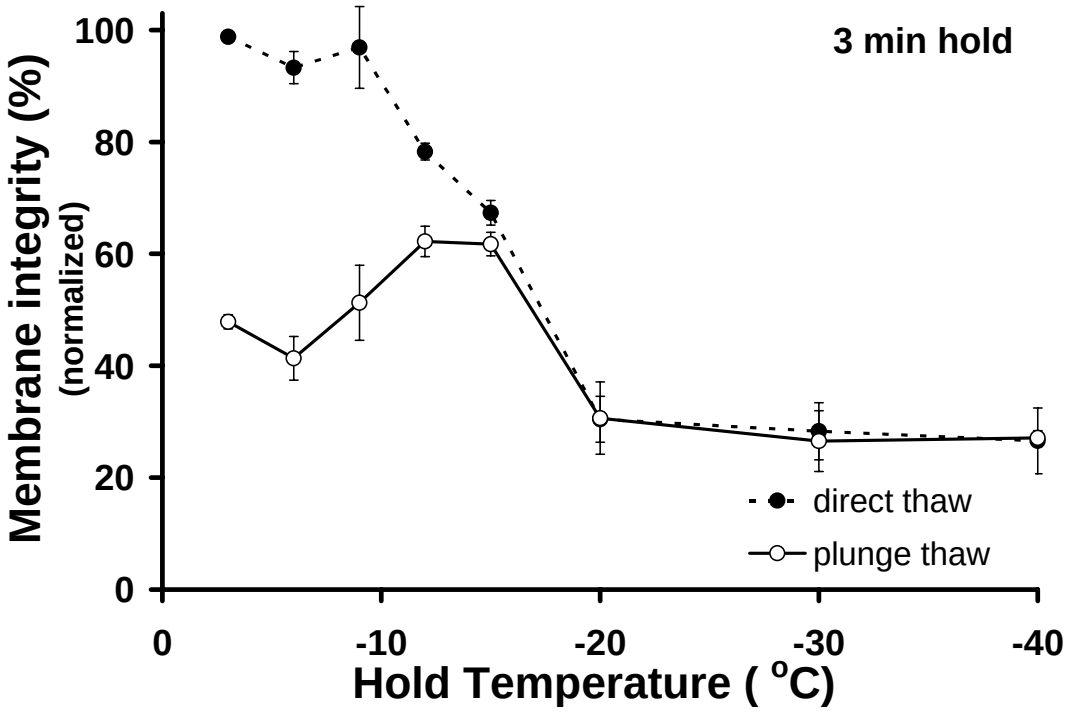

Figure 3-3. Two-step freezing. Membrane integrity for TF-1 cells (± sem; normalized to controls) in serum-free RPMI media cooled to various subzero plunge temperatures from room temperature, held 3 minutes, and then either thawed directly (dashed) or plunged into liquid nitrogen (solid) before being thawed.

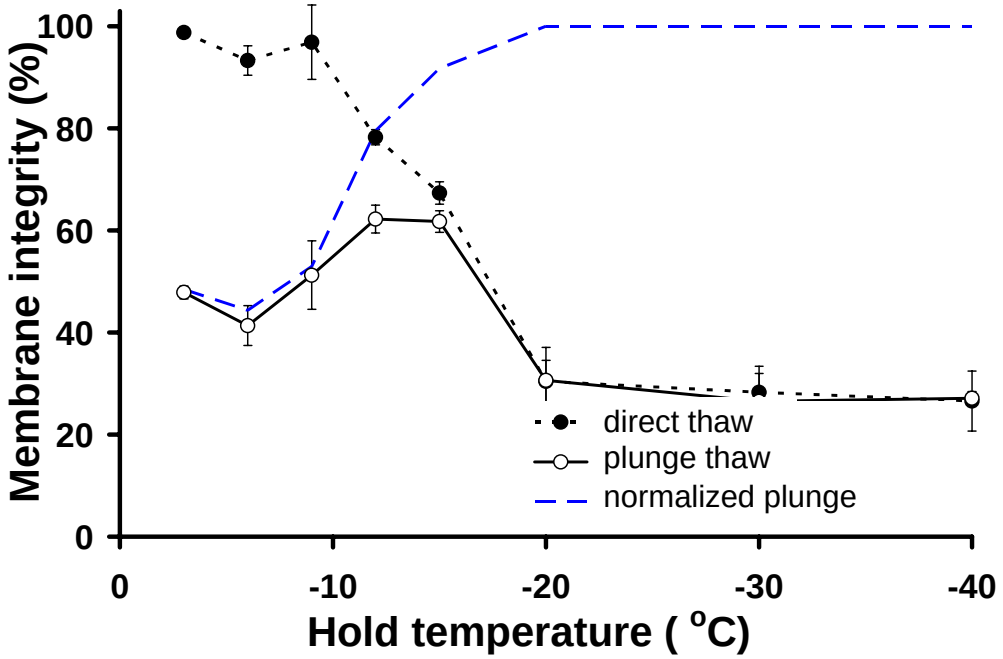

Figure 3-4. Membrane integrity for TF-1 cells (± sem; normalized to controls) in serum-free RPMI following two-step freezing with a 3 minute hold time, including a plunge-thaw curve normalized with (i.e. as a percentage of) the direct-thaw data (long dashes).

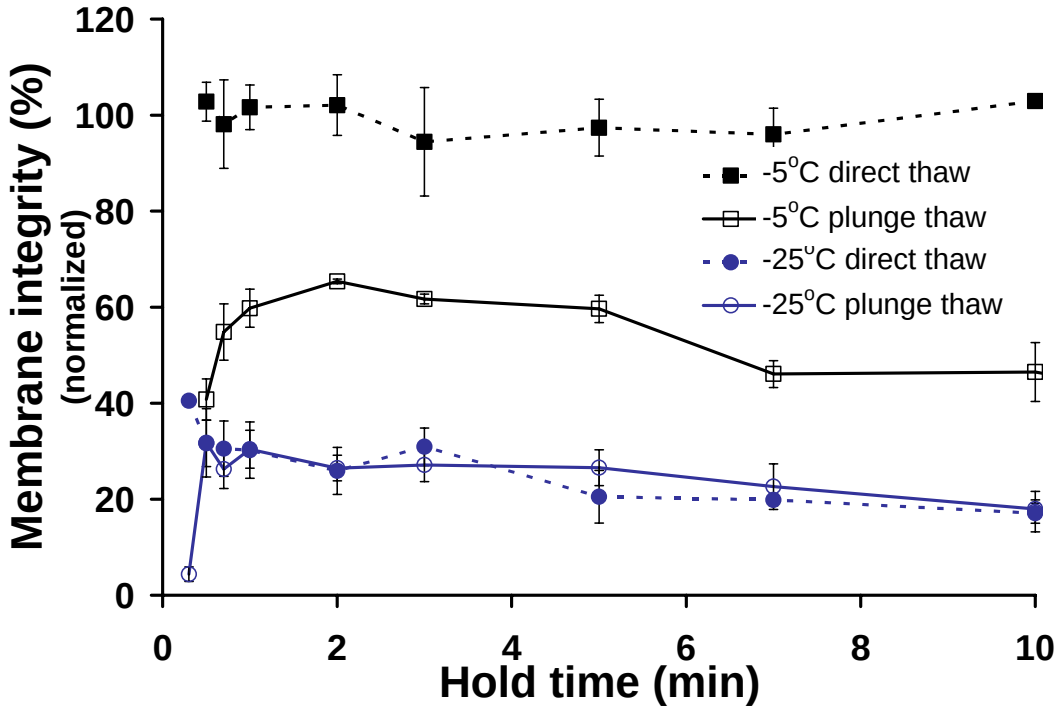

Figure 3-5. The membrane integrity of TF-1 cells (± sem; normalized to controls) in serum-free RPMI media as a function of hold time for cells cooled rapidly to -5 °C (black) or -25 °C (blue), held for a period of time before either thawed directly (dashed) or plunged into liquid nitrogen (solid) before being thawed.

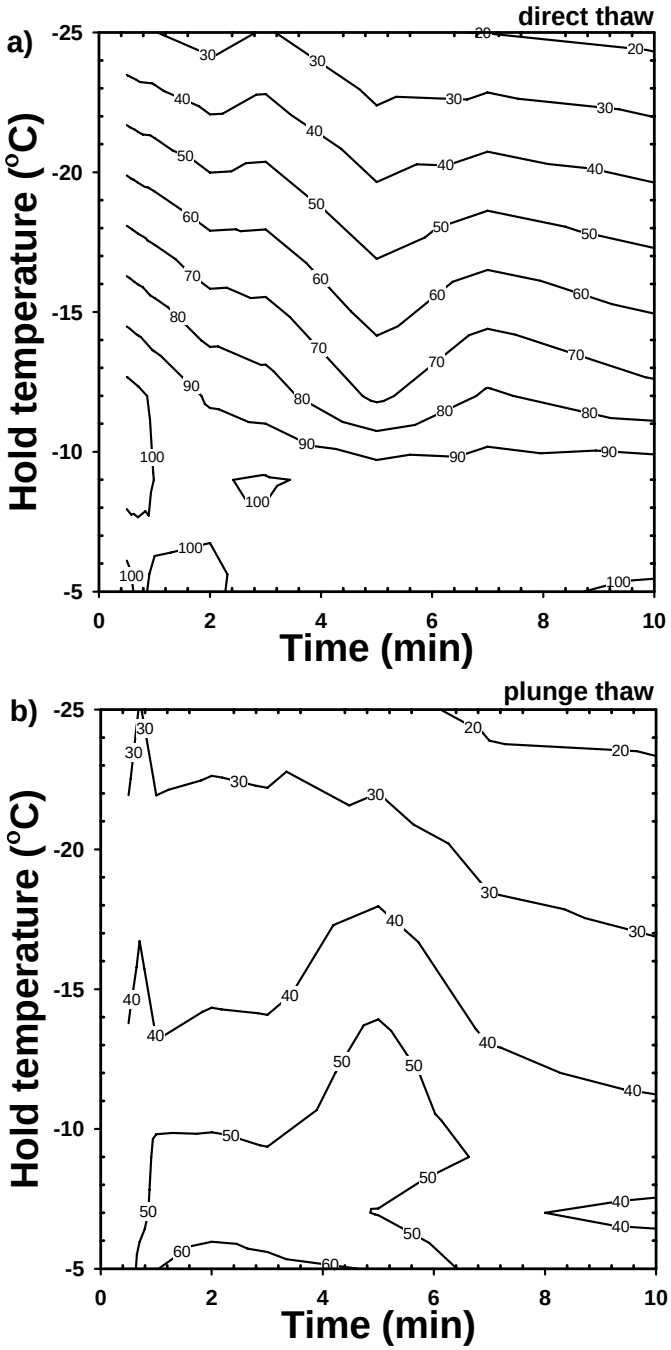

Figure 3-6. Contours of membrane integrity of TF-1 cells (normalized to controls) in serum-free RPMI media after being cooled rapidly to various subzero hold temperatures and held for a duration ranging from 0.5 to 10 minutes before being either (a) thawed directly or (b) plunged into liquid nitrogen prior to thawing.

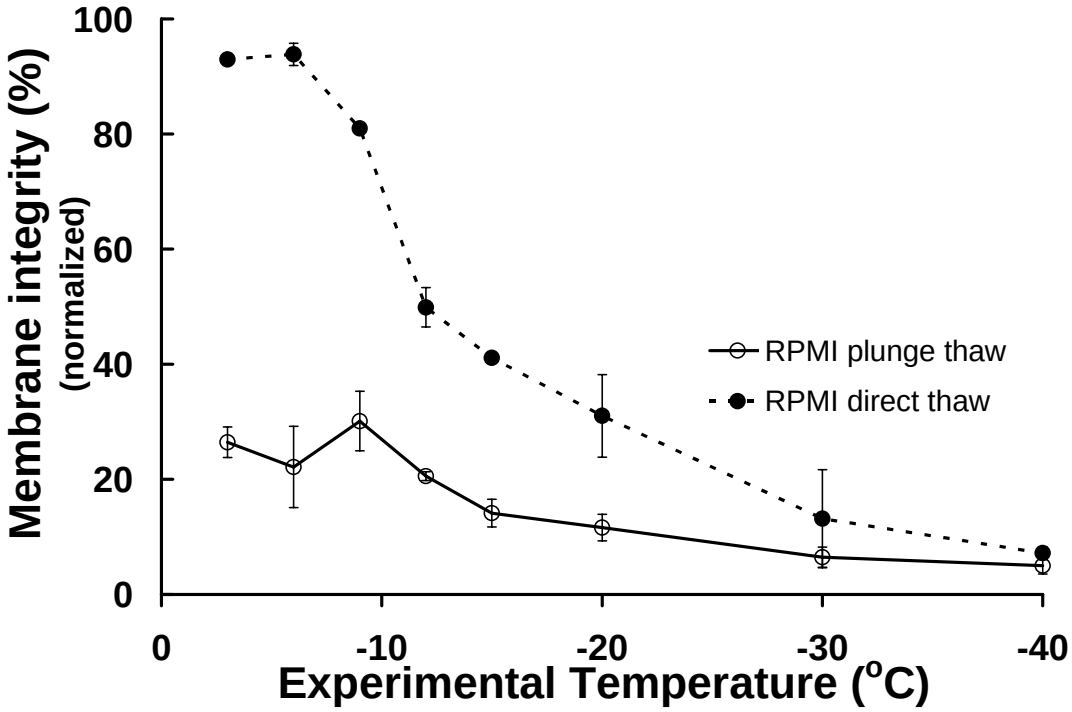

Figure 3-7. Graded freezing without cryoprotectant. Membrane integrity of TF-1 cells (± sem; normalized to controls) in serum-free RPMI media after being cooled at 0.9 °C/min to various subzero experimental temperatures and either thawed directly (dashed) or plunged into liquid nitrogen (solid) prior to thawing.

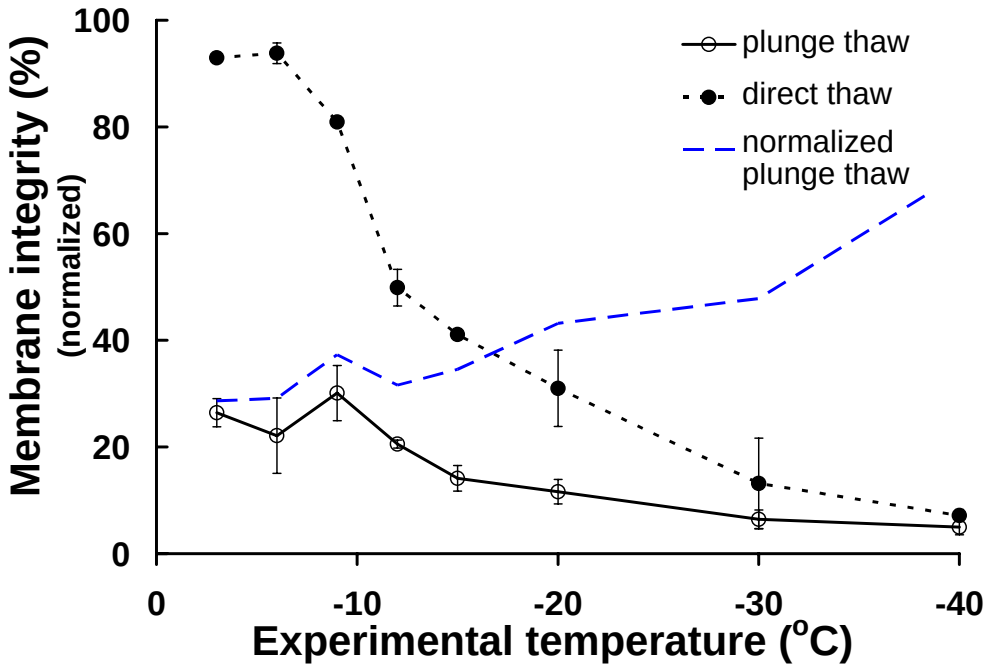

Figure 3-8. Membrane integrity for TF-1 cells (± sem; normalized to controls) in serum-free RPMI following graded freezing, including a plunge-thaw curve normalized with (i.e. as a percentage of) the direct-thaw data (blue long dashes).

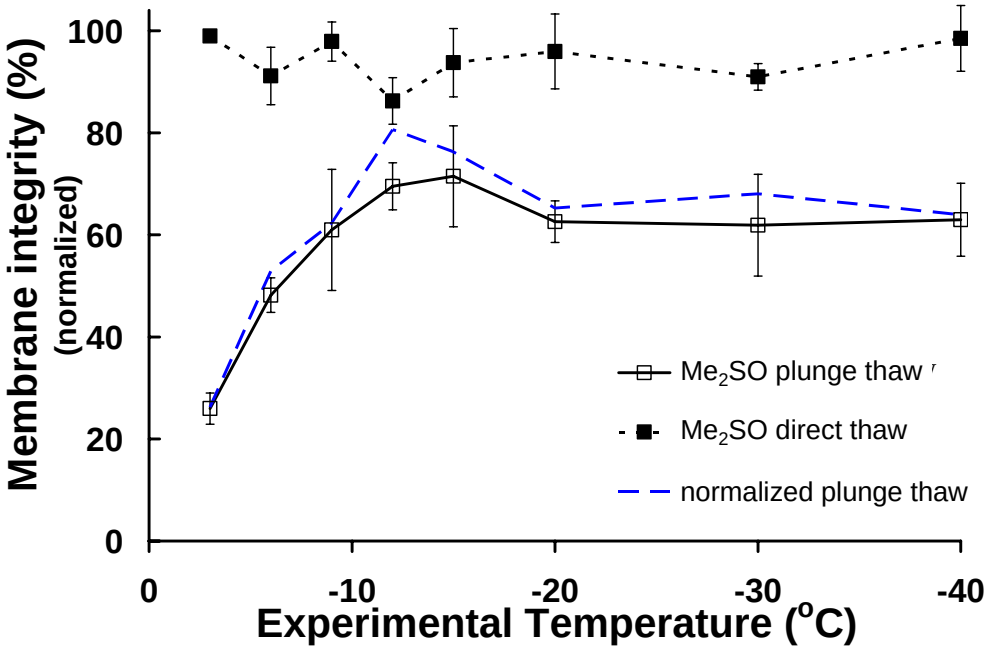

Figure 3-9. Graded freezing with Me_2SO. Membrane integrity of TF-1 cells (± sem; normalized to controls) in 10 % Me_2SO in RPMI media after being cooled at 0.9 °C/min to various subzero experimental temperatures and either thawed directly (dashed) or plunged into liquid nitrogen (solid) prior to thawing. Graph includes a plunge-thaw curve normalized with (i.e. as a percentage of) the direct-thaw data (blue long dashes).

Chapter 4. Simulations of the two-step freezing (rapid cooling interrupted with a hold time) of TF-1 cells[1]

4.1 Introduction

Successful transplantation of hematopoietic stem cells (HSC) depends critically on the number of functional cells transplanted. With the range of stem cell applications in transplant medicine recently expanding beyond hematopoietic applications to cardiology [26] and neurology [41], and with the increasing use of umbilical cord blood (UCB) as a source for stem cell transplants, the need for adequate quantities of stem cells for various applications has become even more apparent. These applications continue to motivate interest in maximizing recovery of stem cells by more effective means of cryopreservation and storage. Specifically, the use of only clinically-approved reagents while achieving high cell recovery and function requires further investigations.

The current procedures for the cryopreservation of HSC use dimethyl sulfoxide (Me_2SO) to alter the intracellular and extracellular solution properties in order to achieve high recovery after cooling at a constant rate to low temperatures. Even with the widespread use of cryopreserved HSC in autologous transplantation, there is morbidity and mortality associated with the use of Me_2SO [6,11,43,56]. With Me_2SO not being

[1] This chapter with minor modifications has been submitted to Cryobiology (2009) as "Investigating cryoinjury using simulations and experiments: 1. TF-1 cells during the two-step freezing (rapid cooling interrupted with a hold time) procedure", L.U. Ross-Rodriguez, J.A.W. Elliott, and L.E. McGann

approved for human use in stem cell transplantation, measures have been taken to reduce or eliminate Me_2SO in the cryopreservation process. One approach has been to wash Me_2SO from the product before infusion, resulting in undesirable cell loss [47,55]. While this loss may not to be significant for peripheral blood stem cell samples [47] where an excess number of stem cells can be collected from the patient, the number of stem cells is a limiting factor in applications of UCB transplants, so additional cell loss due to washing is unacceptable. Other approaches have simply reduced the amount of Me_2SO used in the cryopreservation protocol and there are reports that a minimum of 5 % Me_2SO is necessary for high post-thaw recovery [1,4]. Others have combined a reduced concentration of Me_2SO with a non-penetrating cryoprotectant such as hydroxyethyl starch (HES) [9,16,20]. In clinical trials, high levels of engraftment were maintained with 3.5 % Me_2SO combined with 5 % HES [16]. While these studies attempted to reduce Me_2SO concentration, the same cooling and warming conditions were used, although it has been demonstrated that the optimal cooling and warming rates depend on the nature and concentration of cryoprotectant [25].

Mazur et al.'s 'two-factor hypothesis' [33] proposed that there are two primary mechanisms of damage during cryopreservation: 1) slow cooling injury related to exposure to high solute concentrations as ice forms and solutes concentrate in the residual liquid, and 2) rapid cooling injury related to the presence of ice inside the cell. The current study uses a

two-step cooling procedure as a model for rapid cooling to explore associated cryoinjury. This two-step cooling procedure was described by Farrant et. al. [13,34] as a logical method to investigate the effect of freezing injury on cell recovery. The procedure is based on exposure of cells to a subzero temperature in the presence of extracellular ice for various time intervals before either thawing or rapid cooling to a low storage temperature (-196 °C). This procedure has been used to investigate cryoinjury in several cell types, including hamster lung fibroblasts [14,34], lymphocytes [23], mouse embryos [52], renal cortical slices [5] and islets of Langerhans [3]. Using this procedure (Chapter 3), we have verified that there is a pattern of cell recovery that is consistent for most cell types. For cells thawed directly from the subzero hold temperature, there is a progressive decline in viability at lower hold temperatures. Furthermore, for cells plunged into liquid nitrogen from the hold temperatures before thawing, cell recovery is low at high subzero hold temperatures, and increases at intermediate hold temperatures. This increase is limited by damage incurred during the first cooling step. It is then possible to differentiate between damage incurred during the first cooling step, including the hold time, and during the second cooling step. However, our understanding of cryoinjury using empirical studies alone is still limited.

In contrast to purely empirical studies, this study proposes a fundamentally different approach - to reduce or avoid the need for

cryoprotectants such as Me_2SO by using solution thermodynamic properties (phase diagrams) and knowledge of osmotic transport to generate temperature profiles that will minimize the major causes of cryoinjury. Computer simulations of cellular responses to low temperatures that are based on mathematical calculations of changes in cell volume have previously been used to further understanding of cellular low temperature responses. These models use the osmotic properties of the cell plasma membrane and their temperature dependencies, specific to each cell type, to express theoretical cellular responses to the changes in extracellular osmolality that results from ice formation. The permeability characteristics of the cell membrane regulate water transport and, in turn, intracellular osmolality and intracellular freezing point. Traditionally, cryopreservation protocols have been optimized empirically, but some researchers have explored the use of simulations as a means of predicting low temperature responses of various cell types: peripheral blood stem cells [48]; cord blood stem cells [53]; bull spermatozoa [50]; bovine erythrocytes [24]; rat embryos [27]; porcine chondrocytes [54]; yeast [45]; hamster ova [46]; and human corneal epithelial, endothelial and stromal cells [10]. Karlsson et al. developed a theoretical model for predicting intracellular ice formation during cryopreservation by coupling crystal-growth, ice nucleation, and water transport models [19].

In this study, measured osmotic properties of the TF-1 cells (Chapter 2) were used in simulations of osmotic responses during two-step cooling

procedures to minimize supercooling associated with intracellular ice formation. The erythroleukemic human cell line TF-1 is of particular interest as a model for cryopreservation of HSC, since it expresses the $CD34^+$ antigen and is able to differentiate into the various hematopoietic lineages [21,22,30]. In this study, simulated outcomes were compared to the experimental measurements of TF-1 cell recovery after two-step freezing from Chapter 3. In calculating intracellular supercooling, these simulations used non-dilute solution thermodynamic descriptions of the extra- and intracellular solutions to better describe the solution properties at the high concentrations that occur during the two-step freezing procedures. The correlation between freezing experiments and simulations was used to further our understanding of two-step freezing and the cryopreservation of stem cells without Me_2SO.

4.2 Simulation specifications

Our simulations of cellular responses at low temperatures used four main elements: 1) the change in the composition of the extracellular solution as ice forms at low temperatures; 2) cellular osmotic responses to changes in composition of the extracellular solution and the resulting change in the composition of the intracellular solution; 3) the temperature dependence of the cellular osmotic permeability parameters; and 4) changes in sample temperature as a function of time [42].

4.2.1 Osmolality of the intracellular and extracellular solutions

Phase diagram information [8,12,51] was used to calculate concentrations in the liquid phase for the extracellular and/or intracellular components (Table 4-1a). The extracellular components were assumed to be sodium chloride (NaCl) and potassium chloride (KCl), and the intracellular components were assumed to be NaCl, KCl, and protein. Initial concentrations are given in Table 4-1a. Parameters for the intracellular protein are discussed in the '*Impact of including intracellular protein and nucleation heat*' section, where simulations with and without intracellular protein are compared. The osmotic virial equation (OVE) [12,39] was used to describe the osmolality of binary solutions, taking into account the non-ideal behaviour of real solutes:

$$\pi = m + B m^2 + C m^3; \qquad 4\text{-}1$$

where m is the molality of the solute (moles solute/kg solvent), and B and C are fitting constants for specific solutes in water ((mole/kg solvent)$^{-1}$) (Table 4-1b). For electrolytes, the molality is multiplied by an empirically-determined dissociation constant [37-39]. The constant C in the osmotic virial equation is non-zero only for solutes with highly nonlinear behaviour, such as macromolecules [15,17,40]. The following multisolute OVE, proposed by Elliott et al. [12], was used to calculate osmolality of solutions containing n solutes:

$$\pi = \sum_{i=1}^{n} m_i + \sum_{i=1}^{n}\sum_{j=1}^{n}\left(\frac{B_i + B_j}{2} m_i\, m_j\right) + \sum_{i=1}^{n}\sum_{j=1}^{n}\sum_{k=1}^{n}\left(C_i\, C_j\, C_k\right)^{1/3} m_i\, m_j\, m_k \; ; \qquad 4\text{-}2$$

where, in addition to the terms arising from the summation of an Eq. 4-1 for each solute, Eq. 4-2 includes terms describing interactions between solutes (*i*, *j* and *k*). The freezing point depression of the solution is related to the osmolality by:

$$T_{FP}^{o} - T_{FP} = 1.86\pi \; ; \qquad 4\text{-}3$$

where T_{FP}^{o} is the freezing point of the pure solvent (water) and T_{FP} is the freezing point of the solution.

4.2.2 Cellular osmotic parameters

The cellular osmotic parameters for TF-1 cells were previously determined from experimental measurements using an electronic particle counter in Chapter 2. The cellular osmotic parameters used in the simulations are the isotonic volume, the hydraulic conductivity, and the osmotically-inactive fraction. Jacobs and Stewart [18] used the following equation to describe the rate of water movement across the plasma membrane:

$$\frac{dV}{dt} = L_p ART\rho(\pi_i - \pi_e); \qquad 4\text{-}4$$

where V is the volume of water in the cell (μm^3), t is the time (min), L_p is the hydraulic conductivity ($\mu m^3/\mu m^2/min/atm$), A is the cell surface area (μm^2), R is the universal gas constant ($\mu m^3 \cdot atm/mol/K$), T is the absolute temperature (K), ρ is the density of water (assumed to be constant at 1.0 x 10^{-15} $kg/\mu m^3$), π_e is the extracellular osmolality (osmoles/kg of water), and π_i is the intracellular osmolality (osmoles/kg of water). In these calculations, the cell surface area was calculated from the spherical cell volume.

The osmotically-inactive fraction is the fraction of the cell volume not involved in the osmotic activities of the cell. The Boyle van't Hoff relationship [29] was used to express equilibrium cell volume in solutions of impermeant solutes:

$$\frac{V}{V_o} = \frac{\pi^o}{\pi}(1-b)+b \quad ; \qquad 4\text{-}4$$

where V is the equilibrium cell volume (μm^3) at osmolality π (osmoles/kg water), V_o is the isotonic cell volume (μm^3), π^o is the isotonic osmolality (osmoles/kg water), and b is the osmotically-inactive fraction of the cell volume, a parameter calculated by fitting Eq. 4-5 to experimental data. The temperature dependence of L_p is normally described with an Arrhenius relationship [35]:

$$L_p = k \exp(\frac{-E_a}{RT}); \quad \text{4-5}$$

where k is a pre-exponential factor ($\mu m^3/\mu m^2/min/atm$), E_a is the Arrhenius activation energy (kcal/mol), R is the universal gas constant (kcal/mol/K), and T is the absolute temperature (K). Values for all the osmotic parameters are reported in Table 4-1c. Given these parameters, cell volume can be calculated for the simulations at a specific temperature, osmolality, and time.

4.2.3 The temperature profile

The two-step freezing procedure involves rapidly cooling samples to various subzero hold temperatures, holding at that temperature for a duration ("hold time"), and then either thawing samples directly in a 37 °C water bath (direct thaw) or plunging samples into liquid nitrogen first and then thawing (plunge thaw) (Figure 4-1). Simulations used the actual measured temperature profiles.

4.2.4 Numerical methods

A computer program was developed (L. E. McGann) with the Delphi programming language to perform the calculations in Eqs. 4-2 to 4-6, using Euler's method with sufficiently small discretization to solve the differential equations. Measured temperature profiles in the experimental samples were used in the simulations. Since the cells are initially in osmotic equilibrium with the isotonic extracellular solution, no osmotic changes occur before ice nucleation. The assumptions used in the

simulations are a) the simulation begins on ice nucleation at the freezing point of the extracellular solution, b) the extracellular solution remains in equilibrium with extracellular ice. The simulations do not include the formation of intracellular ice; rather, we use intracellular supercooling as an indicator of the likelihood of intracellular ice formation.

Simulations were performed using measured osmotic parameters of TF-1 cells, i.e. the isotonic cell volume, V_o, the osmotically-inactive fraction, b, the pre-exponential factor, k_1, and the activation energy, E_a, for L_p, previously described in more detail in Chapter 2 and listed in Table 4-1c. Results of the simulations were compared with previously-reported two-step freezing experimental results for TF-1 cells (Chapter 3).

4.3 Experimental materials and methods

4.3.1 TF-1 cell freezing experiments

Descriptions of the TF-1 cell culture and freezing experiments have been previously reported in detail (Chapter 3). Briefly, TF-1 cells (ATCC, Manassas, VA, USA) were cultured according to ATCC guidelines. Samples of 0.2 mL TF-1 cell suspension, in serum-free RPMI (ATCC), in glass tubes (6x50 mm; Fisher, Edmonton, AB, Canada) were transferred into a stirred methanol bath (FTS Systems, Inc., Stone Ridge, NY, USA) preset at -3, -6, -9, -12, -15, -20, or -30 °C and allowed to equilibrate for 2 minutes at that temperature prior to ice nucleation with cold forceps. After nucleation, samples were held at the experimental temperature for

3 minutes before either thawing in a 37 °C water bath or being plunged into liquid nitrogen. Samples were kept in liquid nitrogen for a minimum of 1 hour prior to being thawed in a 37 °C water bath. SYTO®13 (Molecular Probes, Eugene, OR, USA) and ethidium bromide (EB) (Sigma, Mississauga, ON, Canada) were used as a cell membrane integrity assay for freeze-thaw injury.

4.3.2 Cooling profiles

Cooling profiles were measured using a Type T thermocouple (Omega, Laval, QC, Canada) in samples paralleling the two-step freezing experiments. Simulations for the two-step freezing technique used measured temperature profiles of the experimental system.

4.4 Results and discussion

4.4.1 Two-step cooling simulations

Figure 4-2 shows the temperature measurements of samples placed in baths at various hold temperatures ranging from -3 °C to -30 °C, nucleated, and then held for 3 minutes prior to rapidly cooling to liquid nitrogen temperature (250 °C/min) (profiles shown to -40 °C). These temperature profiles were used in the simulations, beginning at the freezing point of the solution after ice nucleation, as shown in the inset of Figure 4-2. The first step and the second (plunge) step of the cooling process, as well as the hold temperatures, are indicated on the figure. Using these temperature profiles and the parameters listed in Table 4-1,

cellular osmotic responses were calculated. Figure 4-3a shows the calculated cell volumes as a function of time for the corresponding cooling profiles shown in Figure 4-2. Cell volumes decreased with time during the 3 minute hold, with the degree of shrinkage dependent on the hold temperature. There was a small additional cell shrinkage during the plunge step. Figure 4-3b shows the calculated cell volumes as a function of temperature, which allows correlation of changes in cell volume with the stage of the cooling protocol. Cell volumes decreased with hold temperature during the hold time, with a small additional decrease during the plunge step.

Figure 4-4a shows calculated intracellular supercooling as a function of time after nucleation and demonstrates varying degrees of intracellular supercooling during the first cooling step to the hold temperature and during the second step (i.e. supercooling reached in the second step by the time the cells are cooled to -40 °C). For the first step, the lower the hold temperature, the higher the degree of intracellular supercooling. All hold temperatures then have a decrease in supercooling during the hold time as water leaves the cell. There is an additional increase in calculated supercooling during the second (plunge) step. Figure 4-4b shows supercooling as a function of temperature and demonstrates a similar pattern of supercooling for all hold temperatures, with the exception of -3 °C. There is an initial increase in supercooling during the first step, followed by a decrease to 0 °C supercooling during

the hold time, and then followed by another increase in supercooling during the second step. This figure illustrates how the increases in supercooling during each step of the two-step freezing procedure differ for different hold temperatures. This is the direct result of the cell not losing as much water during the previous stages of the cooling profile. Cells are likely to freeze intracellularly at higher degrees of supercooling. The simulations were stopped at -40 °C since it has been suggested previously that when no cryoprotectant is present, injury resulting from exposure to low temperatures occurs at temperatures above -40 °C [14,28], the homogeneous nucleation temperature for water is -39 °C, and the accuracy of extrapolating simulations to lower temperatures is questionable.

The maximum supercooling for all the cooling profiles was calculated for each step of the freezing procedure and plotted in Figure 4-5. There is a progressive increase in the amount of supercooling reached in the first cooling step with decreasing hold temperature, indicating an increased likelihood of intracellular ice formation. There is also a progressive decrease in supercooling in the second cooling step, as cells become increasingly dehydrated at the lower hold temperatures before plunging into liquid nitrogen.

4.4.2 Comparison of two-step freezing experiments with simulations

The maximum intracellular supercooling calculated for each step of the cooling profile was used to interpret loss of membrane integrity after

two-step cooling experiments. Previously shown (Chapter 3) membrane integrity data as a function of hold temperature for TF-1 cells with a 3 minute hold time are shown in Figure 4-6. This figure divides the temperature scale into 3 sections. In section 1, there is minimal loss of membrane integrity for the direct thaw samples; in section 2, there is a decline in membrane integrity for the direct thaw samples with decreasing hold temperatures; and in section 3, there is no further change in membrane integrity with decreasing hold temperatures. The first section (0 to -9 °C) shows minimal loss of membrane integrity for direct-thaw samples and the corresponding section 1 in Figure 4-5 shows low maximum supercooling in the first step. TF-1 cells can therefore withstand ~4 °C of supercooling for 3 minutes without loss of membrane integrity. The decrease in membrane integrity at lower subzero temperatures (sections 2 and 3) also corresponds to an increase in supercooling in the first step. The membrane integrity decreases to 20 % at 18 °C of supercooling and there is no further decrease at lower hold temperatures.

The plunge-thaw membrane integrity results could also be interpreted using calculated maximum supercooling in the second step. In section 1 of Figure 4-5 (0 to -9 °C), high maximum supercooling in the second step corresponded with ~50 % loss of membrane integrity. Section 2 in Figure 4-6 (-9 to -20 °C) shows an increase in membrane integrity, which is consistent with a decrease in maximum supercooling reached in the second step. However, membrane integrity in this section

is limited by damage incurred in the first cooling step, a trend that is continued in section 3 (-20 to -30 °C).

An overall comparison between maximum supercooling (Figure 4-5) and membrane integrity (Figure 4-6) indicates that TF-1 cells can withstand a smaller amount of supercooling in the first step than in the second step. For example, TF-1 cells, with a hold temperature of -20 °C for the first step, and supercooled by a maximum of 18 °C during the first step, have low membrane integrity (~30 %). Conversely, TF-1 cells, with a hold temperature of -15 °C, and supercooled by a maximum of 21 °C in the second step are less damaged (membrane integrity ~62 %). Mazur also proposed that there is a 10 °C limit to supercooling, above which the probability of the formation of intracellular ice is significantly increased [31]. In this study, greater than ~4 °C supercooling in the first step (at higher temperatures) and ~20 °C in the second step (at lower temperatures) leads to membrane damage associated with intracellular ice formation. Hence, it is at intermediate hold temperatures (-6 to -15 °C) for a 3 minute hold time that an optimal range of hold temperatures may occur that minimizes the likelihood of intracellular ice formation after both steps of the freezing protocol.

4.4.3 Impact of including intracellular protein and nucleation heat

Solution properties of the cytoplasm are complex and have yet to be elucidated for nucleated cells. We assumed the non-ideality of the solution thermodynamics of the cytoplasm to be attributed to proteins and

electrolytes. We also assumed the protein component in TF-1 cells to have similar thermodynamic properties to hemoglobin, which are well known. It has been reported that red blood cells contain approximately 7.3 mmol of hemoglobin per kg of intracellular water [8,44,49]. The amount of intracellular protein in nucleated cells has been reported to be more than half the dry weight of the cell [2]. Since the intracellular protein content for TF-1 cells is not known, we used a value of 3.65 mmolal which was 50 % the molality of hemoglobin in red blood cells. In simulations reported by de Freitas et al. [7], an intracellular protein concentration of 4 mosmol/L was used, which is similar to the concentration used in this study. The inclusion of protein as an intracellular component had a minimal effect on the calculated maximum supercooling in simulations of two-step cooling (Figure 4-7).

Simulations in this study were based on measured temperature profiles from two-step freezing experiments that included the effects of nucleation heat. Figure 4-8a shows temperature as a function of time for cooling profiles which did not include the change in temperature associated with nucleation. The effects of the assumed temperature profile and the measured temperature profile on the calculated maximum supercooling are shown in Figure 4-8b. Using a measured temperature profile, which includes the effects of nucleation heat, changes the calculated maximum supercooling for both steps of the cooling profile only at high subzero temperatures.

4.5 Conclusions

This study used an approach of calculating supercooling of the cytoplasm in the presence of extracellular ice as an indicator of the likelihood of cryoinjury. A non-dilute solution thermodynamic description [12] of the extra- and intra-cellular solutions was used to calculate intracellular supercooling. Simulations of an empirical approach of two-step freezing were used to examine the role of exposure to subzero hold temperatures and exposure time. A comparison of simulations and experimental measurements of membrane integrity supports the concept that, for two-step cooling, increasing intracellular supercooling is the primary contributor to potential freezing injury due to the increase in the likelihood of intracellular ice formation. These studies also support the upper limit for tolerable intracellular supercooling previously reported by others during the first step of cooling [31,32,36]. However, a comparison of experimental data with simulations showed that TF-1 cells were able to withstand considerably higher degrees of supercooling in the second step than during the first step.

Supercooling appears to play a determining role in cell recovery in two-step cryopreservation protocols, particularly for cells plunged from high subzero hold temperatures. By calculating intracellular supercooling for each step separately and comparing these calculations with cell recovery data, it was demonstrated that it is not optimal simply to limit overall supercooling during two-step freezing procedures. More aptly,

appropriate limitations of supercooling differ from the first step to the second step. Since water movement across the cell membrane is temperature-dependent, cells need to be exposed to conditions (i.e. subzero hold temperatures) that allow sufficient osmotic water efflux from the cell before cooling to lower subzero temperatures, to prevent high supercooling and the likelihood of intracellular ice formation. During the hold step at high subzero hold temperatures, the incidence of intracellular ice formation is low because supercooling is low. However, during the subsequently plunge step, the amount of supercooling is high because of limited cellular dehydration. At intermediate subzero hold temperatures, the supercooling is higher (i.e. more extracellular ice) so cells become more dehydrated. During the plunge step, the additional supercooling before cells reach -40 °C is minimized thus decreasing the chance of intracellular ice formation. Therefore, in order to ensure that cells are sufficiently dehydrated before the plunge step, cells must be exposed to higher amounts of supercooling at higher subzero hold temperatures. The proposed target hold temperature determined from experimental results was suggested to be between -5 °C and -15 °C (Chapter 3), corresponding to a maximum supercooling of less than 10 °C in the first step. In this study using TF-1 cells, supercooling greater than ~4 °C in the first step and ~20 °C in the second step resulted in membrane damage associated with intracellular ice formation.

Based on the sensitivity analysis, the inclusion of protein, as an

intracellular component, minimally affected maximum supercooling. Also, using an assumed temperature profile, instead of a measured temperature profile (i.e. including the effects of nucleation heat) in this experimental set-up, changes the calculated maximum supercooling for both steps of the cooling profile at high subzero hold temperatures. This change was minimal, so it would be acceptable to neglect the effects of nucleation heat for two-step simulations without cryoprotectant for small volume systems.

This study demonstrates the usefulness of simulations, combined with two-step freezing experiments, in attempting to provide understanding into the complexities of establishing cryopreservation protocols for a particular cell type. Specifically, two-step freezing provides useful insight into the mechanisms of damage inflicted by cooling over a range of subzero temperatures [14], allowing manipulation of different variables of the cryopreservation protocol for any cell type for which the osmotic parameters are known. The implications for this work extend beyond TF-1 and stem cells, to any cell type with known osmotic parameters. This study also demonstrates the value of a combination of theoretical and empirical work for interpretation of cryopreservation protocols. Based on the results presented in this work, the use of rapid non-linear cooling profiles in simulations were integral to understanding the successful results for the cryopreservation of TF-1 cells without Me_2SO.

4.6 References

[1] J.F. Abrahamsen, A.M. Bakken, and O. Bruserud, Cryopreserving human peripheral blood progenitor cells with 5-percent rather than 10-percent DMSO results in less apoptosis and necrosis in CD34+cells. Transfusion 42 (2002) 1573-1580.

[2] B. Alberts, D. Bray, J. Lewis, M. Raff, K. Roberts, and J.D. Watson, Molecular biology of the cell, Garland Publishing, Inc, New York & London, 1994.

[3] H.L. Bank, and L. Reichard, Cryogenic preservation of isolated islets of Langerhans: two-step cooling. Cryobiology 18 (1981) 489-96.

[4] F. Beaujean, J.H. Bourhis, C. Bayle, H. Jouault, M. Divine, C. Rieux, M. Janvier, C. Le Forestier, and J.L. Pico, Successful cryopreservation of purified autologous CD34(+) cells: influence of freezing parameters on cell recovery and engraftment. Bone Marrow Transplant. 22 (1998) 1091-1096.

[5] P. Clark, H.E. Hawkins, and A.M. Karow, The Influence of Temperature on the Function of Renal Cortical Slices Frozen in Various Cryoprotectants. Cryobiology 22 (1985) 156-160.

[6] J.M. Davis, S.D. Rowley, H.G. Braine, S. Piantadosi, and G.W. Santos, Clinical toxicity of cryopreserved bone-marrow graft infusion. Blood 75 (1990) 781-786.

[7] R.C. de Freitas, K.R. Diller, J.R. Lakey, and R.V. Rajotte, Osmotic behavior and transport properties of human islets in a dimethyl

sulfoxide solution. Cryobiology 35 (1997) 230-239.

[8] D.A.T. Dick, and L.M. Lowenstein, Osmotic equilibria in human erythrocytes studied by immersion refractometry. Proceedings of the Royal Society of London Series B-Biological Sciences 148 (1958) 241-256.

[9] C. Donaldson, W.J. Armitage, P.A. DenningKendall, A.J. Nicol, B.A. Bradley, and J.M. Hows, Optimal cryopreservation of human umbilical cord blood. Bone Marrow Transplant. 18 (1996) 725-731.

[10] S.L. Ebertz, and L.E. McGann, Osmotic parameters of cells from a bioengineered human corneal equivalent and consequences for cryopreservation. Cryobiology 45 (2002) 109-117.

[11] M.J. Egorin, D.M. Rosen, R. Sridhara, L. Sensenbrenner, and M. Cottler-Fox, Plasma concentrations and pharmacokinetics of dimethylsulfoxide and its metabolites in patients undergoing peripheral-blood stem-cell transplants. Journal of Clinical Oncology 16 (1998) 610-615.

[12] J.A.W. Elliott, R.C. Prickett, H.Y. Elmoazzen, K.R. Porter, and L.E. McGann, A multi-solute osmotic virial equation for solutions of interest in biology. Journal of Physical Chemistry B 111 (2007) 1775-1785.

[13] J. Farrant, S.C. Knight, L.E. McGann, and J. O'Brien, Optimal recovery of lymphocytes and tissue culture cells following rapid cooling. Nature 249 (1974) 452-3.

[14] J. Farrant, C.A. Walter, H. Lee, and L.E. McGann, Use of two-step

cooling procedures to examine factors influencing cell survival following freezing and thawing. Cryobiology 14 (1977) 273-286.

[15] J. Gaube, A. Pfennig, and M. Stumpf, Vapor-liquid equilibrium in binary and ternary aqueous solutions of poly(ethylene glycol) and dextran. J. Chem. Eng. Data 38 (1993) 163-166.

[16] P. Halle, O. Tournilhac, W. Knopinska-Posluszny, J. Kanold, P. Gembara, N. Boiret, C. Rapatel, M. Berger, P. Travade, S. Angielski, J. Bonhomme, and F. Demeocq, Uncontrolled-rate freezing and storage at-80 degrees C, with only 3.5-percent DMSO in cryoprotective solution for 109 autologous peripheral blood progenitor cell transplantations. Transfusion 41 (2001) 667-673.

[17] C.A. Haynes, R.A. Beynon, R.S. King, H.W. Blanch, and J.M. Prausnitz, Thermodynamic properties of aqueous polymer solutions: poly(ethylene glycol)/Dextran. J. Phys. Chem. 93 (1989) 5612-5617.

[18] M.H. Jacobs, and D.R. Stewart, A simple method for the quantitative measurement of cell permeability. J. Cell. Comp. Physiol. 1 (1932) 71-82.

[19] J.O.M. Karlsson, E.G. Cravalho, and M. Toner, A model of diffusion-limited ice growth inside biological cells during freezing. Journal of Applied Physics 75 (1994) 4442-4445.

[20] Y. Katayama, T. Yano, A. Bessho, S. Deguchi, K. Sunami, N. Mahmut, K. Shinagawa, E. Omoto, S. Makino, T. Miyamoto, S. Mizuno, T. Fukuda, T. Eto, T. Fujisaki, Y. Ohno, S. Inaba, Y. Niho,

and M. Harada, The effects of a simplified method for cryopreservation and thawing procedures on peripheral blood stem cells. Bone Marrow Transplant. 19 (1997) 283-287.

[21] T. Kitamura, T. Tange, T. Terasawa, S. Chiba, T. Kuwaki, K. Miyagawa, Y.F. Piao, K. Miyazono, A. Urabe, and F. Takaku, Establishment and characterization of a unique human cell line that proliferates dependently on GM-CSF, IL-3, or erythropoietin. J. Cell. Physiol. 140 (1989) 323-34.

[22] T. Kitamura, A. Tojo, T. Kuwaki, S. Chiba, K. Miyazono, A. Urabe, and F. Takaku, Identification and analysis of human erythropoietin receptors on a factor-dependent cell-line, TF-1. Blood 73 (1989) 375-380.

[23] S.C. Knight, J. Farrant, and L.E. McGann, Storage of human lymphocytes by freezing in serum alone. Cryobiology 14 (1977) 112-5.

[24] S.P. Leibo, Freezing damage of bovine erythrocytes - simulation using glycerol concentration changes at subzero temperatures. Cryobiology 13 (1976) 587-598.

[25] S.P. Leibo, J. Farrant, P. Mazur, M.G. Hanna, Jr., and L.H. Smith, Effects of freezing on marrow stem cell suspensions: interactions of cooling and warming rates in the presence of PVP, sucrose, or glycerol. Cryobiology 6 (1970) 315-32.

[26] A.C. Lindsay, and J.P. Halcox, Stem cells as future therapy in

cardiology. Hosp. Med. 66 (2005) 215-20.

[27] J. Liu, E.J. Woods, Y. Agca, E.S. Critser, and J.K. Critser, Cryobiology of rat embryos II: A theoretical model for the development of interrupted slow freezing procedures. Biology of Reproduction 63 (2000) 1303-1312.

[28] J.E. Lovelock, The mechanism of the protective action of glycerol against haemolysis by freezing and thawing. Biochim Biophys Acta 11 (1953) 28-36.

[29] B. Lucke, and M. McCutcheon, The living cell as an osmotic system and its permeability to water. Physiol. Rev. 12 (1932) 68-139.

[30] M. Marone, G. Scambia, G. Bonanno, S. Rutella, D. de Ritis, F. Guidi, G. Leone, and L. Pierelli, Transforming growth factor-beta 1 transcriptionally activates CD34 and prevents induced differentiation of TF-1 cells in the absence of any cell-cycle effects. Leukemia 16 (2002) 94-105.

[31] P. Mazur, Kinetics of water loss from cells at subzero temperatures and the likelihood of intracellular freezing. The Journal of General Physiology 47 (1963) 347-369.

[32] P. Mazur, Role of intracellular freezing in death of cells cooled at supraoptimal rates. Cryobiology 14 (1977) 251-272.

[33] P. Mazur, S.P. Leibo, and E.H. Chu, A two-factor hypothesis of freezing injury. Evidence from Chinese hamster tissue-culture cells. Exp. Cell Res. 71 (1972) 345-55.

[34] L.E. McGann, and J. Farrant, Survival of tissue culture cells frozen by a two-step procedure to -196 degrees C. I. Holding temperature and time. Cryobiology 13 (1976) 261-268.

[35] J.J. McGrath, Membrane transport properties. in: J.J. McGrath, and K.R. Diller, (Eds.), Low temperature biotechnology emerging applications and engineering contributions, The American Society of Mechanical Engineers, New York, 1988, pp. 273-330.

[36] K. Muldrew, and L.E. McGann, Mechanisms of intracellular ice formation. Biophysical Journal 57 (1990) 525-532.

[37] R.H. Petrucci, and W.S. Harwood, General Chemistry: principles and modern applications, Prentice-Hall, Upper Saddle River, New Jersey, USA, 2007.

[38] R.C. Prickett, J.A.W. Elliott, and L.E. McGann, Application of multisolute osmotic virial equation to solutions containing electrolytes. In preparation (2009).

[39] R.C. Prickett, J.A.W. Elliott, and L.E. McGann, Application of the osmotic virial equation in cryobiology. Cryobiology (accepted) (2009).

[40] S.J. Rathbone, C.A. Haynes, H.W. Blanch, and J.M. Prausnitz, Thermodynamic properties of dilute aqueous polymer solutions from low-angle laser-light-scattering measurements. Macromolecules 23 (1990) 3944-3947.

[41] C.M. Rice, C.A. Halfpenny, and N.J. Scolding, Stem cells for the treatment of neurological disease. Transfus. Med. 13 (2003) 351-61.

[42] L.U. Ross-Rodriguez, Using simulations to design a cryopreservation procedure for hematopoietic stem cells without DMSO, Medical Sciences - Laboratory Medicine and Pathology, University of Alberta, Edmonton, 2003, pp. 111.

[43] N.C. Santos, J. Figueira-Coelho, J. Martins-Silva, and C. Saldanha, Multidisciplinary utilization of dimethyl sulfoxide: pharmacological, cellular, and molecular aspects. Biochem. Pharmacol. 65 (2003) 1035-1041.

[44] D. Savitz, V.W. Sidel, and A.K. Solomon, Osmotic Properties of Human Red Cells. Journal of General Physiology 48 (1964) 79-94.

[45] G.J. Schwartz, and K.R. Diller, Osmotic response of individual cells during freezing .1. Experimental volume measurements. Cryobiology 20 (1983) 61-77.

[46] M. Shabana, and J.J. Mcgrath, Cryomicroscope investigation and thermodynamic modeling of the freezing of unfertilized hamster ova. Cryobiology 25 (1988) 338-354.

[47] R. Syme, M. Bewick, D. Stewart, K. Porter, T. Chadderton, and S. Gluck, The role of depletion of dimethyl sulfoxide before autografting: on hematologic recovery, side effects, and toxicity. Biol. Blood Marrow Transplant. 10 (2004) 135-41.

[48] M.R. Tijssen, H. Woelders, A. de Vries-van Rossen, C.E. van der Schoot, C. Voermans, and J.M. Lagerberg, Improved postthaw viability and in vitro functionality of peripheral blood hematopoietic

progenitor cells after cryopreservation with a theoretically optimized freezing curve. Transfusion 48 (2008) 893-901.

[49] F.T. Williams, C.C. Fordham, III, W. Hollander, Jr., and L.G. Welt, A Study of the Osmotic Behaviour of the Human Erythrocyte. Journal of Clinical Investigation 38 (1959) 1587-98.

[50] H. Woelders, and A. Chaveiro, Theoretical prediction of 'optimal' freezing programmes. Cryobiology 49 (2004) 258-271.

[51] J. Wolfe, and G. Bryant, Freezing, drying, and/or vitrification of membrane- solute-water systems. Cryobiology 39 (1999) 103-129.

[52] M.J. Wood, and J. Farrant, Preservation of mouse embryos by two-step freezing. Cryobiology 17 (1980) 178-80.

[53] E.J. Woods, J. Liu, K. Pollok, J. Hartwell, F.O. Smith, D.A. Williams, M.C. Yoder, and J.K. Critser, A theoretically optimized method for cord blood stem cell cryopreservation. J Hematother Stem Cell Res 12 (2003) 341-350.

[54] W.T. Wu, S.-R. Lyu, and W.H. Hsieh, Cryopreservation and biophysical properties of articular cartilage chondrocytes. Cryobiology 51 (2005) 330-338.

[55] H. Yang, Effects of incubation temperature and time after thawing on viability assessment of peripheral hematopoietic progenitor cells cryopreserved for transplantation. Bone Marrow Transplant. 32 (2003) 1021-1026.

[56] A. Zambelli, G. Poggi, G. Da Prada, P. Pedrazzoli, A. Cuomo, D.

Miotti, C. Perotti, P. Preti, and G.R. Della Cuna, Clinical toxicity of cryopreserved circulating progenitor cells infusion. Anticancer Res. 18 (1998) 4705-4708.

Table 4-1. Parameters used in simulations: (a) isotonic solution composition, (b) solution parameters, and (c) osmotic parameters for TF-1 cells

a) Isotonic solution composition

	Extracellular	Intracellular
NaCl	0.170 molal	0.010 molal
KCl	0.005 molal	0.133 molal
Protein	0	0.004 molal
Total Osmolality	0.300 osm/kg	0.300 osm/kg

b) Solution parameters [12]

	B (mol/kg solvent)$^{-1}$	C (mol/kg solvent)$^{-2}$	K
NaCl	0.02986	0	1.702
KCl	0	0	1.742
Protein†	49.3	3.07×10^{4}	1

c) Osmotic parameters [Chapter 2]

Isotonic volume, V_o	916 μm^3
Inactive fraction, b	0.361
E_a (Activation Energy for L_p)	14.2 kcal/mol
k_1 (Pre-exponential factor for L_p)	1.33×10^{10} $\mu m^3/\mu m^2$/min/atm

†based on values reported for hemoglobin
L_p is for hydraulic conductivity

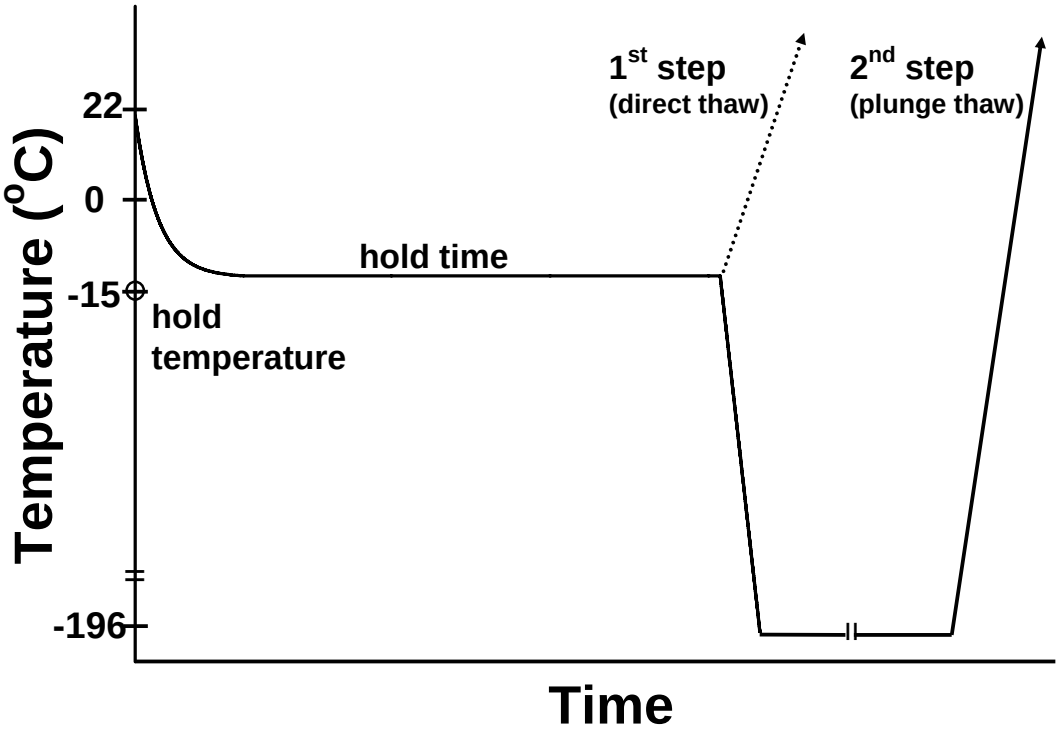

Figure 4-1. A schematic of two-step freezing, including initial rapid non-linear cooling to hold temperature, hold time, and either directly thawing, or plunging, and then thawing, following storage time (Chapter 3).

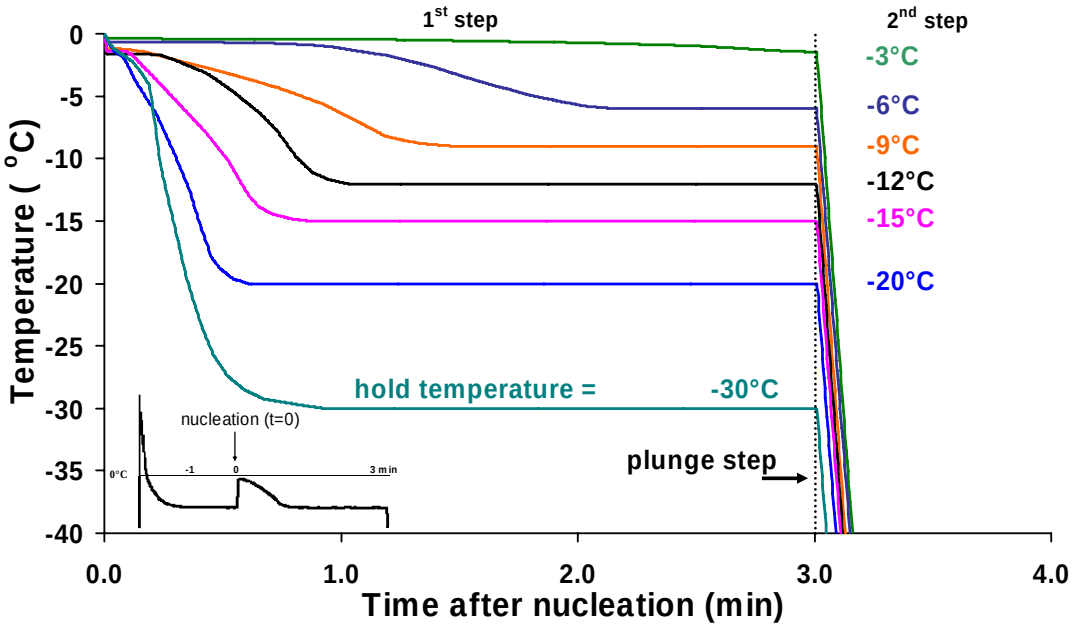

Figure 4-2. Simulation input temperature as a function of time, measured post-nucleation during equilibration at various subzero hold temperatures (-3°C to -30°C) for 3 minutes, prior to rapid cooling (250°C/min). The nucleation and hold step (1st step), and the plunge step (2nd step) are indicated on the graph. The figure insert shows the entire measured temperature profile including prior to the nucleation step for one set of experimental conditions.

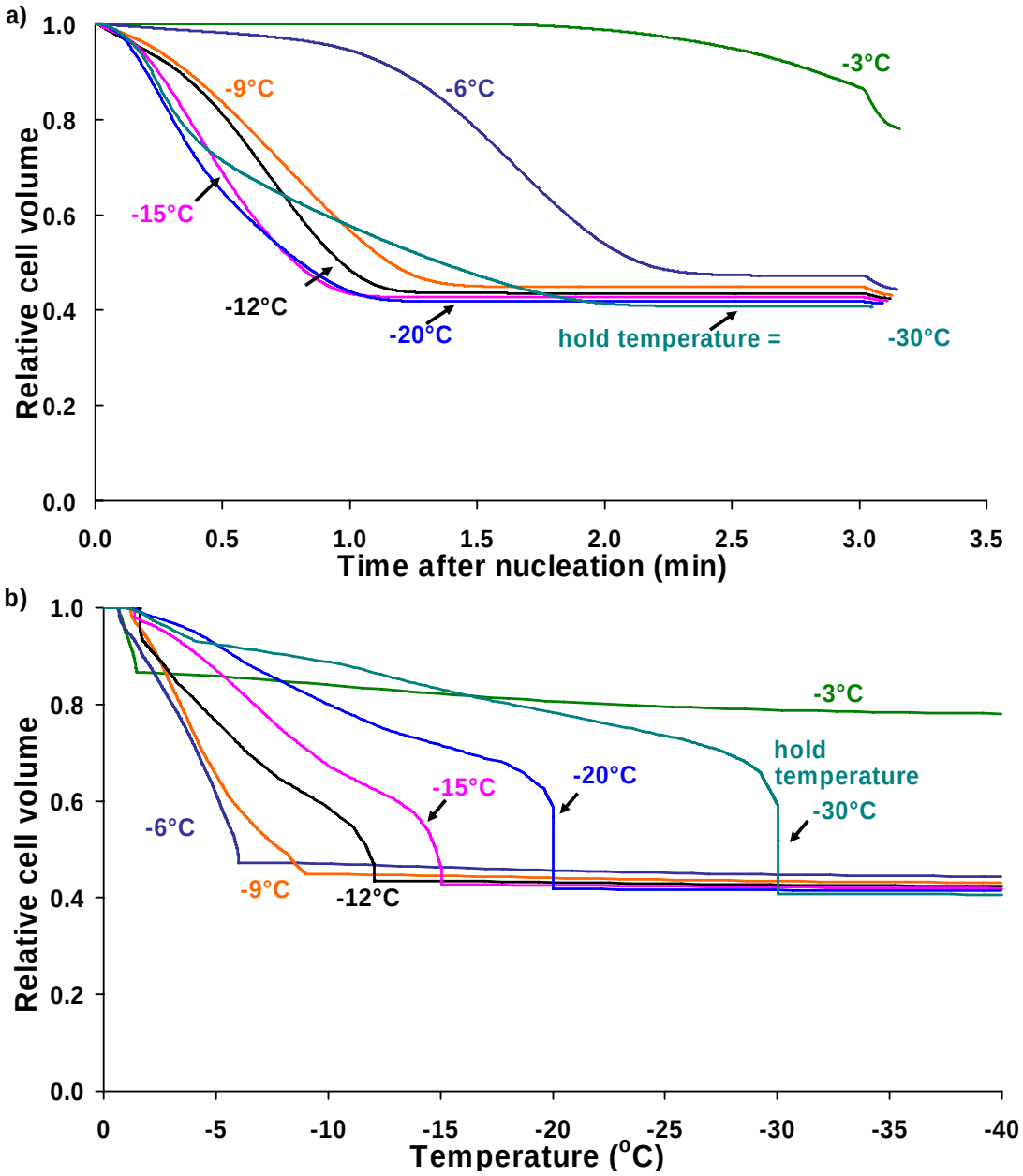

Figure 4-3. Calculated relative cell volume as a function of (a) time after nucleation and (b) temperature for TF-1 cells cooled according to the temperature profiles in Figure 4-2.

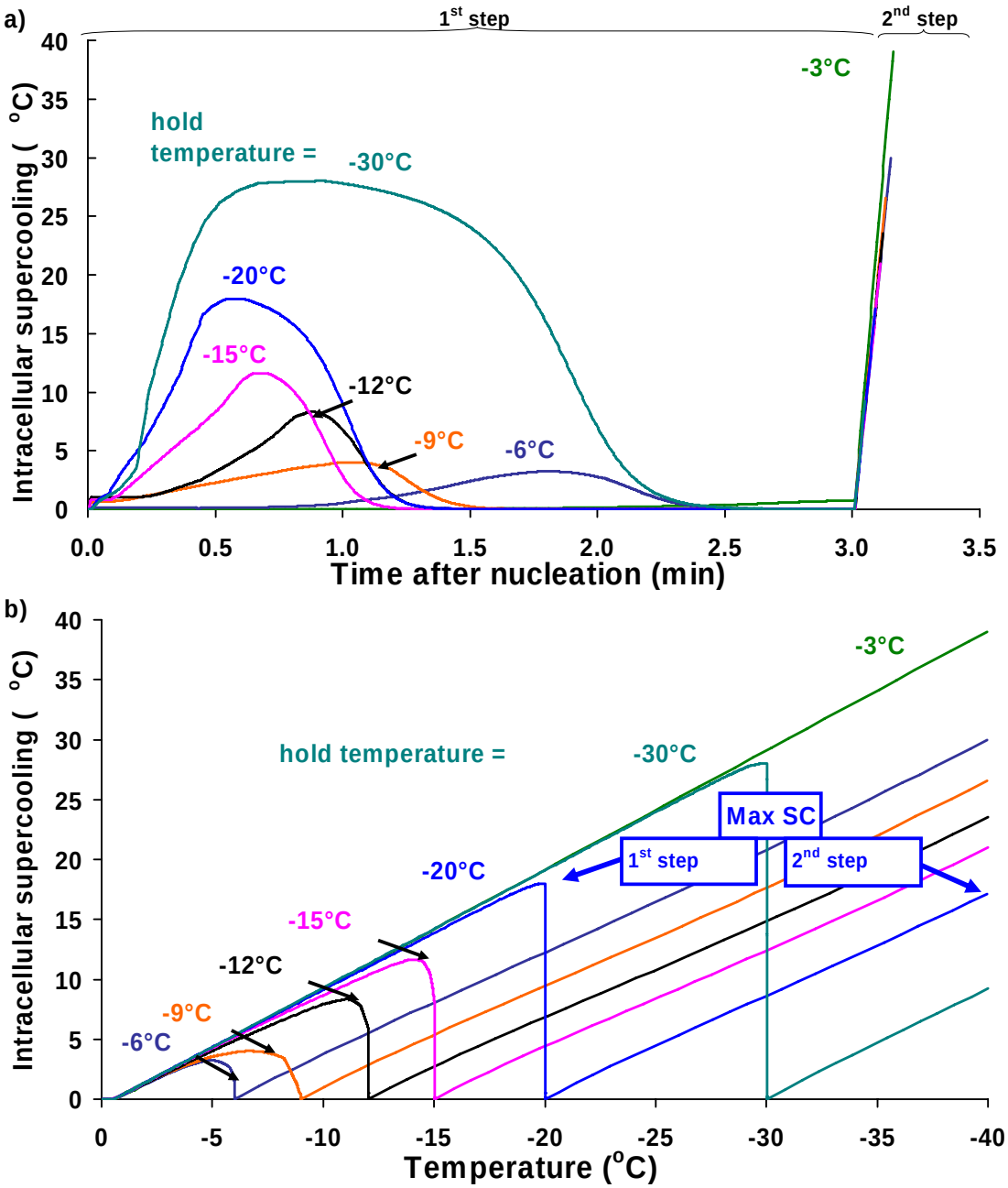

Figure 4-4. Calculated intracellular supercooling as a function of (a) time after nucleation and (b) temperature for TF-1 cells cooled according to the temperature profiles in Figure 4-2. "Max" indicates where the maximum supercooling occurs during the 1st and 2nd steps (for simulations down to -40 °C), where simulations were stopped) for a particular hold temperature.

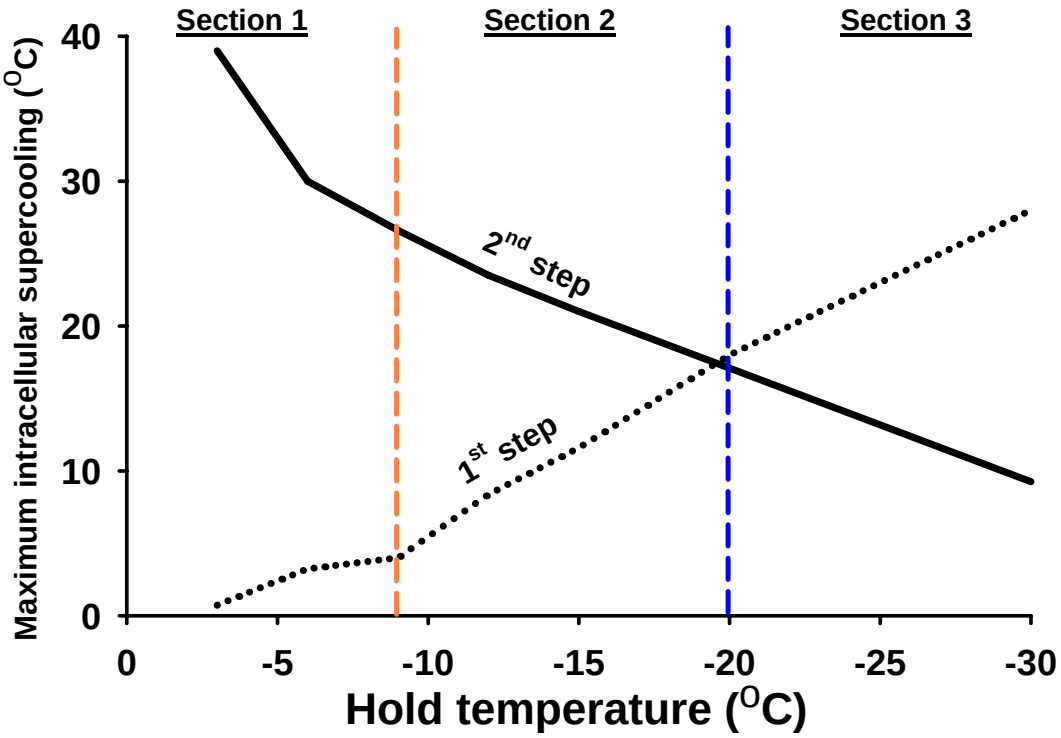

Figure 4-5. Maximum intracellular supercooling during the 1st step (dotted line) and the 2nd step (solid line) as a function of hold temperature for TF-1 cells (for simulations down to -40 °C). Vertical dashed lines are for reference in Figure 4-6.

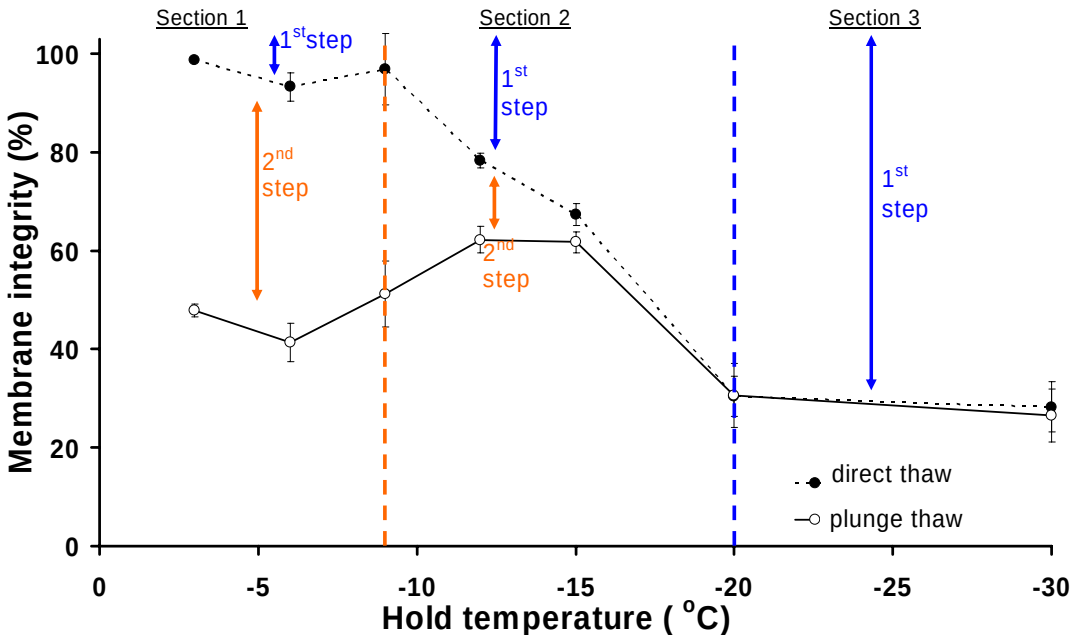

Figure 4-6. Membrane integrity for TF-1 cells (±SEM; normalized to controls) in serum-free RPMI following two-step freezing with a 3 minute hold time and includes sections on the figure where loss of membrane integrity is a result of either supercooling in the 1st or 2nd step, or both, of the two-step freezing procedure [42].

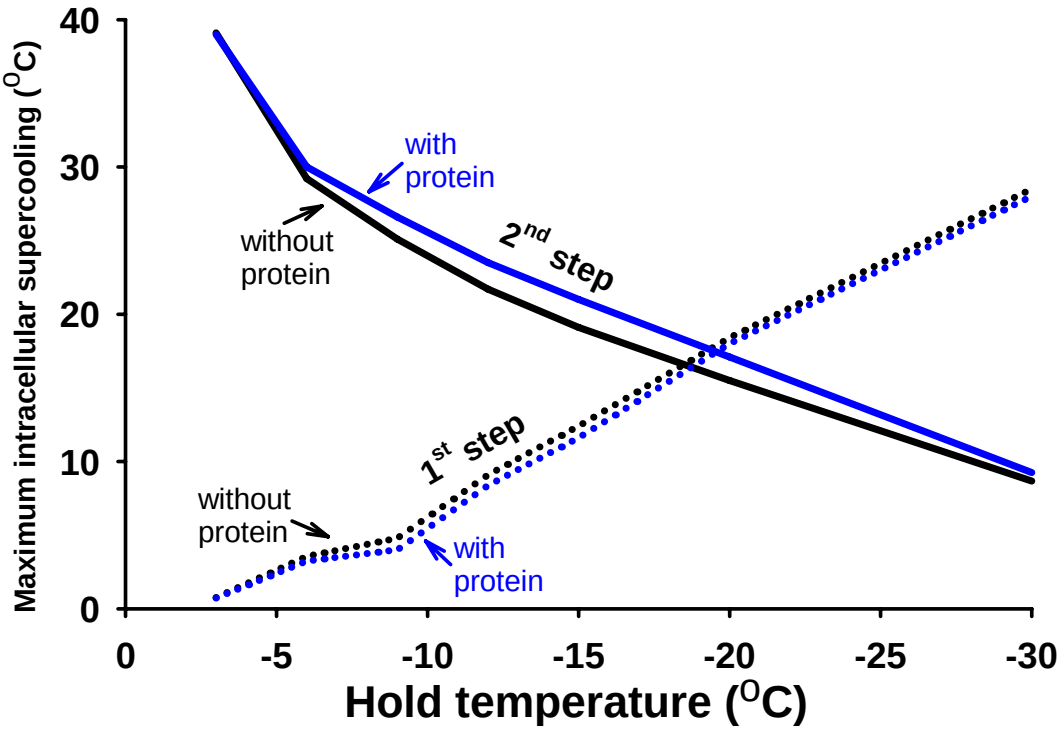

Figure 4-7. Cell model with (black) and without (blue) intracellular protein. Maximum intracellular supercooling during the 1st step (dotted line) and the 2nd step (solid line) as a function of hold temperature for TF-1 cells.

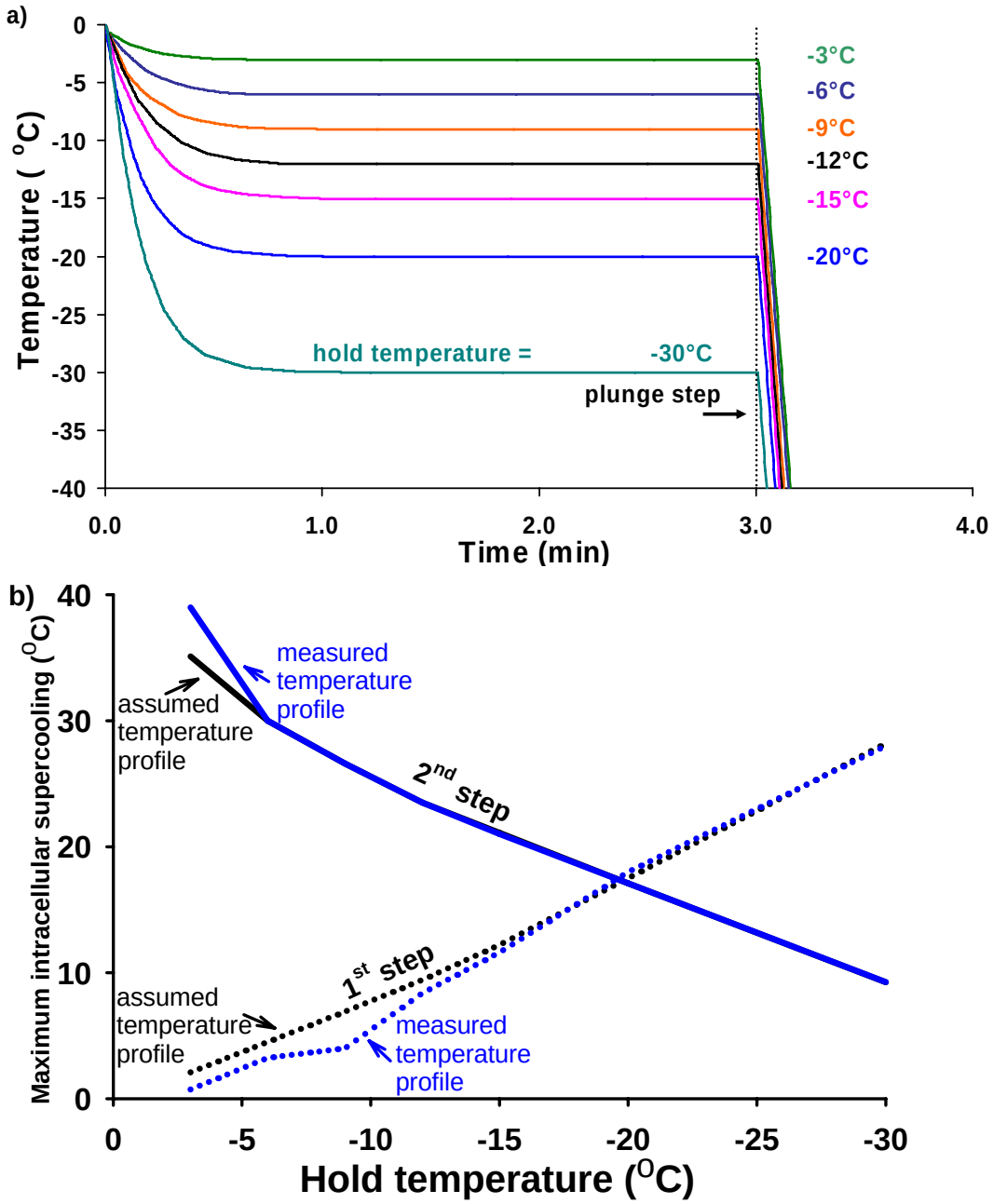

Figure 4-8. Effect of using an assumed temperature profile rather than a measured temperature profile which includes nucleation heat. (a) Simulation input temperature as a function of time and (b) the corresponding calculated maximum supercooling during the 1st step (dotted line) and the 2nd step (solid line) as a function of hold temperature for TF-1 cells.

Chapter 5. Dissecting cryoinjury using simulations of a graded freezing (interrupted slow cooling without hold time) procedure[1]

5.1 Introduction

Some researchers have explored the use of simulations as a means of predicting low temperature responses of various cell types, including peripheral blood stem cells [22]; cord blood stem cells [24]; bull spermatozoa [23]; bovine erythrocytes [6]; rat embryos [8]; porcine chondrocytes [25]; yeast [20]; hamster ova [21]; and human corneal epithelial, endothelial and stromal cells [3]; even though the traditional approach to optimizing cryopreservation protocols has been empirical. For simulations to be used in designing cryopreservation protocols, it is necessary to compare simulations with empirical data to further understand the relationship between calculated parameters and related experimental outcomes. Graded freezing (interrupted slow cooling without hold time) [15] provides insights into the two types of freezing injury which can affect cell recovery: solution effects and intracellular ice formation [14]. McGann used this freezing procedure to explore the two major types of freezing injury by determining the subzero temperature ranges where

[1] This chapter with minor modifications has been submitted to Cryobiology (2009) as "Investigating cryoinjury using simulations and experiments: 2. TF-1 cells during the graded freezing (interrupted slow cooling without hold time) procedure", L.U. Ross-Rodriguez, J.A.W. Elliott, and L.E. McGann

different sources of cryoinjury occur [15]. The graded freezing procedure involves slow cooling (1°C/min for many nucleated mammalian cells) to various subzero temperatures and then either thawing directly or rapid cooling by plunging into liquid nitrogen and later thawing (see schematic - Figure 5-1). With this procedure it is possible to separate injury sustained during the slow cooling phase to the subzero experimental temperatures, from that sustained upon rapid cooling to storage temperatures. Various cooling rates can also be used to explore the effect of time during cooling on cell recovery.

Mazur previously used simulations to explore the effects of solutions, osmotics and temperatures on cellular systems [11], and reported that the water permeability and its temperature dependence are important parameters necessary to predict changes in the volume of intracellular water with temperature during cooling in the presence of extracellular ice. Furthermore, that study reported that predictions of the probability of intracellular ice formation can be made based on the amount of intracellular water and the temperature of the cell. Subsequently, Mazur indicated that cooling rates greater than 1°C/min would result in a supercooled cytoplasm in yeast [11,13]. Supercooling is the degree to which a solution is cooled below its thermodynamic freezing point and was used as an indicator of the potential for intracellular ice formation [14]. Ebertz also reported the use of supercooling as an indicator for intracellular ice formation for simulations on corneal endothelial, epithelial

and stromal cells [3]. Mazur reported that intracellular ice nucleation was likely when supercooling exceeded 10 °C [11,13]. Diller further examined the probability of intracellular ice formation based on the synergistic interaction of cooling rates and supercooling [2]. During cooling, the cell approaches osmotic equilibrium across the plasma membrane either by osmotic dehydration or the formation of ice. Therefore, at low cooling rates, cells dehydrate, resulting in low supercooling. At high cooling rates, there is insufficient time for dehydration, so supercooling increases, making intracellular freezing more likely [2]. Karlsson et al. developed a mechanistic model, including water transport across the cell membrane, ice nucleation, and crystal growth, for predicting the kinetics of intracellular ice formation [4].

In Chapter 4, we have demonstrated that intracellular supercooling can be used as the sole indicator for cryoinjury in two-step freezing (rapid interrupted cooling with a hold time). However, based on Mazur et al.'s 'two-factor hypothesis', solution effects injury must also be considered to determine the optimal cooling rate for cryopreserving a cell type using slow cooling [14]. Karlsson et al. have also shown the need for an effective model of solution effects injury [5]. During slow cooling, cell injury is related to prolonged exposure to the high solute concentrations resulting from extracellular ice formation [14]. This study explores the use of intracellular supercooling, as an indicator of intracellular freezing, and intracellular osmolality, as an indicator of solution effects injury, to

distinguish between the two major types of injury sustained during the different phases of the cooling protocol.

The objective of this study was to perform simulations of interrupted slow cooling freezing experiments using parameters for TF-1 cells as previously reported in Chapter 2 and listed in Table 5-1, and to compare the cell survival outcomes (Chapter 3) with calculations of intracellular supercooling and intracellular osmolality, as cells were cooled slowly to various subzero temperatures before rapid cooling.

5.2 Simulation specifications

The specifications for the simulations of cellular responses at low temperatures have previously been described in detail in Chapter 4. Briefly, there are four main elements to the simulations: 1) the change in the composition of the extracellular solution as ice forms at low temperatures; 2) cellular osmotic responses to changes in composition of the extracellular solution and the resulting change in the composition of the intracellular solution; 3) the temperature dependence of the cellular osmotic permeability parameters; and 4) changes in sample temperature as a function of time.

Measured temperature profiles in the experimental samples were used in the simulations. Since the cells are initially in osmotic equilibrium with the isotonic extracellular solution, no osmotic changes occur before ice nucleation. The assumptions in our simulations are that a) the

simulation begins on ice nucleation at the freezing point of the extracellular solution and b) the extracellular solution remains in equilibrium with extracellular ice. The simulations used measured osmotic parameters of TF-1 cells, as reported previously Chapter 2 and listed in Table 5-1c.

5.3 Experimental materials and methods

5.3.1 TF-1 cell freezing experiments

Descriptions of TF-1 cell culture and freezing experiments have been previously reported in detail in Chapter 3. Briefly, TF-1 cells (ATCC, Manassas, VA, USA) were cultured according to ATCC guidelines. Samples of 0.2 mL cell suspension in serum-free RPMI (ATCC) were transferred to glass tubes (6x50 mm; Fisher, Edmonton, AB, Canada) and cooled in a 0 °C wet ice bath for 5 min. Control samples were removed and either warmed in a 37 °C water bath or plunged into liquid nitrogen. Experimental samples were transferred into a methanol bath (FTS Systems, Inc., Stone Ridge, NY, USA) preset at -3 °C and allowed to equilibrate for 5 min prior to ice nucleation in each tube with cold forceps. After ice was nucleated at -3 °C, samples were held for 3 minutes to allow for the dissipation of the nucleation heat. The bath was then cooled at 0.9 °C/min, and the temperature monitored using a Type T thermocouple (Omega, Laval, QC, Canada). At each experimental temperature (-3, -6, -9, -12, -15, -20, -30, and -40 °C), one set of duplicate samples was

thawed directly in a 37 °C water bath and another set was plunged into liquid nitrogen (250 °C/min). Plunge samples were kept in liquid nitrogen for a minimum of one hour prior to being thawed in a 37 °C water bath. Cell membrane integrity (SYTO® 13 (Molecular Probes, Eugene, OR, USA) and ethidium bromide (Sigma, Mississauga, ON, Canada) was used as an indicator of cell damage during freezing, as it has been shown that the membrane is a primary site of freezing-thawing injury [1]. It has also been shown that there is a correlation between intracellular freezing and membrane damage for cells in suspension [1,12].

5.4 Results and discussion

5.4.1 Graded freezing simulations

Figure 5-2 shows the measured temperature profiles used in the simulations (profiles shown to -40 °C). After ice nucleation at -3 °C, the sample temperature increased to the freezing point of the solution (-0.6 °C). Figure 3 shows calculated cell volumes as a function of temperature for the corresponding cooling profiles shown in Figure 2. As expected for linear cooling, simulations show that cell volumes during the various experimental temperature profiles only differ during the plunge step. Specifically, the calculated volume for the -3 °C experimental temperature profile differs considerably from the other experimental temperatures.

Figure 5-4 shows the calculated supercooling in TF-1 cells cooled at 1°C/min to various subzero temperatures before rapid cooling. For all cooling profiles, there was a small increase in supercooling after ice nucleation, followed by a decrease as the cell dehydrates. TF-1 cells maintained equilibrium (i.e. no increase in supercooling) during slow cooling, indicating that 1 °C/min was sufficiently low enough to allow the cells to remain in osmotic equilibrium during cooling to all the experimental temperatures below -3 °C. During the plunge step, there was an additional increase in supercooling as a result of rapid cooling, with the pattern similar for all experimental temperatures.

Figure 5-5 shows the calculated intracellular osmolality during cooling at 1°C/min to various temperatures before rapid cooling. After extracellular ice nucleation, there was an increase in intracellular osmolality as the cell dehydrated in response to the increased extracellular osmolality to the experimental temperatures. During the plunge step, there was a lower increase in intracellular osmolality during the subsequent rapid cooling step.

5.4.2 Maximum intracellular supercooling and osmolality during cooling

It has been suggested previously that most damage resulting from exposure to low temperatures occurs at temperatures above -40 °C [10]. The highest degree of supercooling was calculated between ice nucleation and -40 °C and was reached at the end of the cooling profiles

(i.e. supercooling reached in the plunge step by the time the cells are cooled to -40 °C). The pattern of supercooling was consistent for all experimental temperatures. In Figure 5-4, the arrow indicates where the maximum supercooling was determined for the -3 °C experimental temperature, as an example. The maximum supercooling for each experimental temperature profile was separated into the maximum supercooling which occurred down to the experimental temperature (direct thaw) and the maximum supercooling which occurred during the plunge step (plunge). The results were then summarized and plotted as a function of experimental temperature (Figure 5-6). The maximum supercooling calculated for the direct thaw group was low (~2 °C) and since it occurred during the ice nucleation step, it was equal for all experimental temperature profiles. This indicates that there should be no damage due to intracellular ice formation for TF-1 cells cooled slowly to -40 °C. However, high maximum supercooling was calculated for the plunge group at high subzero experimental temperatures, decreasing at lower experimental temperatures. This indicates that there should be significant damage due to intracellular ice formation for TF-1 cells plunged from at least the higher experimental temperatures. This analysis indicates that intracellular ice formation plays a role in freezing injury only during the plunge step.

Similar to the pattern for intracellular supercooling, the highest intracellular osmolality was reached at the end of the cooling profiles

(i.e. osmolality reached in the plunge step by the time the cells are cooled to -40 °C). The arrows in Figure 5-5 indicate where the maximum osmolality was determined for direct thaw and plunge for the -20 °C experimental temperature, as an example. The maximum osmolality for each experimental temperature profile was separated into the maximum osmolality which occurred down to the experimental temperature (direct thaw) and the maximum osmolality which occurred during the plunge step (plunge). The results were then summarized and plotted as a function of experimental temperature (Figure 5-6). The maximum osmolality calculated for the direct thaw group increased with decreasing experimental temperature, where cells are exposed to the increasing osmolalities for longer durations. The maximum osmolality calculated for the plunge group also increased with decreasing experimental temperature.

5.4.3 Comparison of theoretical and experimental results

The maximum intracellular supercooling and osmolality calculated throughout the cooling profiles were used to interpret loss of membrane integrity after graded freezing experiments. Figure 5-7 shows previously determined membrane integrity as a function of experimental temperature (Chapter 3) with the results divided into 2 sections.

5.4.3.1 Direct thaw

In Section 1 (-3 to -6 °C; yellow), there is minimal loss of membrane integrity for the direct thaw samples; while in Section 2 (yellow), there is a

decline in membrane integrity for the direct thaw samples with decreasing experimental temperature. For directly thawed samples in Section 1, the corresponding section in Figure 5-6 shows low maximum supercooling and in Figure 5-6 shows low maximum intracellular osmolality. TF-1 cells can therefore tolerate exposure during slow cooling to a calculated 3 Osm/kg. Lovelock reported that exposure to and dilution from 0.8 M salt concentration causes sensitivity to thermal and mechanical stresses and from 3 M salt concentration causes hemolysis of human red blood cells [9]. The experimental data for TF-1 cells demonstrated that there was a progressive decrease in membrane integrity in Section 2 (below -6 °C), as the calculated intracellular osmolality increased with a 50 % loss in membrane integrity at ~6.6 Osm/kg. Since the calculated supercooling in the direct thaw samples remained low at all experimental temperatures, this loss of membrane integrity can be attributed to high intracellular osmolality (yellow area in Figure 5-7).

5.4.3.2 Plunge

Experimental results from the plunge-thaw samples can also be interpreted using the calculated maximum supercooling and osmolality in the plunge step. In Section 1 of experimental temperatures (-3 to -6 °C; blue), high maximum supercooling (Figure 5-6) and lower increase in osmolality in the plunge step (Figure 5-6) corresponded to approximate 75 % loss of membrane integrity (Figure 5-7). The damage in this section can therefore be attributed to intracellular ice formation (blue area in

Figure 5-7). In Figure 5-7 Section 2 of experimental temperatures (-6 to -30 °C; green) for the plunge step, shows a trend of reduced membrane integrity, with decreasing maximum supercooling and increasing maximum intracellular osmolality (Figure 5-6; green area in Figure 5-7). The two indicators of injury are oppositely dependent on the experimental temperature, resulting in an apparent maximum in recovery for the plunge samples. This maximum has been previously reported [15,17-19,26-30].

Lastly, there is no range of experimental temperatures in this study that minimizes the likelihood of intracellular ice formation and solution effects injury sufficiently to achieve high cell recovery using this graded freezing protocol for TF-1 cells without cryoprotectants.

5.4.4 Impact of including intracellular protein

Solution properties of the cytoplasm are complex and have yet to be elucidated for nucleated cells. We have previously discussed the inclusion of a protein as a component of the cell cytoplasm in simulations (Chapter 4), assuming that the protein in TF-1 cells has thermodynamic properties similar to those of hemoglobin, which are well documented. The inclusion of protein as an intracellular component had little effect on the calculated maximum supercooling (Figure 5-8a) or maximum intracellular osmolality (Figure 5-8b) for direct thaw or plunge profiles. As expected, including protein in the cytoplasm is not expected to change the calculated intracellular osmolality during slow cooling because the cell is in equilibrium with the extracellular solution, where the osmolality is

determined by the temperature. However, the presence of protein did have an effect on the maximum salt (KCl) concentration for the direct thaw cooling profiles (Figure 5-9). This demonstrates that while the inclusion of protein may describe the solution thermodynamics of the cytoplasm more accurately, it does not substantially affect simulation results for graded freezing.

5.5 Contrasting graded freezing and two-step freezing simulations

A previous study (Chapter 4) has shown that decreased membrane integrity due to intracellular ice formation in a two-step freezing procedure (rapid cooling interrupted with a hold time) could be predicted using intracellular supercooling as an indicator of intracellular ice formation for TF-1 cells following two-step freezing. In this study, we also calculated the intracellular osmolality as a function of hold temperature for two-step freezing of TF-1 cells to explore the potential contributions of high intracellular osmolality to decreased membrane integrity. Calculations of maximum intracellular osmolality for the first step were comparable to graded freezing direct thaw calculations. However, the time spent exposed to these conditions is significantly longer using graded freezing and thus contributing to a decrease in membrane integrity. Calculations of maximum intracellular osmolality for the second step were also comparable to graded freezing plunge thaw calculations. However, similarly the time spent exposed to these conditions is low for both

two-step and graded freezing and therefore, damage is primarily associated with high intracellular supercooling. Calculated intracellular supercooling alone could be used to explain membrane integrity results for two-step freezing (rapid cooling interrupted with hold time) over the range of hold times investigated in this study. However, it has been shown for longer hold times (i.e. up to 300 minutes) that solution effects injury plays a role with increased hold time [16] and therefore, calculated intracellular osmolality should still be considered. Calculated intracellular supercooling alone was not sufficient to explain graded freezing (interrupted slow cooling without hold time) results and required calculated intracellular osmolality.

5.6 Conclusions

Empirical approaches have been used to develop most cryopreservation procedures currently in use. However, more difficult to cryopreserve cells and complex cellular structures require application of theoretical understanding of cellular osmotic responses to low temperatures [3,7,20]. This study demonstrated the use of intracellular supercooling and osmolality as indicators of intracellular ice formation and solution effects injury, respectively. For graded freezing direct thaw samples, high intracellular osmolality alone correlated with decreased membrane integrity with lower subzero experimental temperatures. For samples cooled rapidly from -3 and -6 °C, intracellular supercooling alone

was correlated with decreased membrane integrity. However for samples cooled rapidly from lower subzero temperatures, a combination of high intracellular osmolality and supercooling were correlated with decreased membrane integrity which is what one would expect with damage associated with slow cooling.

The impact of including of intracellular protein, as an intracellular component in simulations, minimally affected the calculated maximum supercooling and osmolality during interrupted slow cooling. However, the inclusion of protein in simulations may be important for predicting cellular responses using other cooling profiles and/or cryoprotectants, including vitrification.

Based on the findings of this study and our previous study (Chapter 4) using two-step freezing, we have shown that supercooling alone could be used to explain membrane integrity results for two-step freezing (rapid cooling interrupted with hold time); however, supercooling alone was not sufficient to explain graded freezing (interrupted slow cooling without hold time) results. Therefore, we suggest using both intracellular supercooling and osmolality as indicators of injury for simulations of slow cooling cryopreservation protocols.

This study combined the effects of intracellular supercooling and osmolality as indicators of potential damage due to intracellular ice formation and solution effects, respectively. Furthermore, this study demonstrates the usefulness of simulations, combined with interrupted

freezing in attempting to determine the optimal cryopreservation protocol for a particular cell type. Specifically, interrupted freezing provides useful insight into the mechanisms of damage conferred by slow cooling over a range of subzero temperatures [15]. It allows manipulation of different variables of the cryopreservation protocol, cooling rates, plunge temperatures, cryoprotectants, and storage temperatures, so that a comparison between them can be made. Ultimately, both procedures allow for further understanding of cryoinjury and thus the potential for an optimum protocol to be determined.

5.7 References

[1] J.P. Acker, and L.E. McGann, Membrane damage occurs during the formation of intracellular ice. Cryo-Letters 22 (2001) 241-254.

[2] K.R. Diller, Intracellular freezing - effect of extracellular supercooling. Cryobiology 12 (1975) 480-485.

[3] S.L. Ebertz, and L.E. McGann, Osmotic parameters of cells from a bioengineered human corneal equivalent and consequences for cryopreservation. Cryobiology 45 (2002) 109-117.

[4] J.O.M. Karlsson, E.G. Cravalho, and M. Toner, A model of diffusion-limited ice growth inside biological cells during freezing. Journal of Applied Physics 75 (1994) 4442-4445.

[5] J.O.M. Karlsson, A. Eroglu, T.L. Toth, E.G. Cravalho, and M. Toner, Fertilization and development of mouse oocytes cryopreserved using a theoretically optimized protocol. Human Reproduction 11 (1996) 1296-1305.

[6] S.P. Leibo, Freezing damage of bovine erythrocytes - simulation using glycerol concentration changes at subzero temperatures. Cryobiology 13 (1976) 587-598.

[7] C. Liu, C.T. Benson, D.Y. Gao, B.W. Haag, L.E. Mcgann, and J.K. Critser, Water permeability and Its activation-energy for individual hamster pancreatic-islet cells. Cryobiology 32 (1995) 493-502.

[8] J. Liu, E.J. Woods, Y. Agca, E.S. Critser, and J.K. Critser, Cryobiology of rat embryos II: A theoretical model for the development of interrupted slow freezing procedures. Biology of Reproduction 63 (2000) 1303-1312.

[9] J.E. Lovelock, The haemolysis of human red blood-cells by freezing and thawing. Biochimica et Biophysica Acta 10 (1953) 414-426.

[10] J.E. Lovelock, The mechanism of the protective action of glycerol against haemolysis by freezing and thawing. Biochimica et Biophysica Acta 11 (1953) 28-36.

[11] P. Mazur, Kinetics of water loss from cells at subzero temperatures and the likelihood of intracellular freezing. The Journal of General Physiology 47 (1963) 347-69.

[12] P. Mazur, The role of cell membranes in the freezing of yeast and other cells. Annals of the New York Academy of Science 125 (1965) 658-76.

[13] P. Mazur, Role of intracellular freezing in death of cells cooled at supraoptimal rates. Cryobiology 14 (1977) 251-272.

[14] P. Mazur, S.P. Leibo, and E.H.Y. Chu, A two-factor hypothesis of freezing injury - evidence from chinese-hamster tissue-culture cells. Experimental Cell Research 71 (1972) 345-355.

[15] L.E. McGann, Optimal temperature ranges for control of cooling rate. Cryobiology 16 (1979) 211-216.

[16] L.E. McGann, and J. Farrant, Survival of tissue culture cells frozen by a two-step procedure to -196 degrees C. I. Holding temperature and time. Cryobiology 13 (1976) 261-268.

[17] L.E. McGann, and M.L. Walterson, Cryoprotection by dimethyl sulfoxide and dimethyl sulfone. Cryobiology 24 (1987) 11-16.

[18] L.E. McGann, H.Y. Yang, and M. Walterson, Manifestations of cell damage after freezing and thawing. Cryobiology 25 (1988) 178-185.

[19] K. Muldrew, M. Hurtig, K. Novak, N. Schachar, and L.E. McGann, Localization of freezing injury in articular cartilage. Cryobiology 31 (1994) 31-38.

[20] G.J. Schwartz, and K.R. Diller, Osmotic response of individual cells during freezing .1. Experimental volume measurements. Cryobiology 20 (1983) 61-77.

[21] M. Shabana, and J.J. Mcgrath, Cryomicroscope investigation and thermodynamic modeling of the freezing of unfertilized hamster ova. Cryobiology 25 (1988) 338-354.

[22] M.R. Tijssen, H. Woelders, A. de Vries-van Rossen, C.E. van der Schoot, C. Voermans, and J.M. Lagerberg, Improved postthaw viability and in vitro functionality of peripheral blood hematopoietic progenitor cells after cryopreservation with a theoretically optimized freezing curve. Transfusion 48 (2008) 893-901.

[23] H. Woelders, and A. Chaveiro, Theoretical prediction of 'optimal' freezing programmes. Cryobiology 49 (2004) 258-271.

[24] E.J. Woods, J. Liu, K. Pollok, J. Hartwell, F.O. Smith, D.A. Williams, M.C. Yoder, and J.K. Critser, A theoretically optimized method for cord blood stem cell cryopreservation. J Hematother Stem Cell Res 12 (2003) 341-350.

[25] W.T. Wu, S.-R. Lyu, and W.H. Hsieh, Cryopreservation and biophysical properties of articular cartilage chondrocytes. Cryobiology 51 (2005) 330-338.

[26] H. Yang, J. Acker, A. Chen, and L. McGann, In situ assessment of cell viability. Cell Transplantation 7 (1998) 443-51.

[27] H. Yang, J.P. Acker, J. Hannon, H. Miszta-Lane, J.J. Akabutu, and L.E. McGann, Damage and protection of UC blood cells during cryopreservation. Cytotherapy 3 (2001) 377-386.

[28] H. Yang, F. Arnaud, and L.E. McGann, Cryoinjury in human granulocytes and cytoplasts. Cryobiology 29 (1992) 500-510.

[29] H. Yang, X.M. Jia, J.P. Acker, G. Lung, and L.E. McGann, Routine assessment of viability in split-thickness skin. Journal of Burn Care and Rehabilitation 21 (2000) 99-104.

[30] M.A. Zieger, E.E. Tredget, and L.E. McGann, Mechanisms of cryoinjury and cryoprotection in split-thickness skin. Cryobiology 33 (1996) 376-389.

Table 5-1. Parameters used in simulations: (a) isotonic solution composition, (b) solution parameters, and (c) osmotic parameters for TF-1 cells

a) Isotonic solution composition

	Extracellular	Intracellular
NaCl	0.170 molal	0.010 molal
KCl	0.005 molal	0.133 molal
Protein	0	0.004 molal
Total Osmolality	0.300 osm/kg	0.300 osm/kg

b) Solution parameters

	B (mol/kg solvent)$^{-1}$	C (mol/kg solvent)$^{-2}$	K
NaCl	0.02986	0	1.702
KCl	0	0	1.742
Protein†	49.3	3.07×10^4	1

c) Osmotic parameters [Chapter 2]

Isotonic volume, V_o	916 μm^3
Inactive fraction, b	0.361
E_a (Activation Energy for L_p)	14.2 kcal/mol
k_1 (Pre-exponential factor for L_p)	1.33×10^{10} $\mu m^3/\mu m^2$/min/atm

†based on values reported for hemoglobin
L_p is for hydraulic conductivity

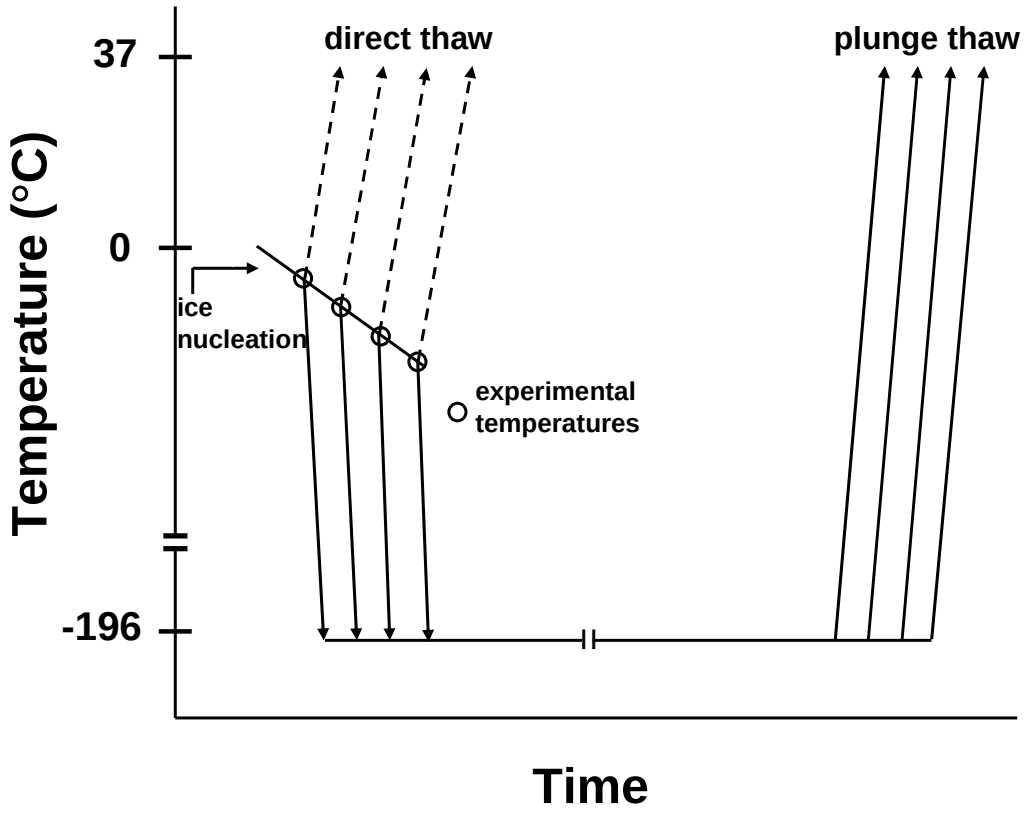

Figure 5-1. A schematic of graded freezing (interrupted slow cooling without hold time) (Chapter 3). Direct-thaw paths are indicated by dashed lines and the plunge-thaw paths are indicated with solid lines. Ice nucleation is indicated. Experimental temperatures are circled.

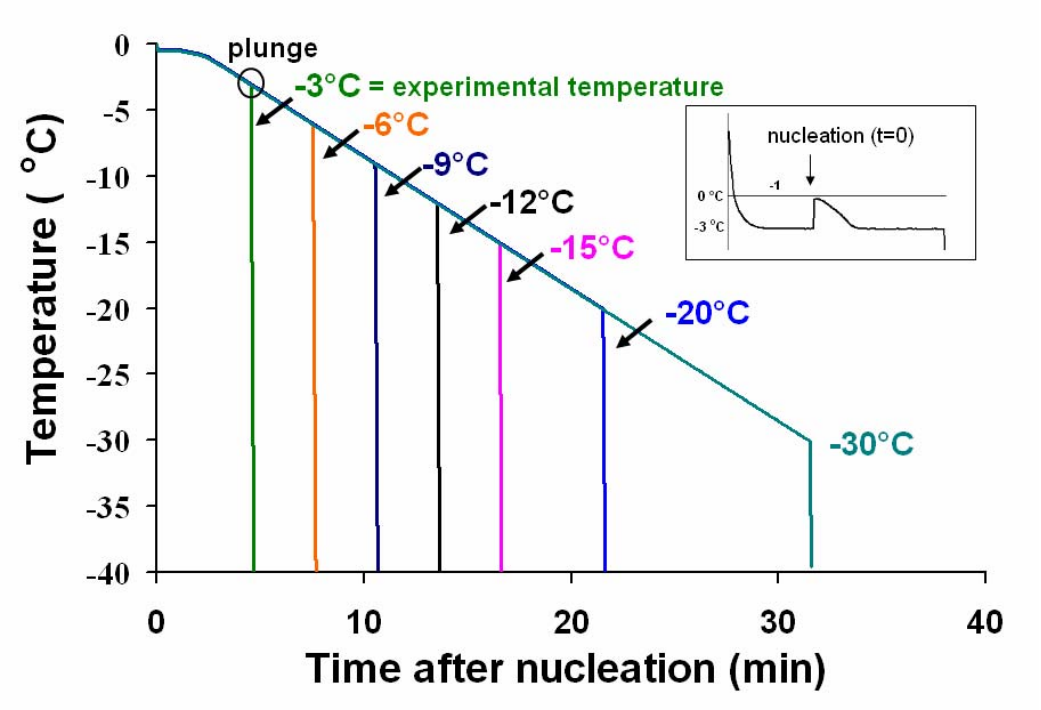

Figure 5-2. Simulation input temperature as a function of time, measured post-nucleation during cooling at 1 °C/min to various subzero experimental temperatures (-3°C to -30°C), prior to rapid cooling (250°C/min). The experimental temperatures are indicated on the graph. The figure insert shows the entire measured temperature profile including prior to the nucleation step for one set of experimental conditions.

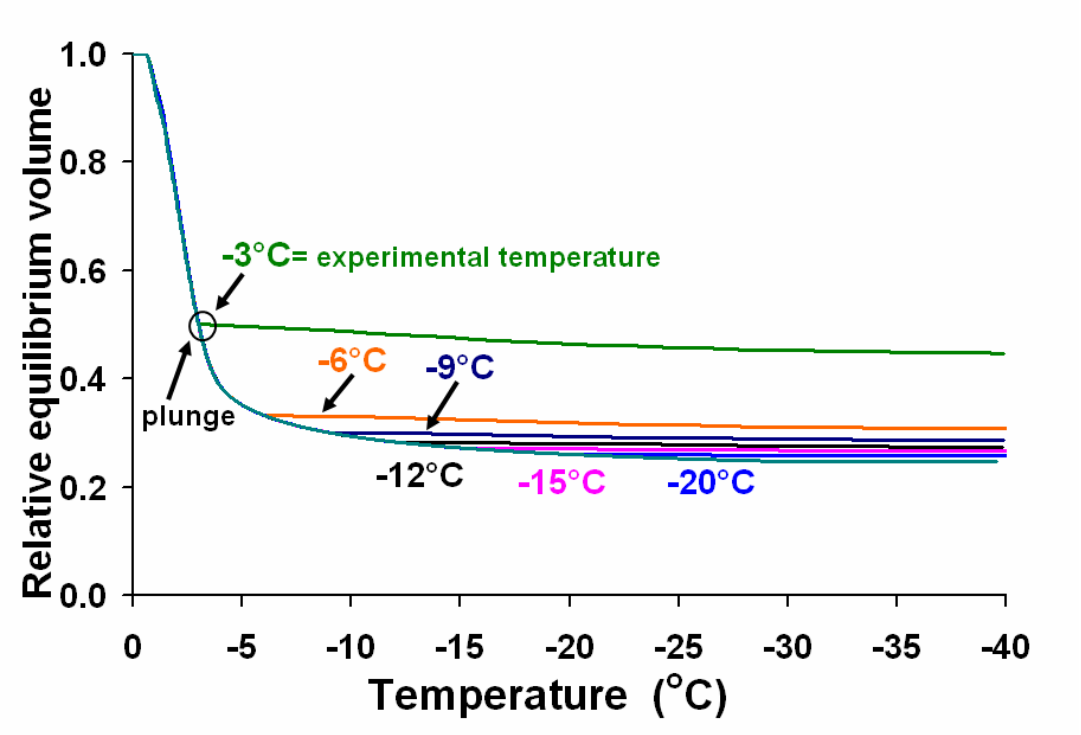

Figure 5-3. Calculated relative cell volume as a function of temperature for TF-1 cells cooled according to the temperature profiles in Figure 5-2.

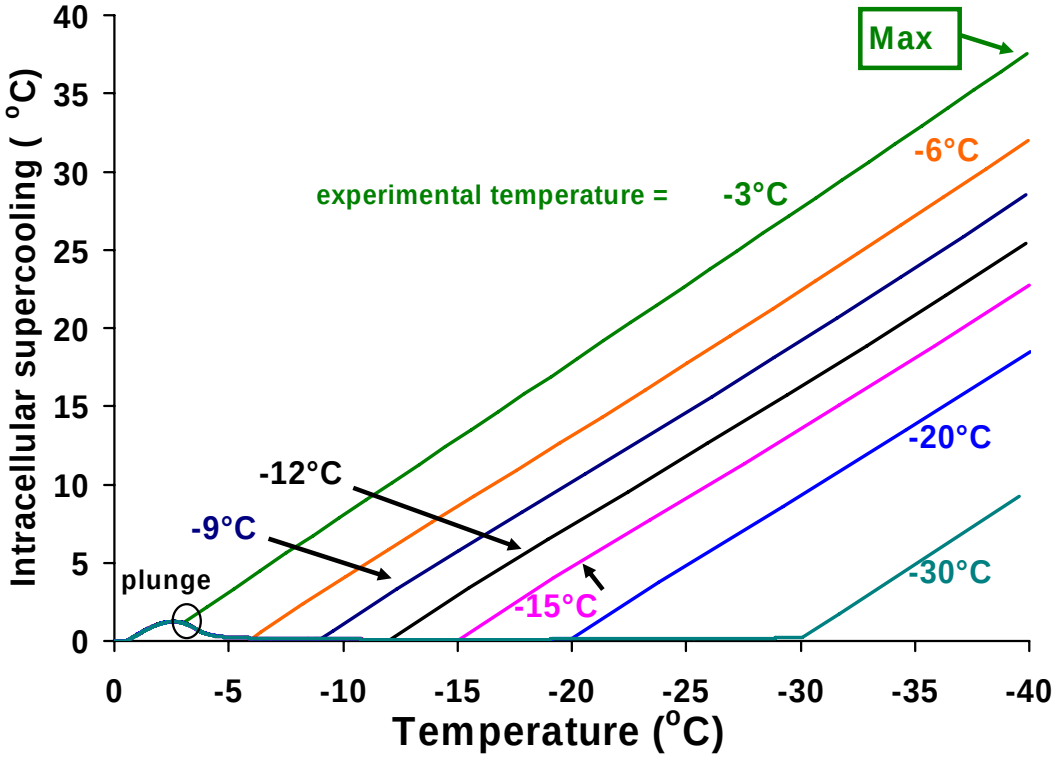

Figure 5-4. Calculated intracellular supercooling as a function of temperature for TF-1 cells cooled according to the temperature profiles in Figure 5-2. "Max" indicates where the maximum supercooling occurs during the cooling profile (for simulations down to -40 °C, where simulations were stopped) for a particular experimental temperature.

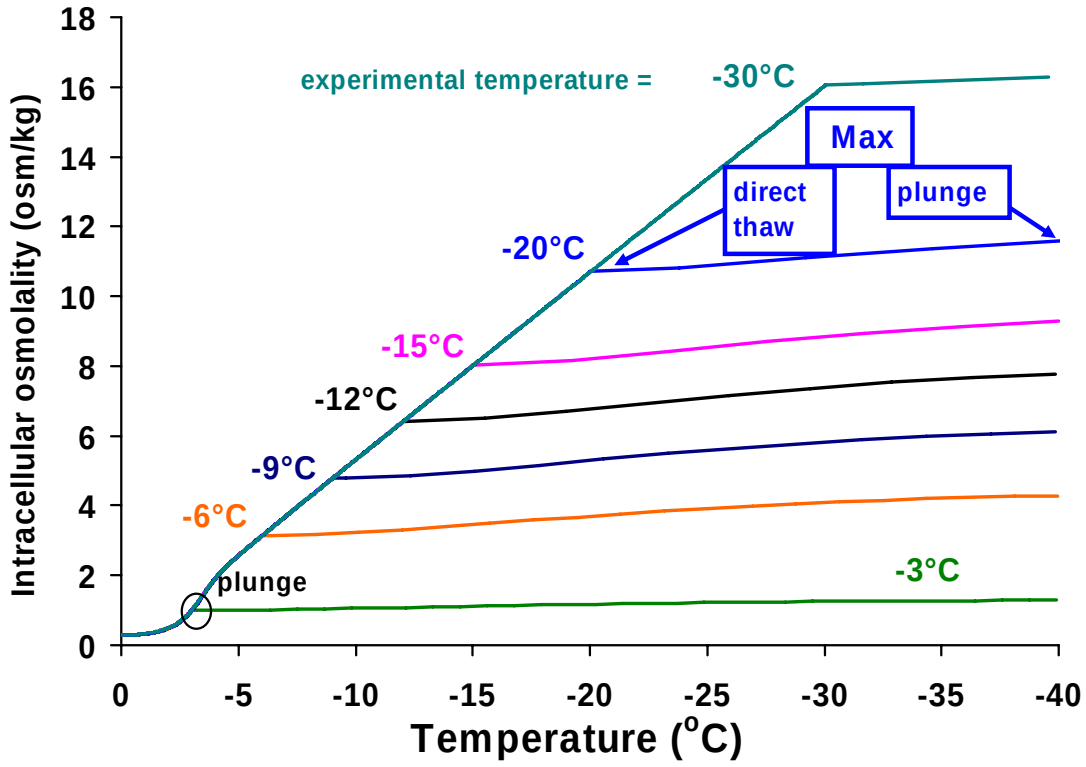

Figure 5-5. Calculated intracellular osmolality as a function of temperature for TF-1 cells cooled according to the temperature profiles in Figure 5-2. “Max” indicates where the maximum intracellular osmolality occurs during the direct thaw and plunge steps of the cooling profile (for simulations down to -40 °C, where simulations were stopped) for a particular experimental temperature.

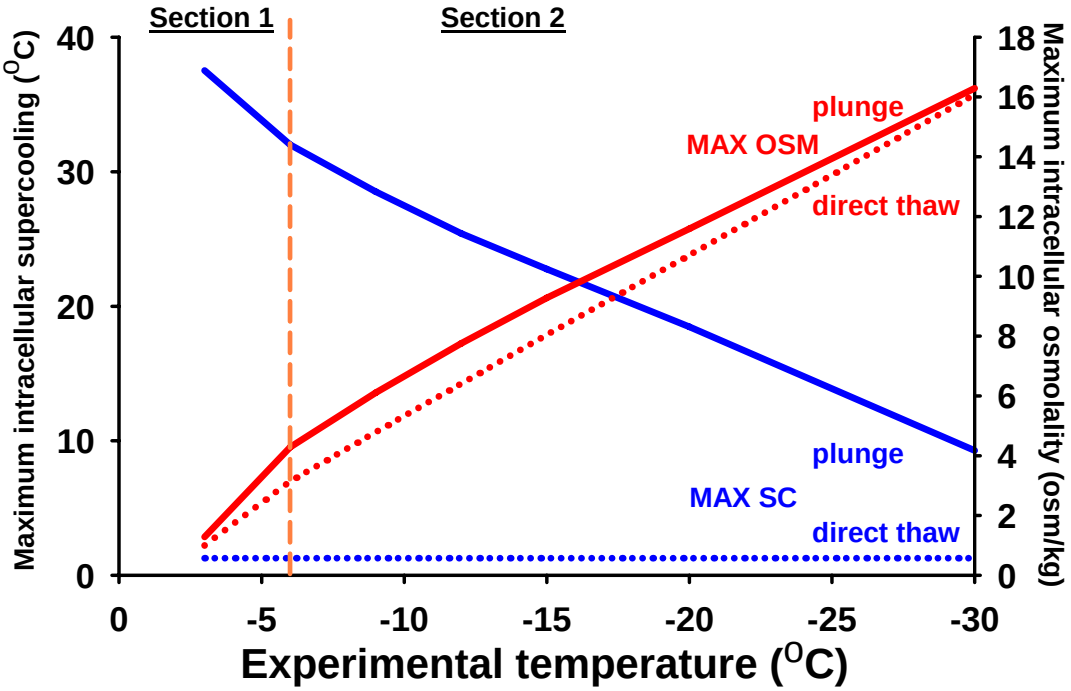

Figure 5-6. Maximum intracellular supercooling (blue) and intracellular osmolality (red) during direct thaw (dotted line) and plunge (solid line) as a function of experimental temperature for TF-1 cells. Vertical dashed line is for reference in Figure 5-8.

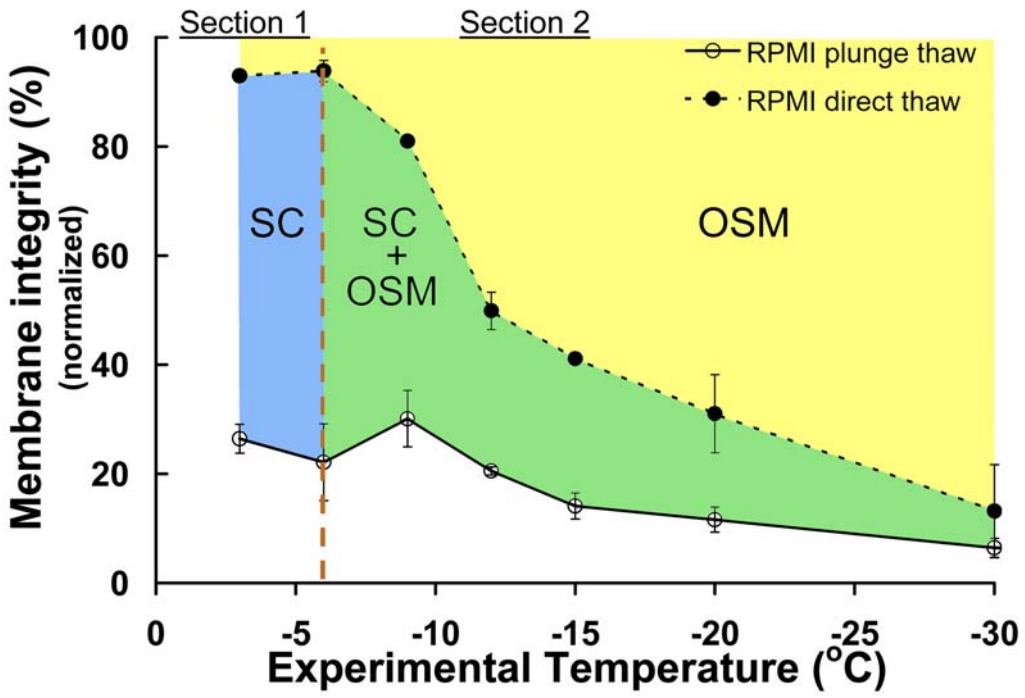

Figure 5-7. Membrane integrity for TF-1 cells (± sem; normalized to controls) in serum-free RPMI following graded freezing (Chapter 3) indicating sections where loss of membrane integrity is a result of supercooling (SC; blue area), osmolality (OSM; yellow area), or both (SC+OSM; green area), for the graded freezing procedure.

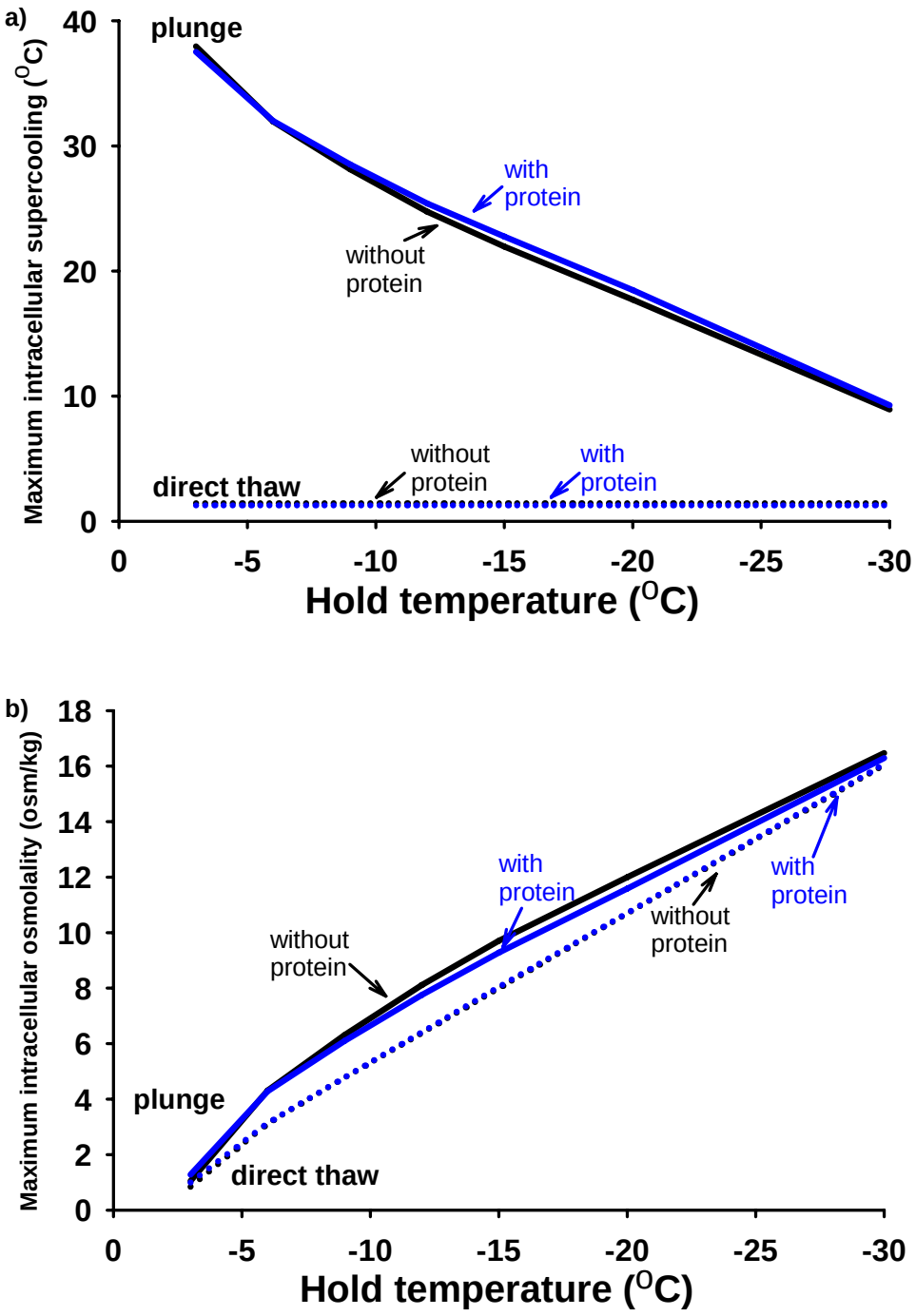

Figure 5-8. Cell model with (blue) and without (black) intracellular protein. (a) Maximum intracellular supercooling and (b) maximum intracellular osmolality during direct thaw (dotted line) and the plunge step (solid line) as a function of experimental temperature for TF-1 cells.

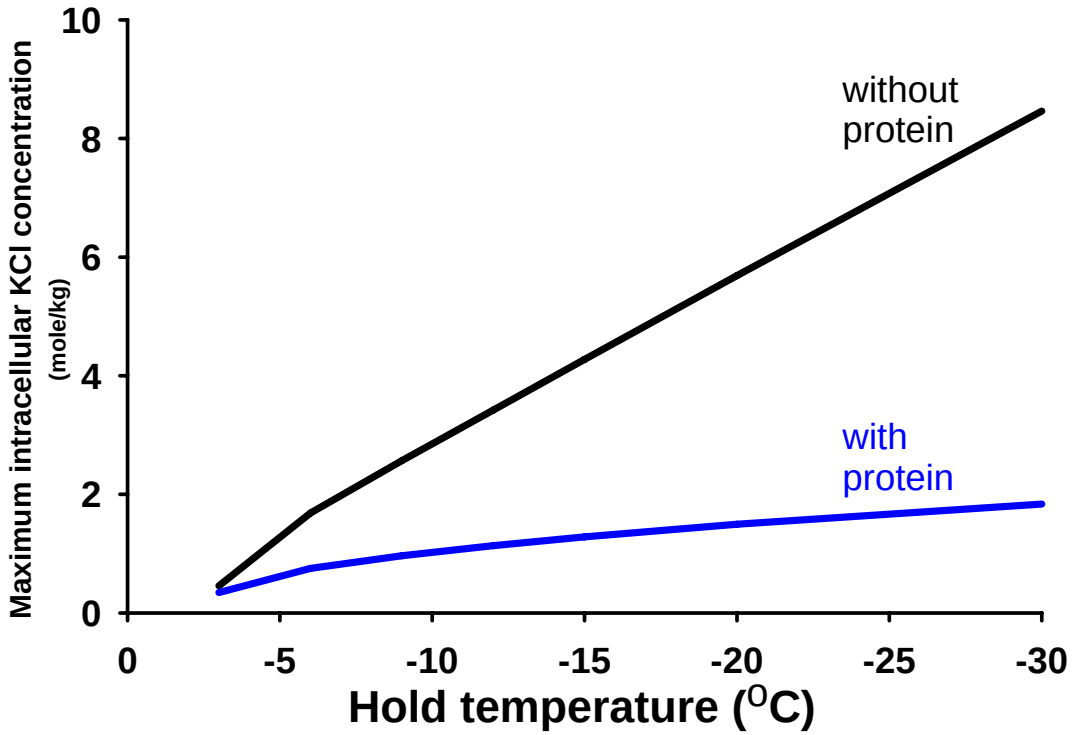

Figure 5-9. Maximum intracellular KCl concentration. Cell model with (blue) and without (black) intracellular protein during direct thaw as a function of experimental temperature for TF-1 cells.

Chapter 6. Thermodynamic solution properties of the cytoplasm of living nucleated cells

6.1 Introduction

Recent advances in the fundamental theories in cryobiology using thermodynamic principles have created new opportunities for innovative methodologies, such as computer simulations. In order for exact calculations of osmotic transport to be used in simulations of cellular responses to low temperatures, more accurate descriptions of the thermodynamic solution properties (specifically osmolality as a function of molality) are required. Osmolality is the basis freezing point depression and water transport. A major component of simulations is the use of thermodynamic descriptions of the intra- and extra-cellular solutions [34], as it is the osmolality difference between these two solutions that drives the water flux across the cell membrane. It has been previously shown that the thermodynamic solution properties affect predicted cellular behavior at low temperatures (Chapters 4 and 5). However, since the solution properties of the cytoplasm of cells, other than erythrocytes have yet to be elucidated, previously described simulations used approximations for the solution properties of the cytoplasm: ideal, dilute ([3,6,9,11,13,14,18,19,22,26,27,36-38,40,41,43,44]; Chapter 4 and 5) in which osmolality is assumed equal to molality:

$$\pi = m; \qquad \text{6-1}$$

where π is osmolality and *m* is molality. Other simulations used a non-ideal assumption, where osmolality is a nonlinear function of molality ([20,21,24]; Chapter 4 and 5). The relationship between osmolality and concentration is well described for a variety of solutions, including the cytoplasm of red blood cells [10,31]; however, the relationship has never been measured for the cytoplasm of a nucleated cell. Nucleated cells have many intracellular components, such as water, organelles, electrolytes, and proteins of varying concentrations [2]. While the solution properties are known for individual components (e.g. hemoglobin [5,10]), and the combination of known components using the osmotic virial equation (e.g. bovine serum albumin and ovalbumin) [10], the cytoplasm is too complex to make use of the individual solute solution properties feasible.

The osmotic virial equation, combined with ESR measurements of the erythrocyte cytoplasm [8,31], has been used to show that modeling the intracellular solution of erythrocytes as hemoglobin and an ideal solute can accurately predict the solution properties [10]. Also, when the modified Boyle van't Hoff equation that was derived was applied to the erythrocytes, it resulted in an osmotically-inactive fraction of the cell that is in closer agreement with dry weight measurements of the cytoplasm [33]. The osmotic virial equation combined with the modified Boyle van't Hoff

equation is the only model in the literature which has been shown to accurately assess the non-ideality of the cytoplasm. Thus, this model was used in this study.

Calculations of the osmotically-inactive fraction of the cell normally assume ideal, dilute solutions, often resulting in high estimates for the osmotically-inactive fraction, as is the case for human erythrocytes [33]. In this work, along with the non-ideal solution properties of the cytoplasm, the osmotically-inactive fraction of the cell was also determined without making ideal, dilute assumptions.

The purpose of this study is to determine a more accurate description of the osmolality as a function of solute molality of the cytoplasm of a living nucleated cell. This study will test the impact of this description on the outcomes of simulations of low temperature cellular responses. Various cell types of interest to cryobiology were used in this study, including cell types used in Chapter 2 (TF-1 cells, human umbilical vein endothelial cells (HUVEC), and porcine chondrocytes), and others (human erythrocytes, porcine hepatocytes, and data from the literature). Measurements of equilibrium cell volumes in hypertonic solutions were used to calculate intracellular osmolality as a function of concentration using either ideal or non-ideal solution assumptions, and the resulting osmotically-inactive fractions of the cell were compared. Osmotic equilibrium data were fit with linear (i.e. assume ideal) and non-linear (i.e. assume non-ideal) (virial [10]) equations of osmolality as a function of

solute concentration of the cytoplasm to determine: a) whether the virial description was required; and b) values of the second osmotic virial coefficients describing the non-linear (quadratic) behavior and the osmotically-inactive fractions of the cytoplasm for the cell types. This study evaluated the range of osmolalities that are necessary to obtain these parameters. The relevance of the measured osmotic virial coefficients and non-ideal osmotically-inactive fraction to cryobiology was assessed using simulations of interrupted cooling profiles (two-step freezing (Chapter 4); graded freezing (Chapter 5)) and calculating intracellular supercooling and osmolality, as indicators of intracellular ice formation and solution effects injury.

6.2 Materials and methods

6.2.1 Cell preparations

Osmotic equilibrium data for TF-1 cells (0.3-1.5 Osm/kg data) (Table 2-1), HUVECs (0.3-2.7 Osm/kg data) (Table 2-2), and porcine chondrocytes (0.3-2.7 Osm/kg data) (Table 2-3) were determined in Chapter 2 and used for analysis in this chapter. In addition, osmotic equilibrium data for additional cell types, including human erythrocytes, human hepatocytes and TF-1 cells (0.3-2.7 Osm/kg data), were obtained using the same methods as describe in Chapter 2.

Ethical approval was obtained from the University of Alberta Faculty of Medicine Research Ethics Board and informed consent was obtained

from all erythrocyte and hepatocyte donors. Human whole blood (7 mL) was collected from healthy donors into vacutainer tubes containing citrate anticoagulant (BD, Fanklin Lakes, NJ, USA) using standard phlebotomy. The sample was centrifuged at 1500 g for 10 min at 4 °C (Eppendorf Centrifuge 5810R, Westbury, NY, USA). Plasma supernatant and buffy coat were removed and the erythrocyte pellet was washed three times with phosphate buffered saline (PBS; GIBCO Invitrogen Corp., Carlsbad, CA, USA). Erythrocytes were then resuspended in 5 mL of PBS buffer. Hepatocytes were isolated by technician Jamie Lewis in the laboratory of Dr. Norm Kneteman (as previously described [30,35]). Erythrocytes and hepatocytes were used for experiments immediately following isolation. TF-1 cells were cultured and prepared according to methods described in Chapter 2.

6.2.2 Cell volume measurements

The same methods used to obtain cell volume as a function of osmolality data for TF-1 cells (0.3-1.5 Osm/kg data), HUVECs, and porcine chondrocytes in Chapter 2 were used for TF-1 cells (0.3-2.7 Osm/kg) and human erythrocytes and hepatocytes.

Briefly, a Coulter Electronic Particle Counter (ZB1, Coulter Inc., Hialeah, FL, USA), fitted with a pulse-height analyzer (The Great Canadian Computer Company, Spruce Grove, AB, Canada) was used to monitor cell volume as the cells passed through the 50 µm (erythrocytes)

or 100 µm (TF-1, hepatocytes) aperture [15-17,29]. The cell suspension (150-200 µL) was injected into well-mixed hypertonic experimental solutions (10 mL). Pulse heights, which are proportional to the cell volume, were digitized as each cell traversed the aperture of the Coulter counter [29]. Latex beads (5 µm diameter (erthryocytes); 20 µm diameter (hepatocytes); Beckman Coulter, Miami, FL, USA) were used as calibrators to convert pulse heights to actual volumes in 1X PBS and in the experimental solutions. In addition for erythrocytes, the calibration factor from the beads was multiplied by a shape factor (1.18 [16]). PBS solutions of various osmolalities were prepared by diluting 10X PBS (GIBCO) with distilled water to final osmolalities ranging from 0.3 Osm/kg (1X) to 2.7 Osm/kg (9X). Osmolalities were measured using a freezing-point depression Osmometer (Precision Systems Inc., Natick, MA, USA). For each experiment, 3 replicate measurements were performed for each experimental solution. The experiments were repeated with cells from three different passages for TF-1 cells, 6 different erythrocyte donors three times each and 3 different hepatocyte donors once.

Cell volume as a function of osmolality data for various cell types of interest in cryobiology were also obtained in the literature and used in the analysis, including human erythrocytes [45], mouse blastocysts [28], mouse eight-cell embryos [28], mouse embryonic stem cells [3], porcine hepatocytes [4], and mouse ova [32].

6.2.3 Traditional Boyle van't Hoff equation

The osmotically-inactive fraction (*b*) of the cell is the fraction of the cell volume that does not contribute in the osmotic response of the cell. The traditional Boyle van't Hoff relationship [23], with ideal, dilute solution assumptions, is used in the literature to express equilibrium cell volume in solutions of impermeant solutes:

$$\frac{V}{V_o} = \frac{\pi^o}{\pi}(1-b)+b\,; \qquad 6\text{-}2$$

where V is the equilibrium cell volume (μm^3) at osmolality (π) (osmoles/kg water), V_o is the isotonic cell volume (μm^3) at isotonic osmolality (π^o), and b is the osmotically-inactive fraction of the cell volume. The osmotically-inactive fraction is found by fitting Eq. 6-2 to data of V at different values of π.

6.2.4 Osmotic virial equation approach

Since the cytoplasm contains many different solutes in varying concentrations, the osmotic virial equation [10] was used to model the thermodynamics of the cytoplasm by treating all cytoplasmic solutes together as one "grouped solute" and assuming this grouped solute has a unique second osmotic virial coefficient:

$$\pi = m + Bm^2; \qquad 6\text{-}3$$

where *m* is the molal concentration of all intracellular solutes combined into one grouped solute (mole/kg solvent) and *B* is the second osmotic virial coefficient ((mole/kg solvent)$^{-1}$). A value of zero for the second osmotic virial coefficient is the ideal dilute solution assumption (Eq. 6-1).

The Boyle van't Hoff equation has been modified by Prickett et al. [33] to eliminate the ideal, dilute solution assumptions. The non-ideal osmotically-inactive fraction (*b**) of the cell is the fraction of the cell volume not involved in the osmotic activities (the * indicating that the value is inferred from data without making ideal, dilute assumptions). The modified Boyle van't Hoff relationship [33] has been used to express equilibrium cell volume in solutions of impermeant solutes:

$$\frac{V}{V_o} = \frac{m(\pi^o)}{m(\pi)}(1 - b^*) + b^*; \qquad 6\text{-}4$$

where $m(\pi)$ is the anisotonic molality as a function of osmolality and *b** is the non-ideal osmotically-inactive fraction of the cell volume, a parameter found by fitting Eq. 6-4 to data.

The modified Boyle van't Hoff equation requires $m(\pi)$, therefore the osmotic virial equation (Eq. 6-3) was inverted:

$$m = \frac{-1+\sqrt{1+4B\pi}}{2B}; \qquad 6\text{-}5$$

and the roots were substituted into Eq. 6.4, so that the modified osmotically-inactive fraction (b*), and the second osmotic virial coefficient (B) could be solved for simultaneously using:

$$\frac{V}{V_o} = \frac{-1+\sqrt{1+4B\pi^o}}{-1+\sqrt{1+4B\pi}}(1-b^*)+b^*; \qquad 6\text{-}6$$

fit to data of V at different values of π.

6.2.5 Statistical analysis[1]

The osmotic equilibrium data were analyzed using linear regression and estimates of the osmotically-inactive fraction were determined (LINEST function, EXCEL). The coefficient of determination [7], R^2, was also calculated to assess the goodness of fit of the data to the traditional Boyle van't Hoff equation:

$$R^2 = 1-\frac{SSE}{SST} = 1-\frac{\sum_n (y_i - f_i)}{\sum_n (y_i - \bar{y})^2}; \qquad 6\text{-}7$$

[1] The author would like to acknowledge Yuri Shardt for his assistance with the statistical analysis.

where *SSE* is the sum of squared errors, also called the residual sum of squares, y_i is the value of the i[th] data point, f_i is the value calculated from the model at the i[th] data point, *n* is the number of data points, the *SST* is the total sum of squares, and $\bar{y}$ is the average of all the data points. However, the standard R^2 does not take into account the number of parameters in the model and may erroneously increase with increasing number of parameters in the equation. The adjusted coefficient of determination, adjusted R^2, is a measure of the goodness of fit of an equation to a data set, which also takes into account the number of parameters in the fitted equation. The adjusted R^2 was used to assess the necessity of adding additional parameters to the model [7]:

$$adjusted\ R^2 = 1 - \frac{SSE/(n-p-1)}{SST/(n-1)} = 1 - (1-R^2)\left(\frac{n-1}{n-p-1}\right); \qquad 6\text{-}8$$

where *p* is the number of parameters in the model (i.e. ideal model *p* = 1).

The osmotic equilibrium data were also analyzed using non-linear regression and estimates of the non-ideal osmotically-inactive fraction and the osmotic virial coefficient were determined (Matrix method, EXCEL) [34]. The adjusted R^2 was calculated where *p* =2 (Eq. 12).

The 95 % confidence intervals for each parameter were calculated, which indicates the reliability of the estimate. If the confidence intervals for the osmotic virial coefficients did not include zero *and* the adjusted R^2

for the non-ideal model was greater than or equal to the ideal model, then it was concluded that the non-ideal model (i.e. osmotic virial coefficient and modified osmotically-inactive fraction) was a better fit to the data than the ideal model (i.e. ideal osmotically-inactive fraction). Therefore, over the range of osmolalities investigated, the modified Boyle van't Hoff with the osmotic virial equation described the data more accurately than the traditional Boyle van't Hoff.

6.2.6 Comparison between ideal and non-ideal solution thermodynamic models

Once (i) the ideal osmotically-inactive fraction (b), and (ii) the non-ideal osmotically-inactive fraction (b^*) and osmotic virial coefficient of the cytoplasm (B) were determined, the parameters were used to compare the ideal and non-ideal models of the cytoplasm with reference to cryobiology. Relative equilibrium volumes were predicted as a function of subzero temperatures using the two models: (i) the ideal solution thermodynamics model, which includes the traditional Boyle van't Hoff equation, which contains ideal, dilute solution assumptions; and (ii) a non-ideal solution thermodynamics model, including the modified Boyle van't Hoff equation [33], and utilizing the osmotic virial equation [10] to remove the ideal, dilute solute assumptions.

A) Ideal solution thermodynamics model

1. $\pi = m$ 6-1

2. $V = V_o\left[\frac{\pi_o}{\pi}(1-b)+b\right]$ 6-2

B) Non-ideal solution thermodynamics model

1. $\pi = m + Bm^2$ 6-3

2. $V = V_o\left[\frac{m(\pi_o)}{m(\pi)}(1-b^*)+b^*\right]$ 6-4

3. $m = \frac{-1+\sqrt{1+4B\pi}}{2B}$ 6-5

4. $\frac{V}{V_o} = \frac{-1+\sqrt{1+4B\pi^o}}{-1+\sqrt{1+4B\pi}}(1-b^*)+b^*$ 6-6

Osmolality was calculated from freezing point depression using a commonly used conversion between osmolality and freezing point [42]:

$$\pi = \frac{T_{FP}^o - T_{FP}}{1.86}\ ; \qquad 6\text{-}9$$

where T_{FP}^o is the freezing point of the pure solvent (water) and T_{FP} is the freezing point of the solution.

In order to assess the difference in using the ideal model (A) versus the non-ideal model (B), the percent difference was calculated using:

$$\%\ difference = \frac{\left|\left[Ideal(A)\right] - \left[Non-ideal(B)\right]\right|}{\left[Non-ideal(B)\right]} \times 100\,. \qquad 6\text{-}10$$

6.2.7 Simulations of TF-1 cells using the osmotic virial coefficient of the cytoplasm

Details of the TF-1 cell parameters, solution composition and solution parameters are explained in detail in Chapters 4 and 5 (values can be found in Table 6-1). Simulations were done using obtained second osmotic virial coefficient of the cytoplasm for TF-1 cells. Maximum intracellular supercooling and osmolality were calculated using the osmotic virial coefficient of the cytoplasm for two-step freezing and graded freezing. These results (non-ideal) were compared with previous simulations in Chapter 4 and 5 using more primitive cytoplasm models of only electrolytes (ideal) or a specified intracellular protein and electrolytes ("protein").

6.3 Results

6.3.1 PBS solutions up to 2.7 Osm/kg

The osmotic equilibrium data were plotted on a traditional Boyle van't Hoff plot, which is equilibrium cell volume as a function of inverse osmolality (Figure 6-1 for TF-1 cells in up to 2.7 Osm/kg solutions)[2]. Data were first analyzed using the traditional Boyle van't Hoff equation (Eq. 6-2). This resulted in an osmotically-inactive fraction, b of 0.357 $\pm$ 0.042 (mean $\pm$ 95 % confidence intervals), with the adjusted R^2 value of 0.993. The R^2 value was also calculated; however, since it does not

[2] Equilibrium volume measurements were calculated from TF-1 experiments conducted by Marc Yu.

take into account the number of parameters in each of the models, the adjusted R^2, being a more rigorous statistical test, was used for subsequent analysis. The data were also analyzed simultaneously using the modified Boyle van't Hoff equation (Eq. 6-4), which uses the osmotic virial equation (Eq. 6-3) to obtain $m(\pi)$ (Eq. 6-5), as shown in Figure 6-1. Non-linear regression, using the Matrix method in EXCEL, was used to fit Eq. 6-5 to the data. This resulted in a non-ideal osmotically-inactive fraction (b^*) of 0.118 $\pm$ 0.004 and an osmotic virial coefficient (B) of 7.559 $\pm$ 0.559 $(\text{mole/kg})^{-1}$). The adjusted R^2 of the non-linear regression was 1.000. Since the adjusted R^2 is greater and the confidence intervals of B did not include zero, we conclude that the non-ideal model of the cytoplasm more accurately describes the equilibrium data than the ideal model where B=0 (Table 6-2). Using the osmotic virial coefficient, the phase diagram of the cytoplasm can be calculated, as demonstrated in Figure 6-2.

The analysis of HUVEC's Boyle van't Hoff data is shown in Figure 6-3. From the linear regression, the osmotically-inactive fraction (b) was 0.598 $\pm$ 0.013 (adjusted R^2 = 0.991). From the non-linear regression, the non-ideal osmotically-inactive fraction (b^*) was 0.524 $\pm$ 0.010 and the osmotic virial coefficient (B) is 2.437 $\pm$ 0.314 $(\text{mole/kg})^{-1}$) (Adjusted R^2 = 0.996). Since the adjusted R^2 is greater and the confidence intervals of B do not include zero, we conclude that for HUVECs and TF-1 cells, the non-ideal model of the cytoplasm more accurately describes the

equilibrium data than the ideal model (Table 6-2). Using the osmotic virial coefficient, the phase diagram of the cytoplasm was calculated (Figure 6-4).

For some of the cell types (porcine chondrocytes, mouse blastocysts, and porcine hepatocytes), the adjusted R^2 remained the same for the non-ideal model of the cytoplasm (Table 6-2), so the non-ideal model is at least as accurate as the ideal model, and since the confidence intervals for B did not include zero, we assert that the non-ideal model is a better description than assuming B=0 (ideal).

The non-ideal model of the cytoplasm did not more accurately represent the other cell types analyzed (human hepatocytes and mouse oocytes). The osmotic virial coefficients were zero and the R^2 adjusted decreased (Table 6-2). Therefore, the osmotic equilibrium data was well described by the traditional Boyle van't Hoff equation and the cytoplasm behaved as an ideal, dilute solution over the range of osmolalities investigated.

For the remaining cell types investigated, including mouse embryonic stem cells [3], mouse ova [32], mouse embryos [28], and human erythrocytes (our data; [45]), the non-ideal model did not converge because the shape of the data was different from ideal, even in the low range of osmolalities where the solution should be ideal, indicating the presence of other effects than thermodynamic solution non-ideality, such as mechanical properties, etc.

6.3.2 PBS solutions up to 1.5 Osm/kg

Since the majority of Boyle van't Hoff analysis in the literature was done using data obtained from hypertonic solutions only up 1.5 Osm/kg, we also compared the ideal and non-ideal models of the cytoplasm for this lower range of osmolalities. The ideal model of the cytoplasm accurately represented this is limited data for many of the cell types analyzed (i.e. the adjusted R^2 decreased when using the non-ideal model), including HUVECs, TF-1 cells, porcine chondrocytes, human hepatocytes, human keratinocytes [1], mouse oocytes [39], porcine islets [12], and hamster ova [36]. Also, with data obtained from hypertonic solutions only up 1.5 Osm/kg, the osmotically-inactive fraction did not change significantly with the modified Boyle van't Hoff equation and the osmotic virial equation. Therefore, data up to only 1.5 Osm/kg is not sufficient to determine estimates of the osmotic virial coefficient for any of the cell types analyzed.

6.3.3 Predictions of low temperature cellular responses

For TF-1 cells and HUVECs, two cell types which had non-ideal solution thermodynamic properties of the cytoplasm, we also investigated the impact of the cytoplasm model in the context of cryobiology. Figure 6-5 shows the relative cell volume of TF-1 cells as a function of subzero temperature for both ideal and non-ideal models of the cytoplasm down to -40 °C. The two models begin to diverge at -5 °C, with the greatest difference being at lower subzero temperatures. Using the ideal model,

the calculated relative cell volume was higher than with the non-ideal model. For example at -40 °C, the relative cell volume using the ideal model was 0.375 compared to the non-ideal model relative cell volume of 0.255. There was a 40 % difference in using the ideal model versus the non-ideal model. Figure 6-6 shows the relative cell volume of HUVECs as a function of subzero temperature. Using the ideal model, the relative cell volume calculated was also higher than with the non-ideal model. For example at -40 °C, the relative cell volume using the ideal model was 0.603 compared to the non-ideal model which was 0.556, where there was an 8.1 % difference in using the ideal model versus the non-ideal model. The disparity between the two models could have consequences when simulating effects of low temperatures on cellular osmotic responses.

Maximum intracellular supercooling and osmolality were calculated using the osmotic virial coefficient of the cytoplasm (cytoplasm model) for TF-1 cells for two-step freezing and shown in Figure 6-7a and 6-7b respectively. These results were also compared with previous two-step freezing simulations using cytoplasm models of only electrolytes (ideal) or a single specified intracellular protein and electrolytes (protein) (Chapter 4). The predicted maximum intracellular supercooling using the cytoplasm model followed a similar trend during both the first step and the second step cooling profiles in the predictions using the ideal and the protein cell models. However, the predicted maximum supercooling using the cytoplasm model was higher in the second step of the profile than the

other models. Furthermore, using the ideal model or the protein model introduced a 17.8 % difference or a 9.6 % difference, respectively (percentage difference calculated at -15 °C). Predicted maximum intracellular osmolality using the cytoplasm model also followed a similar trend for both first step and the second step cooling profiles as the predictions using the ideal and the protein cell models. However, the predicted maximum osmolality using the cytoplasm model was lower in the second step of the profile with a 25.3 % difference using the ideal model and 13.1 % difference using the protein model (percentage difference calculated at -15 °C).

Predicted maximum intracellular supercooling and osmolality were calculated using the osmotic virial coefficient of the cytoplasm (cytoplasm model) for TF-1 cells for graded freezing protocols and are shown in Figure 6-8a and 6-8b, respectively. These results were also compared with previous graded freezing simulations using cytoplasm models of only electrolytes (ideal) or a single specified intracellular protein and electrolytes (Chapter 5). Predicted maximum intracellular supercooling and osmolality using the cytoplasm model followed similar trends for both the direct thaw and plunge cooling profiles as the predictions from the ideal and the protein cell models. The predicted maximum supercooling using the cytoplasm model was higher in the plunge step of the profile, with a 6.0 % difference using the ideal model and 2.6 % difference using the protein model (percentage difference calculated at -15 °C). The

predicted maximum osmolality using the cytoplasm model was lower in the plunge of the profile with an 8.3 % difference using the ideal model and 3.4 % difference using the protein model (percentage difference calculated at -15 °C). Although the predictions when using the ideal or the protein and electrolyte models were close to predictions when using the measured value description of the cytoplasm, there was still some difference associated with these models.

6.4 Discussion

The purpose of this study was to develop and demonstrate a novel technique of inferring the thermodynamic solution properties of the cytoplasm and the modified osmotically-inactive fraction of a living nucleated cell from measurements without making any ideal, dilute solution assumptions. Another purpose of this study was to show that the newly measured osmotic parameters make a difference in predictions of cellular responses to low temperatures.

Based on the results of this study, the osmotic equilibrium data obtained using the conventional range of osmolalities (up to 1.5 Osm/kg) was not sufficient to explore the non-ideality of the cytoplasm. Although these data appears linear when plotted on a traditional Boyle van't Hoff plot, it was limiting as it results in erroneously large values for the osmotically-inactive fraction.

This study demonstrated that in order to obtain second osmotic virial coefficients, exposure to higher osmolality of the hypertonic solutions than is traditionally used (i.e. greater than ~1.5 Osm/kg) is required. The osmotic equilibrium data obtained using hypertonic solutions ranging up to 2.7 Osm/kg, showed the non-ideality of the cytoplasm for several cell types. The modified osmotically-inactive fraction (b^*) and the osmotic virial coefficient (B) were calculated for TF-1 cells, HUVECs, porcine chondrocytes, mouse embryos, and porcine hepatocytes (Table 6-2). The osmotically-inactive fractions of the cells, determined without ideal, dilute solution assumptions, were significantly lower than when using dilute solution assumptions. The other cell types, including human hepatocytes and mouse oocytes, may require additional osmotic equilibrium measurements at an even higher range of osmolalities (i.e. greater than 2.7 Osm/kg) in order to determine their cytoplasmic osmotic virial coefficients. The solution thermodynamics model could not be used to describe the shape of the data for mouse embryonic stem cells [3], mouse ova [32], human erythrocytes (our data; [45]), and mouse embryos [28].

The phase diagram of the cytoplasm of human erythrocytes has been measured using ESR [8,10,25,33]. It has been shown that the solution thermodynamics of human erythrocytes' cytoplasm are highly non-ideal [10,33] and can be accurately described by a multisolute cubic osmotic virial equation [10] assuming the cytoplasm is made up of hemoglobin (B=49.3 $(\text{mole/kg})^{-1}$, C=3.07x10^4 $(\text{mole/kg})^{-1}$) and an ideal

solute (B=0) [10]. In addition, the solutes in the cytoplasm could be treated as a grouped solute, using a slightly different version of a cubic osmotic virial equation, with the following osmotic virial coefficients: A=298.49, B=-66.46 and C=53.42 (note: the coefficients do not have units due to the different form of the osmotic virial equation) [33]. To compare these previous predictions with the results from this study, we fit the hemoglobin and an ideal solute model of the cytoplasm with a quadratic osmotic virial equation to estimate an overall second osmotic virial coefficient for the erythrocyte resulting in B=3.75 $(\text{mole/kg})^{-1}$). TF-1 cells and the mouse blastocysts were more non-ideal (B>3.75 $(\text{mole/kg})^{-1}$) than the erythrocytes, while the other cell types were more ideal (B<3.75 $(\text{mole/kg})^{-1}$) within the range of osmolalities investigated in this study.

The range of osmolalities used in this study correspond to freezing a cell in suspension to -3 °C (1.5 Osm/kg) and -5 °C (2.7 Osm/kg), so it's not surprising that cellular osmotic responses can be adequately described using ideal solutions over this range. Demonstrating the non-ideality of the cytoplasm for some types of nucleated cells provides impetus to extend the range of Boyle van't Hoff measurements beyond the range of this study. Novel methods for obtaining these measurements are required, including the possibility of measurements at low temperatures.

Another significant finding of this study was that the non-ideality of the solution properties of the cytoplasm played a significant role in cellular

osmotic responses at subzero temperatures particularly for the two-step protocol which has segments of rapid cooling. The equilibrium cell volumes at subzero temperatures for TF-1 and HUVECs using the measured osmotic virial coefficient of the cytoplasm were always lower than when using an ideal cytoplasm below -5 °C. Therefore, assuming ideal solution properties of the cytoplasm resulted in higher relative equilibrium volumes than with non-ideal solution properties. Previously in simulations, the solution properties of the cytoplasm used were approximations: ideal, dilute (Chapter 4 and 5) [3,6,9,11,13,14,18,19,22,26,27,36-38,40,41,43,44]; and a single specified intracellular protein and electrolytes (Chapter 4 and 5) [20,21,24]. This study represents novel simulations using the newly measured osmotic parameters of the cytoplasm of nucleated cells. Simulations of TF-1 osmotic responses at low temperatures were investigated using two-step and graded freezing cooling profiles. The newly measured osmotic parameters showed a difference in predictions of intracellular supercooling and osmolality, which can be used as indicators of injury associated with intracellular ice formation and solution effects, respectively. These newly measured parameters are particularly necessary when modeling rapid cooling without cryoprotectants. This could ultimately contribute to more accurate simulations used to design novel cryopreservation protocols for any cell type with known osmotic properties.

6.5 References

[1] J.P. Acker, A. Larese, H. Yang, A. Petrenko, and L.E. McGann, Intracellular ice formation is affected by cell interactions. Cryobiology 38 (1999) 363-371.

[2] B. Alberts, D. Bray, J. Lewis, M. Raff, K. Roberts, and J.D. Watson, Molecular biology of the cell, Garland Publishing, Inc, New York & London, 1994.

[3] C.M.K. Benson, J.D. Benson, and J.K. Critser, An improved cryopreservation method for a mouse embryonic stem cell line. Cryobiology 56 (2008) 120-130.

[4] T.B. Darr, and A. Hubel, Freezing characteristics of isolated pig and human hepatocytes. Cell Transplantation 6 (1997) 173-183.

[5] D.A.T. Dick, and L.M. Lowenstein, Osmotic equilibria in human erythrocytes studied by immersion refractometry. Proceedings of the Royal Society of London Series B-Biological Sciences 148 (1958) 241-256.

[6] K.R. Diller, and M.E. Lynch, An irreversible thermodynamic analysis of cell freezing in the presence of membrane-permeable additives .2. Transient electrolyte and additive concentrations. Cryoletters 5 (1984) 117-130.

[7] N.R. Draper, Applied regression analysis, John Wiley & Sons, Inc., New York, NY, 1998.

[8] J. Du, Biophysical study of mammalian sperm utilizing electron paramagnetic resonance, Purdue University, 1995, pp. 122.

[9] S.L. Ebertz, and L.E. McGann, Osmotic parameters of cells from a bioengineered human corneal equivalent and consequences for cryopreservation. Cryobiology 45 (2002) 109-117.

[10] J.A.W. Elliott, R.C. Prickett, H.Y. Elmoazzen, K.R. Porter, and L.E. McGann, A multi-solute osmotic virial equation for solutions of interest in biology. Journal of Physical Chemistry B 111 (2007) 1775-1785.

[11] G.M. Fahy, Simplified calculation of cell water-content during freezing and thawing in nonideal solutions of cryoprotective agents and its possible application to the study of solution effects injury. Cryobiology 18 (1981) 473-482.

[12] C. Fedorow, L.E. McGann, G.S. Korbutt, G.R. Rayat, R.V. Rajotte, and J.R.T. Lakey, Osmotic and cryoprotectant permeation characteristics of islet cells isolated from the newborn pig pancreas. Cell Transplantation 10 (2001) 651-659.

[13] D.Y. Gao, C. Liu, C.T. Benson, J. Liu, E.S. Critser, J.K. Critser, L.E. McGann, and S. Lin, Theoretical and experimental analyses of optimal experimental design for determination of hydraulic conductivity of cell membrane. in: L.J. Hayes, and R.B. Roemer, (Eds.), Advances in heat and mass transfer in biological systems.,

American Society of Mechanical Engineers., New York, N. Y., 1994, pp. 151-158.

[14] J.A. Gilmore, J. Liu, E.J. Woods, A.T. Peter, and J.K. Critser, Cryoprotective agent and temperature effects on human sperm membrane permeabilities: convergence of theoretical and empirical approaches for optimal cryopreservation methods. Human Reproduction 15 (2000) 335-343.

[15] N.B. Grover, J. Naaman, S. Ben-Sasson, and F. Doljanski, Electrical sizing of particles in suspensions. I: Theory. Biophysical Journal 9 (1969) 1398-1414.

[16] N.B. Grover, J. Naaman, S. Ben-Sasson, and F. Doljanski, Electrical sizing of particles in suspensions. III: Rigid spheroids and red blood cells. Biophysical Journal 12 (1972) 1099-1117.

[17] N.B. Grover, J. Naaman, S. Ben-Sasson, F. Doljanski, and E. Nadav, Electrical sizing of particles in suspensions. II: Experiments with rigid spheres. Biophysical Journal 9 (1969) 1415-25.

[18] J.O.M. Karlsson, E.G. Cravalho, and M. Toner, A model of diffusion-limited ice growth inside biological cells during freezing. Journal of Applied Physics 75 (1994) 4442-4445.

[19] J.O.M. Karlsson, A. Eroglu, T.L. Toth, E.G. Cravalho, and M. Toner, Fertilization and development of mouse oocytes cryopreserved using a theoretically optimized protocol. Human Reproduction 11 (1996) 1296-1305.

[20] R.L. Levin, E.G. Cravalho, and C.E. Huggins, Effect of hydration on water-content of human erythrocytes. Biophysical Journal 16 (1976) 1411-1426.

[21] R.L. Levin, E.G. Cravalho, and C.E. Huggins, Effect of solution non-ideality on erythrocyte volume regulation. Biochimica et Biophysica Acta 465 (1977) 179-190.

[22] J. Liu, E.J. Woods, Y. Agca, E.S. Critser, and J.K. Critser, Cryobiology of rat embryos II: A theoretical model for the development of interrupted slow freezing procedures. Biology of Reproduction 63 (2000) 1303-1312.

[23] B. Lucke, and M. McCutcheon, The living cell as an osmotic system and its permeability to water. Physiol. Rev. 12 (1932) 68-139.

[24] G.A. Mansoori, Kinetics of water-loss from cells at subzero centigrade temperatures. Cryobiology 12 (1975) 34-45.

[25] M. Marone, G. Scambia, G. Bonanno, S. Rutella, D. de Ritis, F. Guidi, G. Leone, and L. Pierelli, Transforming growth factor-beta 1 transcriptionally activates CD34 and prevents induced differentiation of TF-1 cells in the absence of any cell-cycle effects. Leukemia 16 (2002) 94-105.

[26] P. Mazur, Kinetics of water loss from cells at subzero temperatures and the likelihood of intracellular freezing. The Journal of General Physiology 47 (1963) 347-369.

[27] P. Mazur, Studies on rapidly frozen suspensions of yeast cells by differential thermal analysis and conductometry, 1963, pp. 323-353.

[28] P. Mazur, and U. Schneider, Osmotic responses of preimplantation mouse and bovine embryos and their cryobiological implications. Cell Biophysics 8 (1986) 259-285.

[29] L.E. McGann, A.R. Turner, and J.M. Turc, Microcomputer interface for rapid measurements of average volume using an electronic particle counter. Medical & Biological Engineering & Computing 20 (1982) 117-120.

[30] D.F. Mercer, D.E. Schiller, J.F. Elliott, D.N. Douglas, C.H. Hao, A. Rinfret, W.R. Addison, K.P. Fischer, T.A. Churchill, J.R.T. Lakey, D.L.J. Tyrrell, and N.M. Kneteman, Hepatitis C virus replication in mice with chimeric human livers. Nature Medicine 7 (2001) 927-933.

[31] M.M. Moronne, R.J. Mehlhorn, M.P. Miller, L.C. Ackerson, and R.I. Macey, ESR measurement of time-dependent and equilibrium volumes in red-cells. Journal of Membrane Biology 115 (1990) 31-40.

[32] K. Oda, W.E. Gibbons, and S.P. Leibo, Osmotic shock of fertilized mouse ova. Journal of Reproduction and Fertility 95 (1992) 737-747.

[33] R.C. Prickett, J.A.W. Elliott, S. Hakda, and L.E. McGann, A non-ideal replacement for the Boyle van't Hoff equation. Cryobiology 57 (2008) 130-136.

[34] R.C. Prickett, J.A.W. Elliott, and L.E. McGann, Application of the osmotic virial equation in cryobiology. Cryobiology (accepted) (2009).

[35] P.O. Seglen, Preparation of isolated rat liver cells, Prescott, David M., 1976, pp. 29-83.

[36] M. Shabana, and J.J. Mcgrath, Cryomicroscope investigation and thermodynamic modeling of the freezing of unfertilized hamster ova. Cryobiology 25 (1988) 338-354.

[37] S. Thirumala, and R.V. Devireddy, A simplified procedure to determine the optimal rate of freezing biological systems. Journal of Biomechanical Engineering 127 (2005) 295-300.

[38] M.R. Tijssen, H. Woelders, A. de Vries-van Rossen, C.E. van der Schoot, C. Voermans, and J.M. Lagerberg, Improved postthaw viability and in vitro functionality of peripheral blood hematopoietic progenitor cells after cryopreservation with a theoretically optimized freezing curve. Transfusion 48 (2008) 893-901.

[39] M. Toner, E.G. Cravalho, and D.R. Armant, Water transport and estimated transmembrane potential during freezing of mouse oocytes. Journal of Membrane Biology 115 (1990) 261-272.

[40] M. Toner, E.G. Cravalho, and M. Karel, Thermodynamics and kinetics of intracellular ice formation during freezing of biological cells. Journal of Applied Physics 67 (1990) 1582-1593.

[41] M. Toner, E.G. Cravalho, and M. Karel, Cellular-response of mouse oocytes to freezing stress - prediction of intracellular ice formation. Journal of Biomechanical Engineering-Transactions of the Asme 115 (1993) 169-174.

[42] D.J. Winzor, Reappraisal of disparities between osmolality estimates by freezing point depression and vapor pressure deficit methods. Biophysical Chemistry 107 (2004) 317-323.

[43] H. Woelders, and A. Chaveiro, Theoretical prediction of 'optimal' freezing programmes. Cryobiology 49 (2004) 258-271.

[44] E.J. Woods, J. Liu, K. Pollok, J. Hartwell, F.O. Smith, D.A. Williams, M.C. Yoder, and J.K. Critser, A theoretically optimized method for cord blood stem cell cryopreservation. J Hematother Stem Cell Res 12 (2003) 341-350.

[45] G. Zhao, L.Q. He, H.F. Zhang, W.P. Ding, Z. Liu, D.W. Luo, and D.Y. Gao, Trapped water of human erythrocytes and its application in cryopreservation. Biophysical Chemistry 107 (2004) 189-195.

Table 6-1. Parameters used in simulations: (a) isotonic solution composition, (b) solution parameters, and (c) osmotic parameters for TF-1 cells

a) Isotonic solution composition

	Extracellular	Intracellular
NaCl	0.170 molal	0.010 molal
KCl	0.005 molal	0.133 molal
Protein	0	0.004 molal
Total Osmolality	0.300 osm/kg	0.300 osm/kg

b) Solution parameters

	B (mol/kg solvent)$^{-1}$	C (mol/kg solvent)$^{-2}$	K
NaCl	0.02986	0	1.702
KCl	0	0	1.742
Protein†	49.3	3.07×10^4	1

c) Osmotic parameters [Chapter 2]

Isotonic volume, V_o	916 μm^3
Inactive fraction, b	0.361
E_a (Activation Energy for L_p)	14.2 kcal/mol
k_1 (Pre-exponential factor for L_p)	1.33×10^{10} $\mu m^3/\mu m^2$/min/atm

†based on values reported for hemoglobin
L_p is for hydraulic conductivity

Table 6-2. Ideal osmotically-inactive fraction (*b*), non-ideal osmotically-inactive fraction (*b**), osmotic virial coefficient (*B*), R^2, and adjusted R^2 (Adj. R^2) for various cell types.

Cell types	*b* [± 95 % C.I.]	*B* (mole/kg)$^{-1}$ [± 95 % C.I.]	R^2	Adj. R^2	*b** [± 95 % C.I.]	*B* (mole/kg)$^{-1}$ [± 95 % C.I.]	R^2	Adj. R^2
TF-1	0.357 [± 0.042]	0	0.995	0.993	0.118 [± 0.004]	7.559 [± 0.559]	1.000	1.000
Mouse blastocyst[1]	0.234 [± 0.079]	0	0.981	0.976	0.056 [± 0.061]	4.823 [± 3.699]	0.986	0.976
HUVEC	0.598 [± 0.013]	0	0.993	0.991	0.524 [± 0.010]	2.437 [± 0.341]	0.997	0.996
Porcine hepatocyte[2]	0.250 [± 0.006]	0	0.999	0.998	0.185 [± 0.016]	0.606 [± 0.033]	0.999	0.998
Porcine chondrocyte	0.580 [± 0.010]	0	0.997	0.996	0.548 [± 0.010]	0.433 [± 0.016]	0.997	0.996
Human hepatocyte	0.572 [± 0.014]	0	0.992	0.991	0.569 [± 0.017]	0.000***** [± 0.000]	0.990	0.987
Mouse oocyte[3]	0.206 [± 0.063]	0	0.987	0.984	0.198 [± 0.057]	0.000***** [± 0.000]	0.985	0.975

*The results were less than $1x10^{-6}$ which we assumed to be zero.

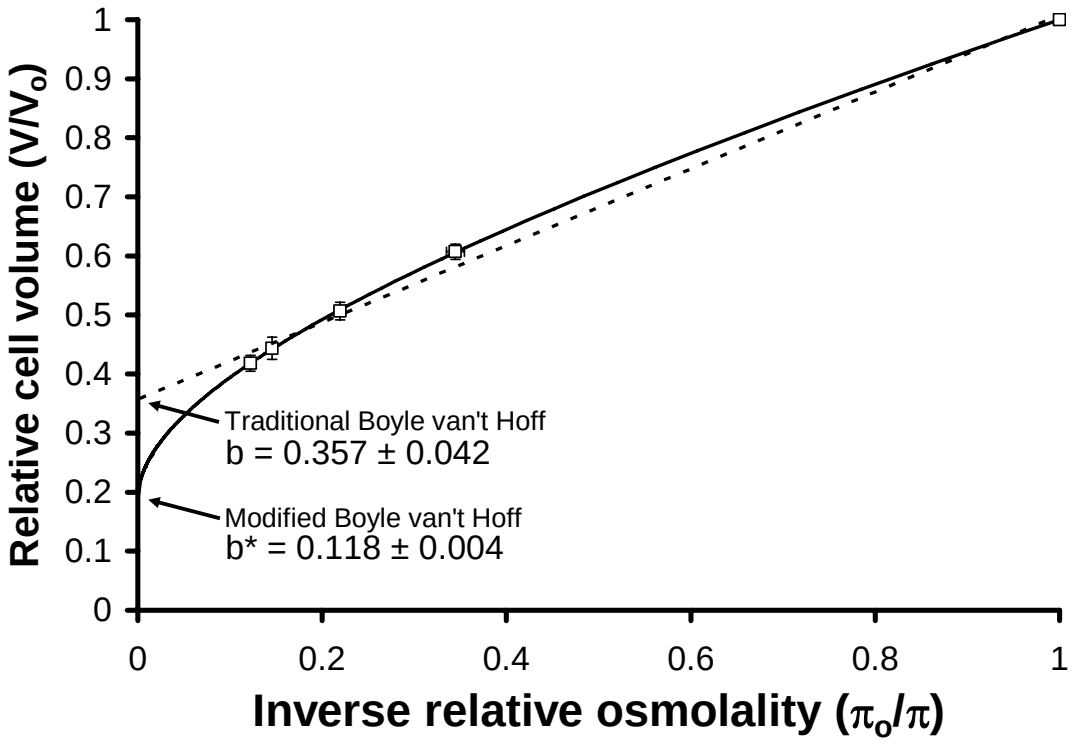

Figure 6-1. Osmotic equilibrium plot for TF-1 cells in phosphate buffered saline. The symbols represent the experimental relative cell volumes in hypertonic solutions (mean ± sem). The dashed line is the Boyle van't Hoff equation and represents the linear regression fit of Eq. 6-2 to the data. The solid line represents the non-linear regression fit of Eq. 6-6 to the data. The y-intercepts (± C.I.) give the ideal osmotically-inactive fraction, *b*, and the non-ideal osmotically inactive fraction, b*. In the modified Boyle van't Hoff equation, inverse relative molality is the independent variable; however we've included the modified Boyle van't Hoff on the traditional Boyle van't Hoff graph for direct comparison.

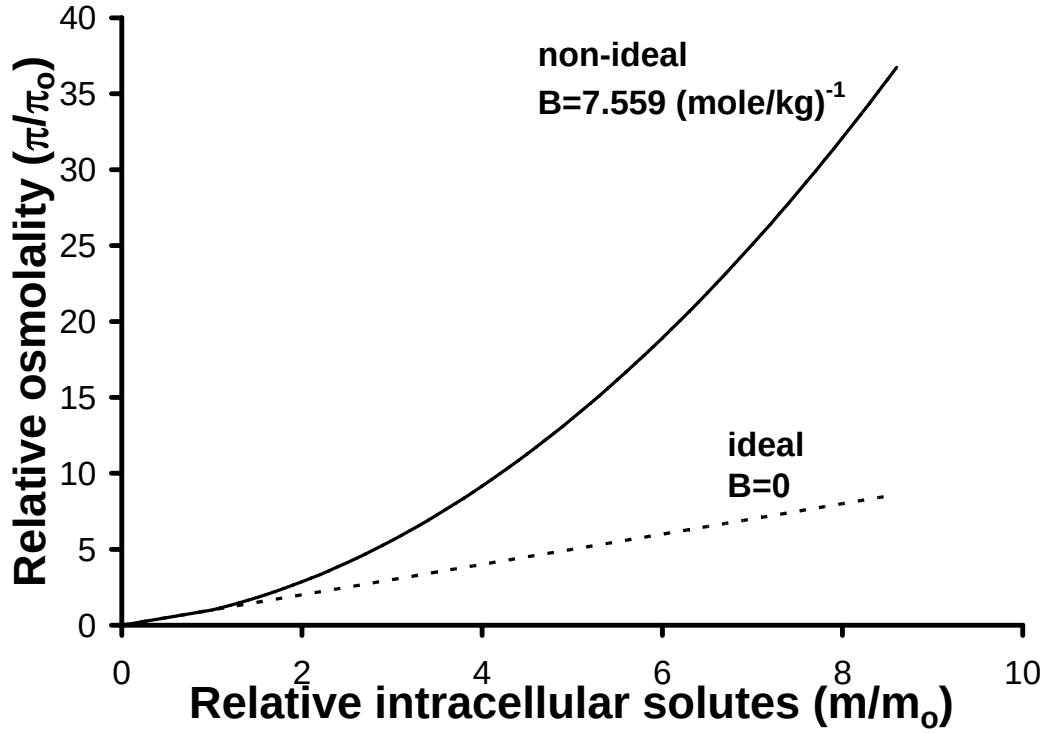

Figure 6-2. Relative osmolality as a function of intracellular solute concentration for TF-1 cells. The dashed line is predicted assuming the cytoplasm behaves as an ideal solution (Eq. 6-1). The solid line is predicted assuming non-ideality of the cytoplasm using the osmotic virial equation (Eq. 6-3) and the measured second osmotic virial coefficient ($B=7.559\ (mole/kg)^{-1}$).

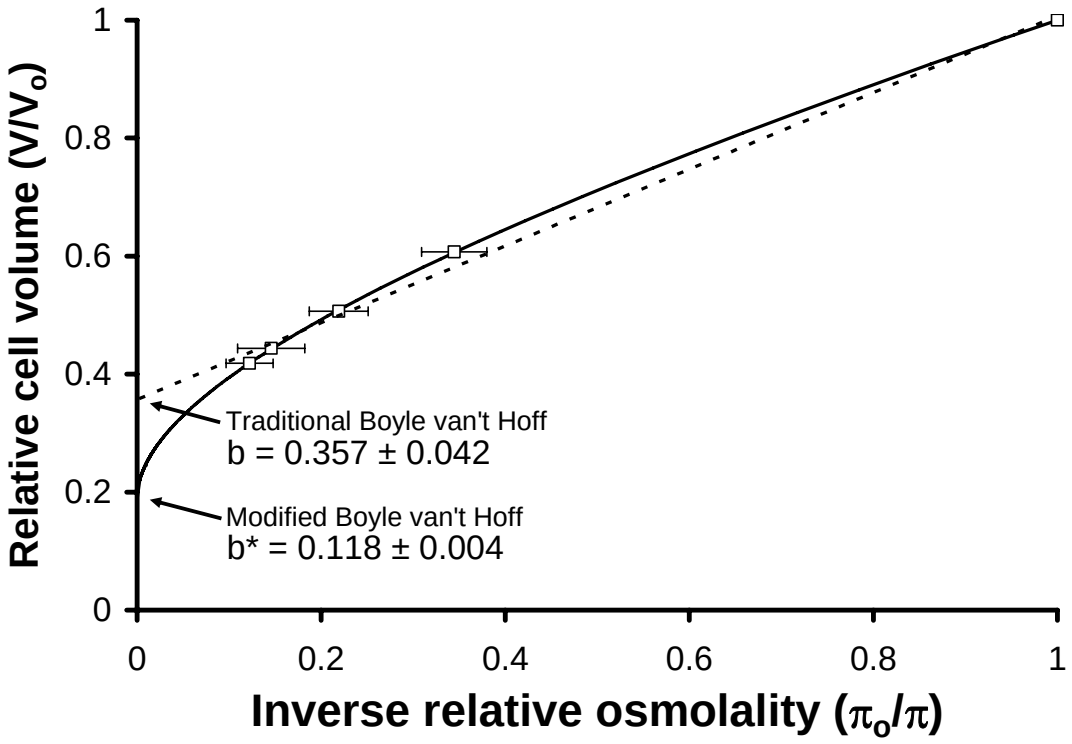

Figure 6-3. Osmotic equilibrium plot for HUVECs in phosphate buffered saline. The symbols represent the experimental relative cell volumes in hypertonic solutions (mean ± sem). The dashed line is the Boyle van't Hoff equation and represents the linear regression fit of Eq. 6-2 to the data. The solid line represents the non-linear regression fit of Eq. 6-6 to the data, which includes a description of the non-ideality of the cytoplasm. The y-intercepts (± C.I.) give the ideal osmotically-inactive fraction, *b*, and the non-ideal osmotically inactive fraction, b*. In the modified Boyle van't Hoff equation, inverse relative molality is the independent variable; however we've included the modified Boyle van't Hoff on the traditional Boyle van't Hoff graph for direct comparison.

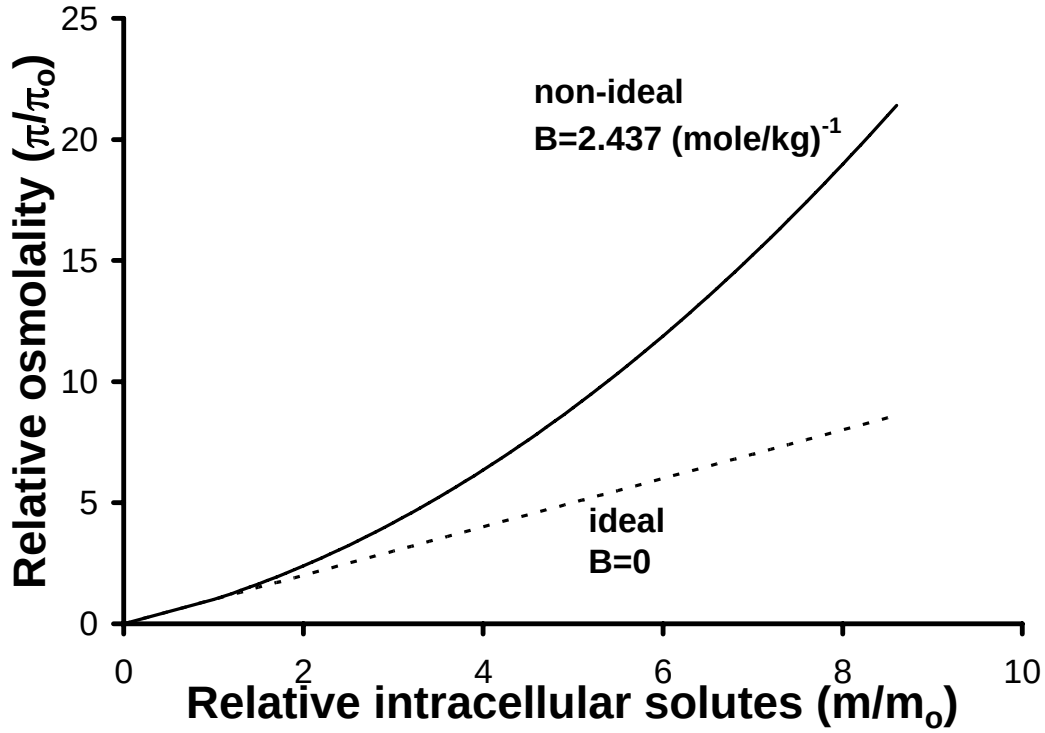

Figure 6-4. Relative osmolality as a function of intracellular solute concentration for HUVECs. The dashed line is predicted assuming the cytoplasm behaves as an ideal, dilute solution (Eq. 6-1). The solid line is predicted assuming non-ideality of the cytoplasm using the osmotic virial equation (Eq. 6-3) and the measured second osmotic virial coefficient (B=2.437 (mole/kg)$^{-1}$).

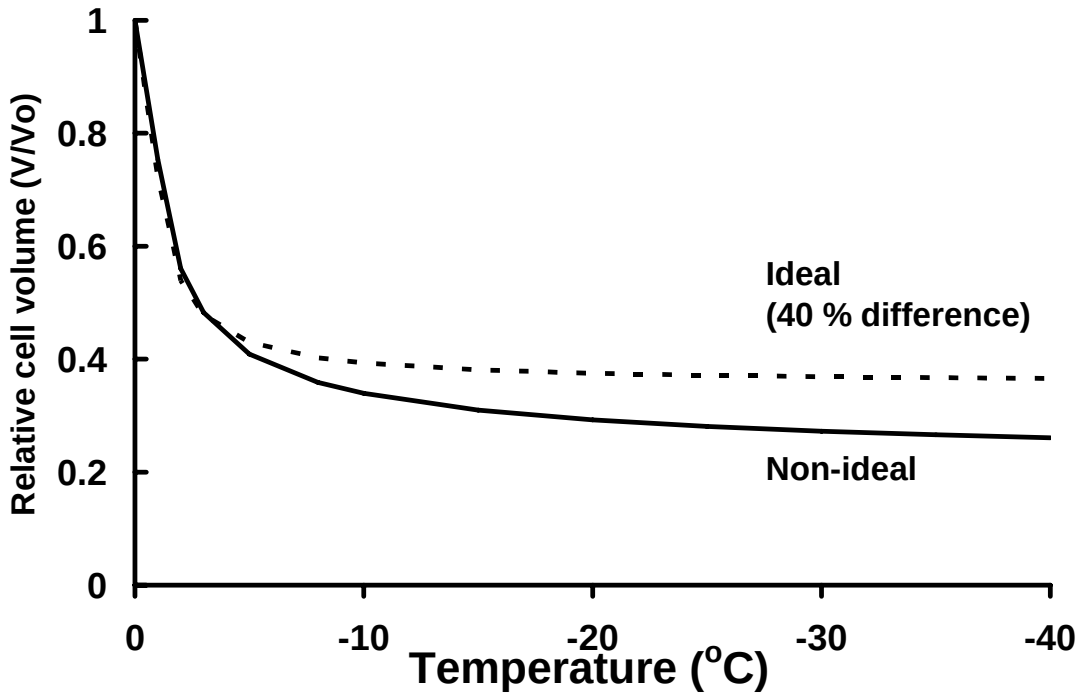

Figure 6-5. The relative cell volume as a function of subzero temperature for TF-1 cells for ideal and non-ideal models of the cytoplasm. The dashed line is using ideal osmotic equilibrium equations (Eqs. 6-1, 6-2) to determine the cell volume as a function of temperature. The solid line is using non-ideal osmotic equilibrium equations (Eqs. 6-3 to 6-6) to determine the cell volume as a function of temperature. The percent difference was calculated at -40 °C.

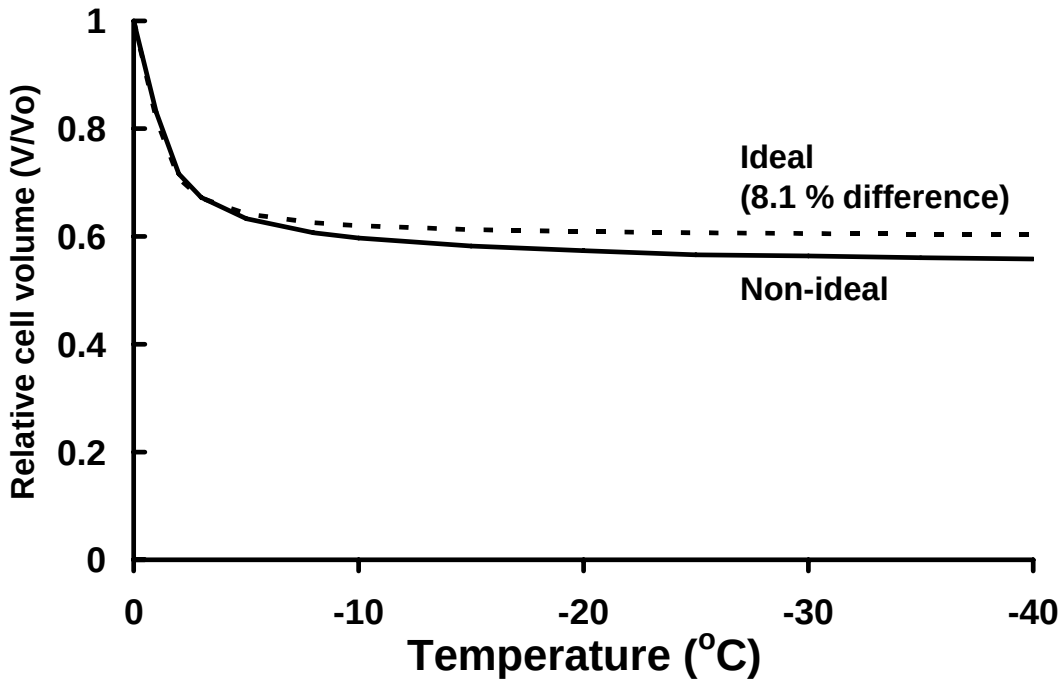

Figure 6-6. The relative cell volume as a function of subzero temperature for HUVECs for ideal and non-ideal models of the cytoplasm. The dashed line is using ideal osmotic equilibrium equations (Eqs. 6-1, 6-6, 6-7) to determine the cell volume as a function of temperature. The solid line is using non-ideal osmotic equilibrium equations (Eqs. 6-4, 6-8, 6-9) to determine the cell volume as a function of temperature. The percent difference was calculated at -40 °C.

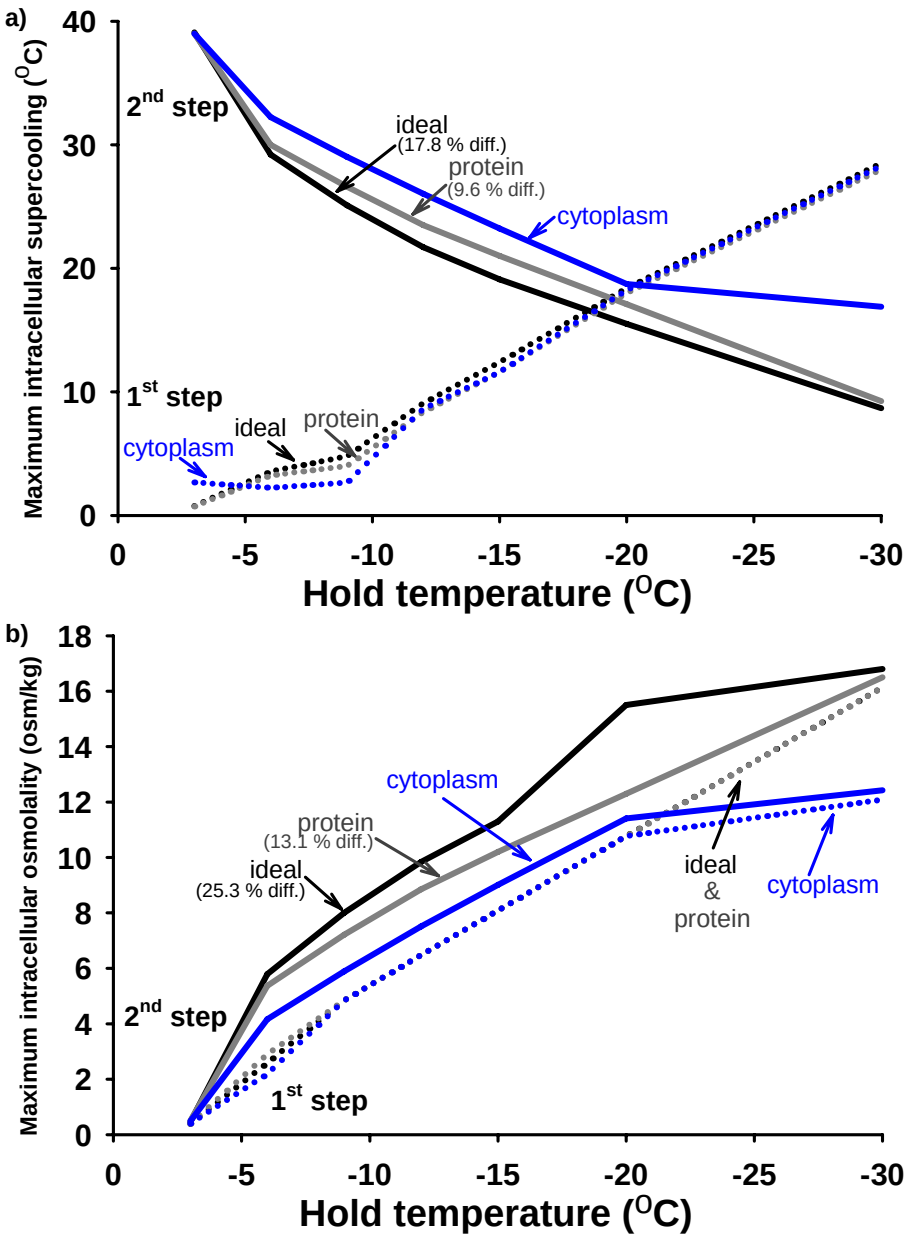

Figure 6-7. Simulations of two-step freezing with various cell models of the cytoplasm: ideal; with a single specified intracellular protein and electrolytes (protein); and non-ideal (cytoplasm). (a) Predicted maximum intracellular supercooling and (b) predicted maximum intracellular osmolality during 1st step (dotted line) and the 2nd step (solid line) as a function of hold temperature for TF-1 cells. The percent difference (% diff.) was calculated at -15 °C.

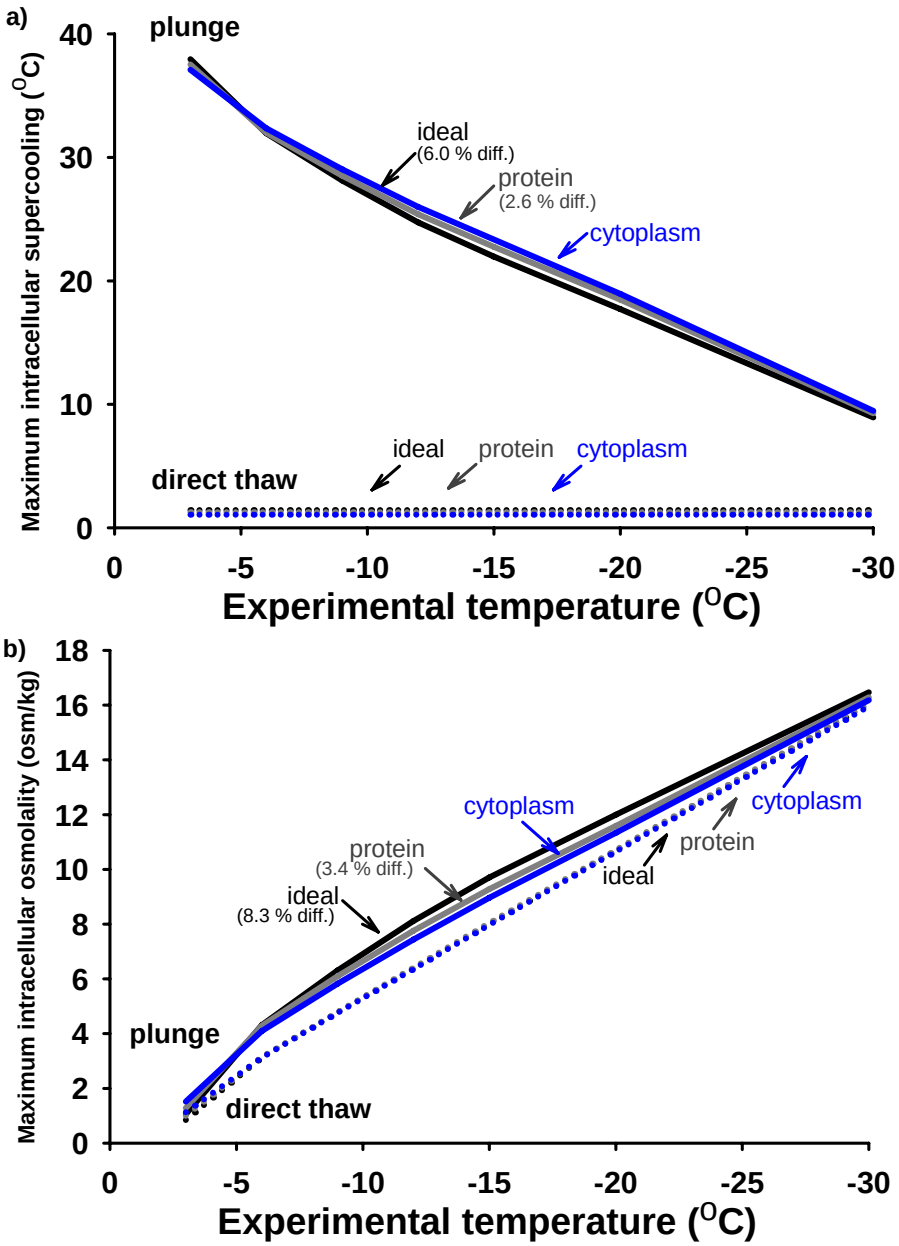

Figure 6-8. Simulations of graded freezing with various cell models: ideal; with a single specified intracellular protein and electrolytes (protein); and non-ideal (cytoplasm). (a) Predicted maximum intracellular supercooling and (b) predicted maximum intracellular osmolality during direct thaw (dotted line) and the plunge step (solid line) as a function of experimental temperature for TF-1 cells. The percent difference (% diff.) was calculated at -15 °C.

Chapter 7. Overall Discussion and General Conclusions

7.1 Summary of thesis

Development of protocols for cryopreservation of cells has largely been approached empirically. Although this has met with success for many cellular systems, protocols may not be achieving the maximum recovery of cells or may be inflicting unnecessary complications, such as dimethyl sulfoxide (Me_2SO) toxicity to patients using cryopreserved hematopoietic stem cells (HSCs). Major challenges exist in maintaining cell viability at a range of subzero temperatures, including liquid nitrogen temperatures (-196°C), without the use of toxic cryoprotectants. These challenges have been approached largely empirically; however, this research proposes a fundamentally different approach: combining theoretical modeling and biological experimentation. In order for this approach to be successful, a more accurate description of the osmotic solution properties of the cell (i.e. osmolality as a function of molality of the cytoplasm) is required. Also, in-depth examination into the correlation between predictions of the two types of cryoinjury and measured post-thaw biological outcomes is necessary. The overall goal of this thesis was to develop approaches using simulations that can be applied to development of cryopreservation procedures for HSCs and other cell types of interest for cellular therapies.

The first study calculated the osmotic parameters, using equations from the literature to fit cell volume measurements. Cell volumes were

determined using a modified Coulter counter, fitted with a cell size analyzer following exposure to hypertonic solutions and their change in volume was monitored over time. Various cell types of interest in cryopreservation were used in this study, including TF-1 cells, a model for HSCs, human umbilical vein endothelial cells (HUVECs), and porcine chondrocytes. Osmotic parameters from this study showed that these cell types were relatively slow responding cells and that the movement of water across the plasma membrane is highly dependent on temperature. This study demonstrated the diversity among cell types and sources indicating that different cell types require different conditions for cryopreservation.

The second study in this thesis was to characterize the cryobiological responses of TF-1 cells using interrupted freezing procedures: two-step freezing (rapid interrupted cooling with hold time); and graded freezing (slow interrupted cooling without hold time). TF-1 cells had higher cell recovery with Me_2SO and graded freezing. Without Me_2SO using two-step freezing, the cell recovery was comparable to the conventional approach (i.e. slow cooling with 10 % Me_2SO), demonstrating the possibilities of alternatives to constant cooling rates and cryoprotectants.

The third study in this thesis was to demonstrate the use of calculated intracellular supercooling, as an indicator of intracellular ice formation, to understand post-thaw biological outcomes. We used

osmotic parameters for TF-1 cells (Chapter 2) to model the two-step freezing procedure (Chapter 3). High amounts of intracellular supercooling were correlated with low cell recovery. Also, it was demonstrated that cells could withstand a higher amount of supercooling in the second step of the cooling profile than in the first step. This study also demonstrated that the inclusion of intracellular protein in the model of the cytoplasm had minimal effect on calculated maximum supercooling. Also, including nucleation heat in simulations changed the calculated maximum supercooling for both steps of the cooling profile only at high subzero temperatures. This study also demonstrated the value of a combining theoretical and empirical work for interpretation of cryopreservation protocols.

The fourth study in this thesis was to dissect the components of cryoinjury using simulations of a graded freezing procedure (slow interrupted cooling without hold time). We also used osmotic parameters for TF-1 cells (Chapter 2) to model the graded freezing procedure (Chapter 3). In addition to intracellular supercooling as an indicator of intracellular ice formation, we used intracellular osmolality as an indicator of solution effects injury, associated with slow cooling. We demonstrated that while intracellular supercooling was sufficient to explain injury with rapid cooling (i.e. two-step freezing up to 10 minutes hold time); both indicators of injury were required to explain injury associated with slow

cooling (i.e. graded freezing) and potentially rapid cooling with long hold times.

The final contribution of this thesis was to develop a new procedure to measure the osmotic solution properties (i.e. osmolality as a function of molality) of the cytoplasm of living cells and evaluate the effect of using these measured properties on calculated indicators of cryoinjury in simulations. We used the osmotic virial equation with the modified Boyle van't Hoff equation to calculate the phase diagram (i.e. osmolality as a function of molality) of the cytoplasm of living cells without any ideal, dilute solution assumptions. Of the various cell types of interest in cryopreservation that we studied, we were able to calculate the second osmotic virial coefficient and modified osmotically-inactive fraction for 7 cell types, including TF-1 cells, HUVECs, porcine chondrocytes, mouse blastocysts, and porcine hepatocytes. Using the newly calculated parameters for TF-1 cells and HUVECs, we demonstrated the magnitude of error introduced by making ideal, dilute solution assumptions in cellular responses to low temperatures, including simulations of interrupted freezing procedures (Chapter 3 and 4).

7.2 Implications of this thesis

Our research approach is to use detailed knowledge of cellular osmotic properties, including osmotic solution properties of the intra- and extracellular solutions, to manipulate cooling profiles in order to replace

cryoprotectants as the method to minimize the two types of cryoinjury. Previously, cellular osmotic properties have been included in these simulations; however, the simulations were limited by the use of a simple cell model (electrolytes + cryoprotectant) of the cytoplasm, permeating cryoprotectants (type and concentration), and linear cooling rates. Our novel approach to simulations is not limited by these constraints. This thesis has shown that simulations coupled with interrupted cooling procedures can be used to determine conditions that minimize the two identified damaging factors in cryopreservation. We have also shown a novel method of obtaining the solution properties (i.e. osmolality as a function of molality) of the cytoplasm of living cells. Previously, the theoretical field of cryobiology has been almost entirely focused on the solution properties of the extracellular solution, with only cursory attention given to the cytoplasm. This research should inspire cryobiologists to conduct more rigorous simulations, including the measured solution properties of the cytoplasm. We have essentially added a new parameter of the cell that allows for more accurate descriptions of cellular low temperature responses. This thesis has now extended the approach to cryopreservation to include the properties of the cell and the physical conditions of the freezing environment. This approach was only possible through the linkage between biological experimentation and simulations.

7.3 Limitations of this study

While this study enabled us to gain considerable understanding of the osmotic characteristics, the characterization of the cryobiological responses and the solution properties of the cytoplasm of various cell types, there are limitations that prevent us from making specific recommendations for transplantation based on these findings. Some of this research was conducted using TF-1 cells, a cell line, as a model of primary cells, such as bone marrow, peripheral blood and cord blood stem cells. Tissue culture cells provide more consistent and repeatable results in both the measurement of osmotic parameters and the assessment of biological outcomes. However, now that the principle has been established, further studies with primary HSCs are required in order to make clinical recommendations.

For proof of principle, we used membrane integrity as the sole indicator for cell viability. Although, the membrane has been shown to be the primary site of cryoinjury for most cell types, functional assays, including cell-specific assays, should be included prior to the use of these findings for clinical applications.

Although this research enabled us to calculate the solution properties of the cytoplasm for some cell types, we did not have sufficient data at the very high ranges of osmolalities. It is at this range that the non-ideality of the cytoplasm becomes very apparent and wherein further research is warranted.

7.4 General conclusions and recommendations

Simulations can be used to theoretically describe osmotic and low temperature responses of cells. As cryobiologists continue to broaden the scope of cells and tissues which require cryopreservation, there is an increased need in utilizing computer modeling. Simulations allow for the development of cryopreservation protocols with specific design criteria, such as non-linear cooling profiles, including interrupted freezing procedures and constant supercooling [1,2], complex solutions both with and without cryoprotectants, and cell-specific requirements.

By combining the knowledge gained through simulations and empirical validations, cryopreservation protocols can be established. Based on results from this research, both intracellular supercooling and osmolality, as indicators of intracellular ice formation and solution effects injury respectively, should be calculated when attempting to compare simulations with biological experimentation. This is of particular importance with slow cooling, which is used to cryopreserve the majority of cells in suspension. Another major recommendation stemmed from obtaining the solution properties of the cytoplasm and the non-ideal osmotically-inactive fraction. It has been shown that volume measurements at higher osmolalities than are universally used (i.e. > 1.5 Osm/kg) are required to accurately obtain these properties of the cell.

Beyond this work, the results from the studies presented in this thesis may also have direct implications for the cryopreservation of tissues, which have multiple cell types in a matrix. This may also prove particularly beneficial in transfusion medicine, when minimizing the amount of manipulation to the sample may reduce potential risks to the recipients. More specifically, in the case of HSC transplants, eliminating Me_2SO as a cryoprotectant would be very beneficial, especially for patients requiring large volumes of bone marrow or leukapheresis products.

This thesis has furthered our knowledge of intracellular osmotic solution properties and applied this insight to understanding cryopreservation protocols for cellular therapies, including cell cryopreservation for transplantation and cellular therapies. By developing a technique to measure the osmotic solution properties of the cytoplasm of a nucleated cell, using osmotic equilibrium data, and combining our theoretical and biological understanding of a cell, important advancements in long-term preservation of cells will result. These results could ultimately contribute to the design of novel cryopreservation protocols for any cell type with known osmotic properties.

7.5 References

[1] M.R. Tijssen, H. Woelders, A. de Vries-van Rossen, C.E. van der Schoot, C. Voermans, and J.M. Lagerberg, Improved postthaw viability and in vitro functionality of peripheral blood hematopoietic progenitor cells after cryopreservation with a theoretically optimized freezing curve. Transfusion 48 (2008) 893-901.

[2] H. Woelders, and A. Chaveiro, Theoretical prediction of 'optimal' freezing programmes. Cryobiology 49 (2004) 258-271.